NASA Reference Publication 1152

AVSCOM Technical Report 84-C-15

1985

Gearing

John J. Coy
Propulsion Directorate
USAARTA-AVSCOM
Lewis Research Center
Cleveland, Ohio

Dennis P. Townsend
and Erwin V. Zaretsky
Lewis Research Center
Cleveland, Ohio

NASA
National Aeronautics
and Space Administration

Scientific and Technical Information Branch

Contents

	Page
Summary	1
1.0 Introduction	1
1.1 Early History of Gearing	1
1.2 Beginning of Modern Gear Technology	2
2.0 Types and Geometry	2
2.1 Parallel-Shaft Gears	2
2.2 Intersecting-Shaft Gears	9
2.3 Nonparallel-Nonintersecting-Shaft Gears	12
3.0 Processing and Manufacture	17
3.1 Materials	17
3.2 Metallurgical Processing Variables	23
3.3 Manufacturing	25
4.0 Stresses and Deflections	26
4.1 Lewis Equation Approach for Bending Stress	26
4.2 Allowable Bending Stress	31
4.3 Other Methods	31
5.0 Gear Life Predictions	34
5.1 Theory of Gear Tooth Life	35
5.2 Gear Life	37
5.3 Gear System Life	37
5.4 Helical Gear Life	38
5.5 Bevel and Hypoid Gear Life	38
6.0 Lubrication	40
6.1 Lubricant Selection	40
6.2 Elastohydrodynamic Film Thickness	41
6.3 Boundary Lubrication	44
6.4 Lubricant Additive Selection	44
6.5 Jet Lubrication	45
6.6 Gear Tooth Temperature	47
7.0 Power Loss Predictions	47
7.1 Sliding Loss	48
7.2 Rolling Loss	49
7.3 Windage Loss	49
7.4 Other Losses	50
7.5 Optimizing Efficiency	50
8.0 Optimal Design of Spur Gear Mesh	51
8.1 Minimum Size	51
8.2 Specific Torque Capacity	52
9.0 Gear Transmission Concepts	53
9.1 Series Trains	53
9.2 Multispeed Gears	54
9.3 Epicyclic Gears	54
9.4 Split-Torque Transmissions	57
9.5 Differential Gearing	57
9.6 Closed-Loop Trains	58
Appendix—Symbols	59
References	62
Bibliography	66

Summary

Gearing technology in its modern form has a history of only 100 years. However, the earliest form of gearing can probably be traced back to fourth century B.C. Greece. This publication draws together current gear practice and integrates it with recent advances in the technology. The history of gearing is reviewed briefly in the "Introduction." Subsequent sections describe types of gearing and their geometry, processing, and manufacture. Both conventional and more recent methods of determining gear stress and deflections are considered. The subjects of life prediction and lubrication are additions to the literature, not having been treated before. New and more complete methods of power loss prediction as well as an optimum design of spur gear meshes are described. Conventional and new types of power transmission system are presented.

1.0 Introduction

Gears are the means by which power is transferred from source to application. Gearing and geared transmissions drive the machines of modern industry. Gears move the wheels and propellers that transport us over the sea, on the land, and in the air. A sizable section of industry and commerce in today's world depends on gearing for its economy, production, and livelihood.

The art and science of gearing have their roots before the common era. Yet many engineers and researchers continue to delve into the areas where improvements are necessary, seeking to quantify, establish, and codify methods to make gears meet the ever-widening needs of advancing technology (ref. 1).

1.1 Early History of Gearing

The earliest written descriptions of gears are said to have been made by Aristotle in the fourth century B.C. (ref. 2). It has been pointed out (refs. 3 and 4) that the passage attributed by some to Aristotle, in "Mechanical Problems of Aristotle" (ca. 280 B.C.), was actually from the writings of his school. In the passage in question there was no mention of gear teeth on the parallel wheels, and they may just as well have been smooth wheels in frictional contact. Therefore the attribution of gearing to Aristotle is most likely incorrect. The real beginning of gearing was probably with Archimedes, who in about 250 B.C. invented the endless screw turning a toothed wheel, which was used in engines of war. Archimedes also used gears to simulate astronomical ratios. The Archimedian spiral was continued in the hodometer and dioptra, which were early forms of the wagon mileage indicator (odometer) and the surveying instrument. These devices were probably based on "thought" experiments of Heron of Alexandria (ca. 60 A.D.), who wrote on theoretical mechanics and the basic elements of mechanisms.

The oldest surviving relic containing gears is the Antikythera mechanism, named for the Greek island near which the mechanism was discovered in a sunken ship in 1900. Professor Price of Yale University has written an authoritative account of this mechanism (ref. 3). The mechanism is not only the earliest relic of gearing, but is also an extremely complex arrangement of epicyclic differential gearing. The mechanism is identified as a calendrical Sun and Moon computing mechanism and is dated to about 87 B.C.

The art of gearing was carried through the European Dark Ages, appearing in Islamic instruments such as the geared astrolabes that were used to calculate the positions of the celestial bodies. Perhaps the art was relearned by the clock- and instrument-making artisans of 14th century Europe, or perhaps some crystallizing ideas and mechanisms were imported from the East after the crusades of the 11th through the 13th centuries.

It appears that an English abbot of St. Alban's monastery, born Richard of Wallingford in 1330 A.D., reinvented the epicyclic gearing concept. He applied it to an astronomical clock that he began to build and that was completed after his death.

A mechanical clock of a slightly later period was conceived by Giovanni de Dondi (1348–1364). Diagrams of this clock, which did not use differential gearing (ref. 3), appear in the sketchbooks of Leonardo da Vinci, who designed geared mechanisms himself (refs. 3 to 5). In 1967, two of Leonardo da Vinci's manuscripts, lost in the National Library in Madrid since 1830, were rediscovered (ref. 6). One of the manuscripts, written between 1493 and 1497 and known as "Codex Madrid I" (ref. 7), contains 382 pages with some 1600 sketches. Included among this display of Leonardo's artistic skill and engineering ability are his studies of gearing. Among these are tooth profile designs and gearing arrangements that were centuries ahead of their "invention."

1.2 Beginning of Modern Gear Technology

In the period 1450 to 1750 the mathematics of gear-tooth profiles and theories of geared mechanisms became established. Albrecht Dürer is credited with discovering the epicycloidal shape (ca. 1525). Philip de la Hire is said to have worked out the analysis of epicycloids and recommended the involute curve for gear teeth (ca. 1694). Leonard Euler worked out the law of conjugate action (ca. 1754) (ref. 5). Gears designed according to this law have a steady speed ratio.

Since the industrial revolution in the mid 19th century, the art of gearing has blossomed, and gear designs have steadily become based on more scientific principles. In 1893, Wilfred Lewis published a formula for computing stress in gear teeth (ref. 8). This formula is in wide use today in gear design. In 1899, George B. Grant, the founder of five gear manufacturing companies, published "A Treatise on Gear Wheels" (ref. 9). New inventions led to new applications for gearing. For example, in the early part of this century (1910), parallel-shaft gears were introduced to reduce the speed of the newly developed reaction steam turbine enough for it to turn the driving screws of ocean-going vessels. This application achieved an overall increase in efficiency of 25 percent in sea travel (ref. 2).

The need for more accurate and quieter running gears became obvious with the advent of the automobile. Although the hypoid gear was within our manufacturing capabilities by 1916, it was not used practically until 1926, when it was used in the Packard automobile. The hypoid gear made it possible to lower the drive shaft and gain more usable floor space. By 1937 almost all cars used hypoid-geared rear axles. Special lubricant anti-wear additives that made it practical to use hypoid gearing were formulated in the 1920's. In 1931, Earle Buckingham, chairman of an ASME research committee on gearing, published a milestone report on the dynamic loading of gear teeth (ref. 10). This led to a better understanding of why faster-running gears sometimes could not carry as much load as slower-running gears.

High-strength alloy steels for gearing were developed during the 1920's and 1930's. Nitriding and case-hardening techniques to increase the surface strength of gearing were introduced in the 1930's. Induction hardening was introduced in 1950. Extremely clean steels produced by vacuum melting processes introduced in 1960 have proven effective in prolonging gear life.

Since the early 1960's there has been increased use of industrial gas turbines for electric power generation. Epicyclic gear systems in the range 746 to 10 445 kW (1000 to 14 000 hp) have been used successfully. Pitch-line velocities are from 50 to 100 m/s (10 000 to 20 000 ft/min). These gearsets must work reliably for 10 000 to 30 000 hr between overhauls (ref. 1).

In 1976, bevel gears produced to drive a compressor test stand ran successfully at 2984 kW (4000 hp) and 203 m/s (40 000 ft/min) for 235 hr (ref. 11). From all indications these gears could be used in an industrial application. A reasonable maximum pitch-line velocity for commercial spiral-bevel gears with curved teeth is 60 m/s (12 000 ft/min) (ref. 12).

Gear system development methods have been advanced in which lightweight, high-speed, highly loaded gears are used in aircraft applications. The problems of strength and dynamic loads, as well as resonant frequencies for such gearing, are now treatable with techniques such as finite-element analysis, siren and impulse testing for mode shapes, and damping (ref. 13). The material presented herein will assist in the design, selection, application, and evaluation of gear drives. Sizing criteria, lubricating considerations, material selection, and methods to estimate service life and power loss are presented.

2.0 Types and Geometry

References 14 and 15 outline the various gear types and include information on proper gear selection. These references classify single-mesh gears according to the arrangement of their shaft axes in a single-mesh gearset (table 1). These arrangements are parallel shafts; intersecting shafts; and nonparallel, nonintersecting shafts.

2.1 Parallel-Shaft Gears

Spur gears.—The external spur gear (figs. 1 and 2) is the most common type of gear. Because the teeth are straight and parallel to the shaft axis, it is also the simplest type of gear. The smaller of two gears in mesh is called the pinion. The larger is customarily designated as "the gear." In most applications the pinion is the driving element and the gear is the driven element. Most spur gear tooth profiles are cut to conform to an involute curve in order to ensure conjugate action. Conjugate action is defined as a constant angular velocity ratio between two meshing gears. Conjugate action can be obtained with any tooth profile shape for the pinion, provided that the mating gear is made with a tooth shape that is conjugate to the pinion tooth shape. The conjugate tooth profiles are such that the common normal at the point of contact between the two teeth will always pass through a fixed point on the line of centers. The fixed point is called the pitch point.

The line of action, or pressure line (fig. 2), is the line that is tangent to both base circles. All points of contact between the two teeth will lie along this line. The pressure angle φ is defined as the acute angle between the line of

TABLE 1.—SIMPLE MESH GEARS

Type	Nominal gear ratio range	Maximum pitch-line velocity		Nominal efficiency at rated power, percent	Remarks
		m/s	ft/min		
Parallel shafts					
Spur	1-5	[a]100 [b]20	[a]20 000 [b]4 000	97-99.5	----------
Helical	1-10	[a]200 [b]20	[a]40 000 [b]4 000		15°-35° Helix angle
Double helical (herringbone)	1-20	[a]200 [b]20	[a]40 000 [b]4 000		----------
Conformal	1-12		------		----------
Intersecting shafts					
Straight bevel	1-8	[a]50 [b]5	[a]10 000 [b]1 000	97-99.5	----------
Spiral bevel	1-8	[a]125 [b]10	[a]25 000 [b]12 000	97-99.5	35° Spiral angle most used
Zerol[c] bevel	1-8	[a]50 [b]5	[a]10 000 [b]1 000	97-99.5	----------
Nonintersecting, nonparallel shafts					
Worm	3-100	[a]50 [b]25	[a]10 000 [b]5 000	50-90	----------
Double-enveloping worm	3-100	[a]50 [b]20	[a]10 000 [b]4 000	50-98	----------
Crossed helical	1-100	[a]50 [b]20	[a]10 000 [b]4 000	50-95	----------
Hypoid	1-50	[a]50 [b]20	[a]10 000 [b]4 000	50-98	Higher ratios have low efficiency

[a]Aircraft high precision.
[b]Commercial.
[c]Registered trademark, The Gleason Works, Rochester, NY.

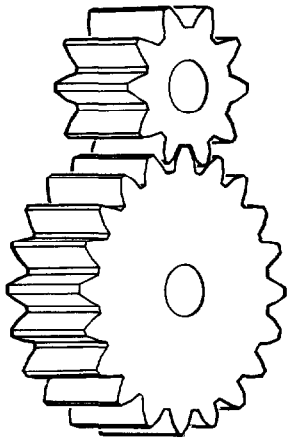

Figure 1.—External spur gears.

action and a line perpendicular to the line of centers. Although the pressure angle can vary for different applications, most spur gears are cut to operate at pressure angles of 20° or 25°. The circular pitch p of a spur gear is defined as the distance on the pitch circle from a point on a tooth to the corresponding point on an adjacent tooth:

$$p = \frac{2\pi r_p}{N} \tag{1}$$

where

r_p pitch circle radius
N number of teeth

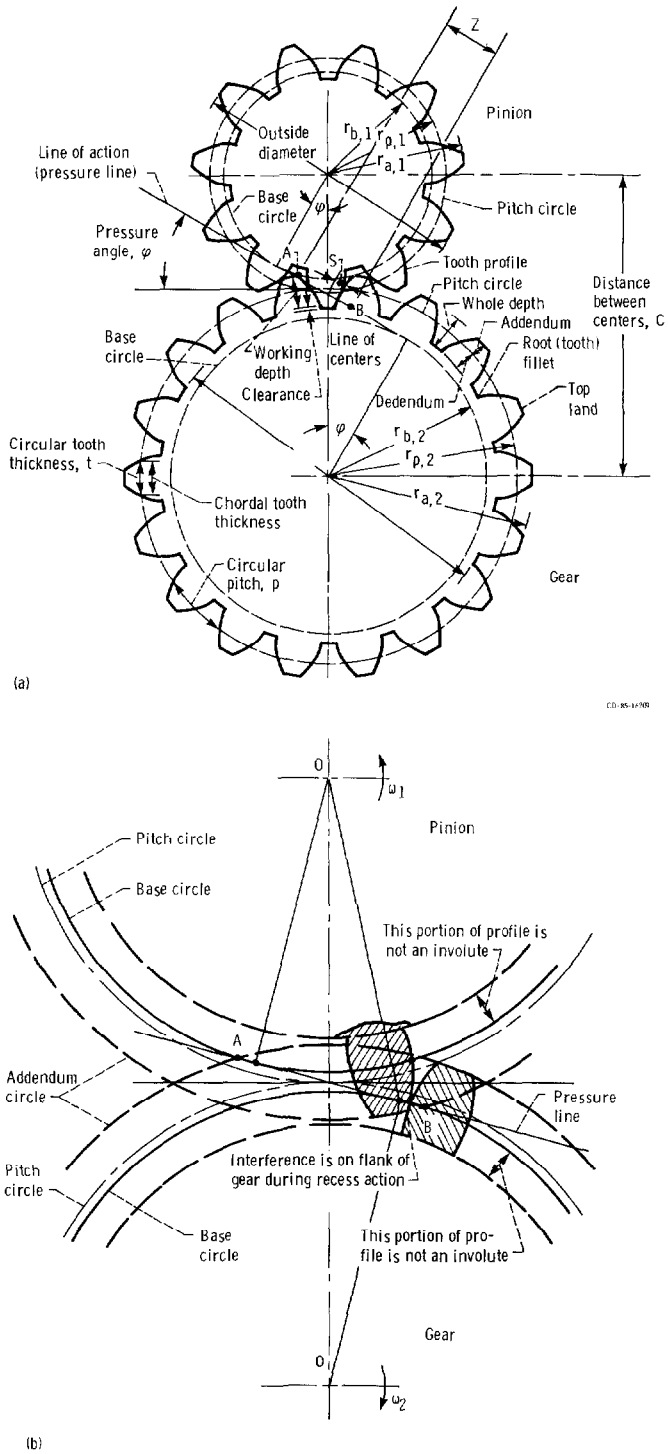

(a) Geometry.

(b) Interference, on flank of pinion during approach action and flank of gear during recess action.

Figure 2.—External spur gear geometry and interference in the action of gear teeth.

Similarly the base pitch p_b is the distance on the base circle from a point on one tooth to the corresponding point on an adjacent tooth:

$$p_b = \frac{2\pi r_b}{N} \tag{2}$$

where r_b is the base circle radius. Also, from geometry

$$p_b = p \cos \varphi \tag{3}$$

The diametral pitch P, defined as the number of gear teeth N divided by the diameter of the pitch circle D, determines the relative sizes of gear teeth:

$$P = \frac{N}{D} \tag{4}$$

where

$$P_p = \pi \tag{5}$$

The larger the value of P, the greater the number of gear teeth and the smaller their size. "Module" is the reciprocal of diametral pitch in concept, but whereas diametral pitch is expressed as the number of teeth per inch, the module is generally expressed in millimeters per tooth. Metric gears (in which tooth size is expressed in modules) and American standard inch diametral pitch gears are not interchangable.

The distance between the centers of two gears (fig. 2) is

$$C = \frac{D_1 + D_2}{2} \tag{6}$$

The space between the teeth must be larger than the mating tooth thickness in order to prevent jamming of the gears. The difference between tooth thickness and tooth space as measured along the pitch circle is called backlash. Backlash can be created by cutting the gear teeth slightly thinner than the space between teeth, or by setting the center distance slightly greater between the two gears. In the second case the operating pressure angle of the gear pair is increased accordingly. The backlash for a gear pair must be sufficient to permit free action under the most severe combination of manufacturing tolerances and operating temperature variations. Backlash should be small in positioning control systems, but it should be quite generous for single-direction power gearing (table 2). If the center distance between mating

TABLE 2.—RECOMMENDED BACKLASH FOR ASSEMBLED GEARS

Diametral pitch, P		Backlash	
		cm	in
m^{-1}	in^{-1}		
25.4	1	0.064–0.10	0.025–0.040
17	1.5	.046–.070	.018–.027
12.7	2	.036–.050	.014–.020
10	2.5	.028–.040	.011–.016
8.5	3	.024–.036	.009–.014
6.4	4	.018–.028	.007–.011
5	5	.015–.023	.006–.009
4.2	6	.013–.020	.005–.008
3.6	7	.010–.018	.004–.007
3.2–2.8	8–9	.010–.015	.004–.006
2.5–2	10–13	.008–.013	.003–.005
1.8–.8	14–32	.005–.010	.002–.004

external gears is increased by ΔC, the resulting increase in backlash ΔB is

$$\Delta B = \Delta C \times 2 \tan \varphi \tag{7}$$

For the mesh of internal gears this equation gives the decrease in backlash for an increase in center distance.

The distance between points A and B (fig. 2), or the length of contact along the line of action, is the distance between the intersections, with the line of action, of the gear addendum circle and the pinion addendum circle. This is the total length along the line of action for which there is tooth contact. This distance can be determined by the various radii and the pressure angle as follows:

$$Z = \left[r_{a,1}^2 - (r_{p,1} \cos \varphi)^2\right]^{1/2} + \left[r_{a,2}^2 - (r_{p,2} \cos \varphi)^2\right]^{1/2} - C \sin \varphi \tag{8}$$

The radii of curvature of the teeth when contact is at a distance s along the line of action from the pitch point can be represented for the pinion as

$$\rho_1 = r_{p,1} \sin \varphi \pm s \tag{9}$$

and for the gear as

$$\rho_2 = r_{p,2} \sin \varphi \pm s \tag{10}$$

Where s is positive for equation (9), it must be negative for equation (10) and vice versa.

To determine how many teeth are in contact, the contact ratio of the gear mesh must be known. The contact ratio m_c is defined as

$$m_c = \frac{Z}{p_b} \tag{11}$$

Gears are generally designed with contact ratios of 1.2 to 1.6. A contact ratio of 1.6, for example, means that 40 percent of the time one pair of teeth will be in contact and 60 percent of the time two pairs of teeth will be in contact. A contact ratio of 1.2 means that 80 percent of the time one pair of teeth will be in contact and 20 percent of the time two pairs of teeth will be in contact.

Gears with contact ratios greater than 2 are referred to as "high-contact-ratio gears." For these gears there are never less than two pairs of teeth in contact. A contact ratio of 2.2 means that 80 percent of the time two pairs of teeth will be in contact and 20 percent of the time three pairs of teeth will be in contact. High-contact-ratio gears are generally used in select applications where long life is required. Figure 3 shows a high-contact-ratio gear and a conventional involute gear. Analyses should be performed when using high-contact-ratio gearing because higher bending stresses may occur in the tooth addendum region. Also, higher sliding in the tooth contact can contribute to distress of the tooth surfaces. In addition, higher dynamic loading may occur with high-contact-ratio gearing (ref. 16).

Interference of the gear teeth is an important consideration. The portion of the spur gear below the base circle is sometimes cut as a straight radial line but never as an involute curve (fig. 2(b)). Hence, if contact should occur below the base circle, nonconjugate action (interference) will occur. The maximum addendum radius of the gear without interference is calculated from the following equation:

$$r_a' = \left(r_b^2 + C^2 \sin^2 \varphi\right)^{1/2} \tag{12}$$

where r_a' is the radial distance from the gear center to the point of tangency of the mating gear's base circle with the line of action. Should interference be indicated, there are several methods to eliminate it. The center distance can be increased, which will also increase the pressure angle and change the contact ratio. Also, the addendum can be shortened, with a corresponding increase in the addendum of the mating member. The method used depends on the application and experience.

Another type of spur gear, internal, has the teeth cut on the inside of the rim (fig. 4). The pitch relationships previously discussed for external gears apply also to internal gears (eqs. (1) to (5)). A secondary type of involute interference called tip fouling may also occur. The geometry should be carefully checked in the region labeled "F" in figure 4 to see if this occurs.

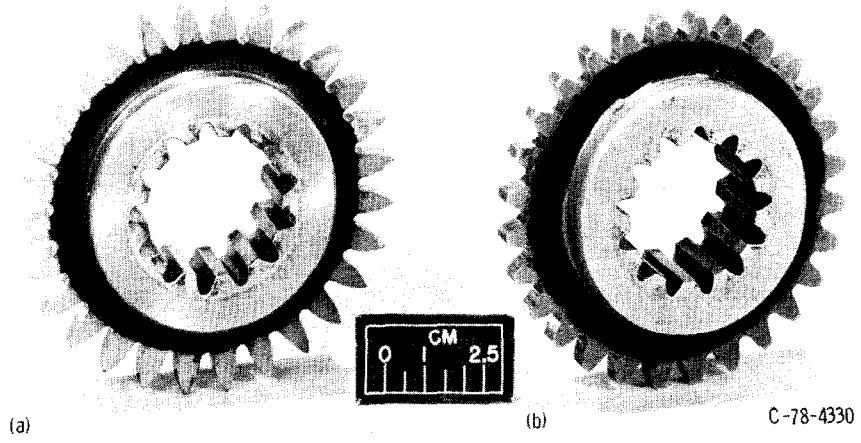

(a) High-contact-ratio gear with modified tooth profile. Contact ratio, 2.25.
(b) Conventional involute gear. Contact ratio, 1.3.

Figure 3.—Comparison of gears.

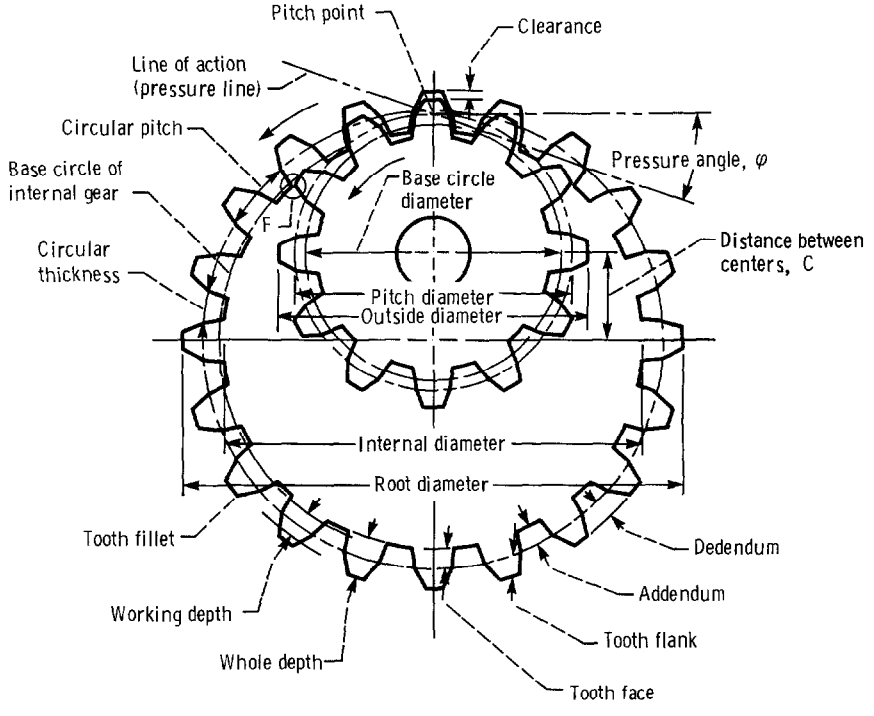

Figure 4.—Internal spur gear geometry.

Helical gears.—In a helical gearset (fig. 5) cylindrical gears have teeth cut in the form of a helix: one gear has a right-hand helix and the mating gear, a left-hand helix. Helical gears have a greater load-carrying capacity than equivalent-size spur gears. Although helical gears vibrate less than spur gears because the teeth overlap, a high thrust load is produced along the axis of rotation. This load results in high rolling-element-bearing loads, which may reduce the life and reliability of a transmission system. This end thrust increases with helix angle.

To overcome the axial thrust load, double-helical gearsets are used (fig. 6). The thrust loads are counterbalanced so that no resultant axial load is transmitted to the bearings. Space is sometimes provided between the two sets of teeth to allow for runout of the tooth cutting tool, or the gear may be assembled in two

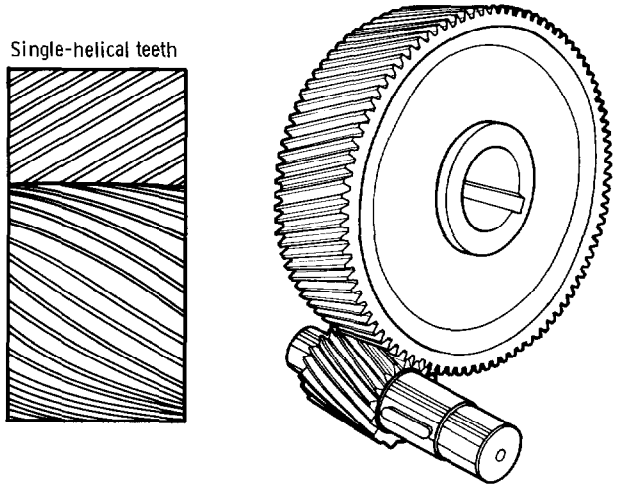

Figure 5.—Single-helical gear pair.

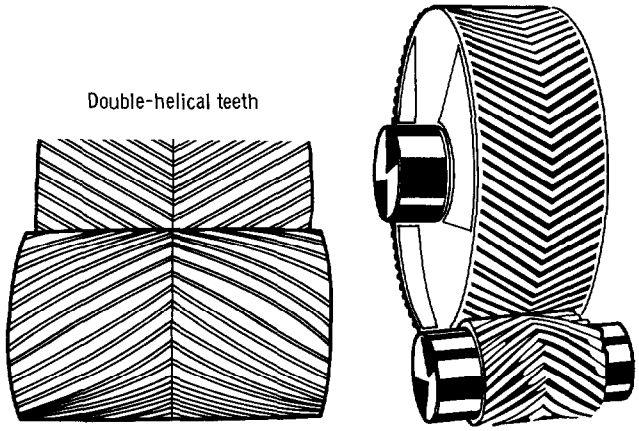

Figure 6.—Double-helical, or herringbone, gear pair.

halves. The space should be small because it reduces the active face width. Double-helical, or herringbone, gears are used for the transmission of high torques at high speeds in continuous service.

Spur gears have only one diametral and one circular pitch; helical gears have two additional pitches. The normal circular pitch p_n is the distance between corresponding points of adjacent teeth as measured in plane B-B (fig. 7), which is perpendicular to the helix.

$$p_n = p_t \cos \Psi \tag{13}$$

where

p_t transverse circular pitch

Ψ helix angle

The transverse circular pitch is measured in plane A-A (fig. 7), which is perpendicular to the shaft axis. The axial

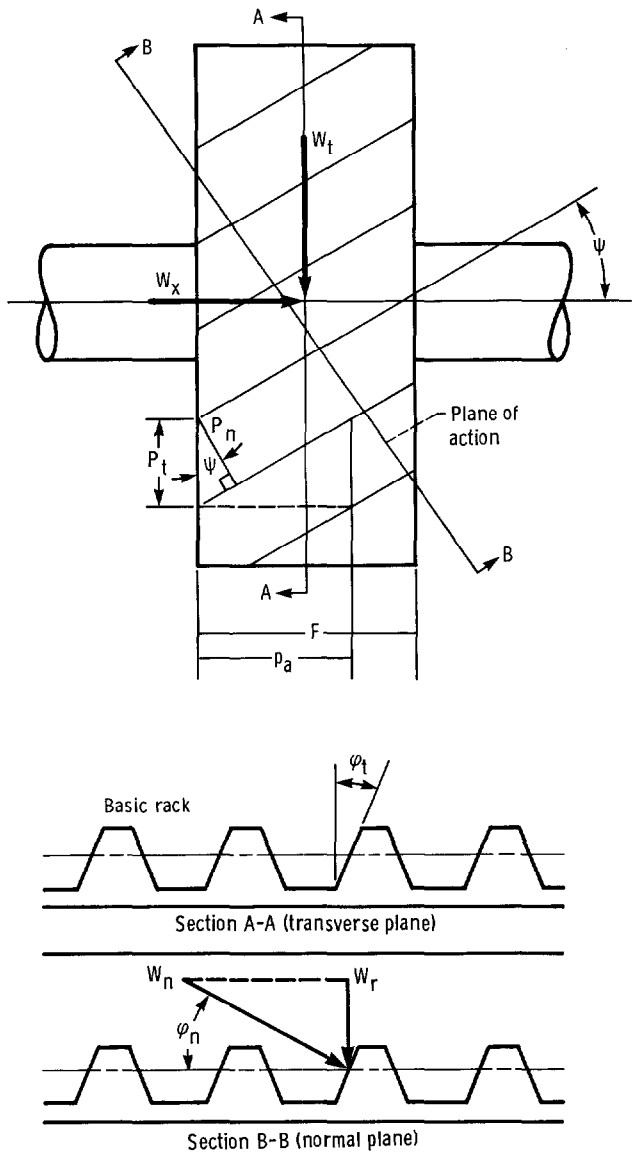

Figure 7.—Helical gear geometry. (Not to scale.).

pitch p_a is a similar distance measured in a plane parallel to the shaft axis:

$$p_a = p_t \cot \Psi \tag{14}$$

The diametral pitch in the transverse plane is

$$P_t = \frac{N}{D} \tag{15}$$

The normal diametral pitch is

$$P_n = \frac{P_t}{\cos \varphi} \tag{16}$$

To maintain contact across the entire tooth face, the minimum face width F must be greater than the axial pitch p_a. However, to ensure a smooth transfer of load during tooth engagement, F should be at least 1.2 to 2 times p_a. The two pressure angles associated with the helical gear, the transverse pressure angle φ_t measured in plane A–A (fig. 7) and the normal pressure angle φ_n measured in plane B–B, can be related as follows:

$$\tan \varphi_n = \tan \varphi_t \cos \Psi \tag{17}$$

The three components of normal load W_N acting on a helical gear tooth can be written as follows:

Tangential:

$$W_t = W_N \cos \varphi_n \cos \Psi \tag{18}$$

Radial:

$$W_r = W_N \sin \varphi_n \tag{19}$$

Axial:

$$W_x = W_N \cos \varphi_n \sin \Psi \tag{20}$$

where W_t is the tangential load acting at the pitch circle perpendicular to the axis of rotation. The direction of the axial thrust load for pairs of helical gears (fig. 8) depends on whether the driver has a right-hand or left-hand helix and the direction of rotation. These loads must be considered when selecting and sizing the rolling-element bearings to support the shafts and gears.

The plane normal to the gear teeth, B–B (fig. 7), intersects the pitch cylinder. The gear tooth profile generated in this plane would be a spur gear, with the same properties as the actual helical gear. The number of teeth of the equivalent spur gear in the normal plane is known as either the virtual or equivalent number of teeth. The equivalent number of teeth is

$$N_e = \frac{N}{\cos^3 \Psi} \tag{21}$$

Conformal (Wildhaber/Novikov) gears.—In 1923, E. Wildhaber filed a U.S. patent application (ref. 17) for helical gearing of a circular arc form. In 1926, he filed a patent application for a method of grinding this form of gearing (ref. 18). Until Wildhaber, helical gears were made only with screw involute surfaces. However, Wildhaber gearing failed to receive the support necessary to develop it into a working system. In 1956, M.L. Novikov in the U.S.S.R. was granted a patent for a similar form of gearing (ref. 19). Conformal gearing then advanced in the U.S.S.R, but the concept found only limited application. Conformal gearing was also the subject of research in Japan and China but did not find widespread industrial application.

The first and probably only aerospace application of conformal gearing was by Westland Helicopter in Great Britain (refs. 20 and 21). Westland modified the geometry of the conformal gears as proposed by Novikov and Wildhaber and successfully applied the modified geometry to the transmission of the Lynx helicopter. The major advantage demonstrated by this transmission system was increased gear load capacity without gear tooth fracture. It is anticipated that the gear system would exhibit improved power-to-weight ratio or increased life and reliability. However, these assumptions have neither been analytically shown nor experimentally proven.

To achieve the maximum contact area in a conformal gear pair (fig. 9), the radii of two mating surfaces r_1 and r_2 should be identical. However, this is not practical. Inaccuracies in fabrication will occur on the curvatures

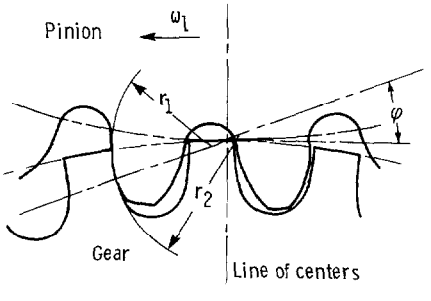

Figure 9.—Conformal tooth geometry.

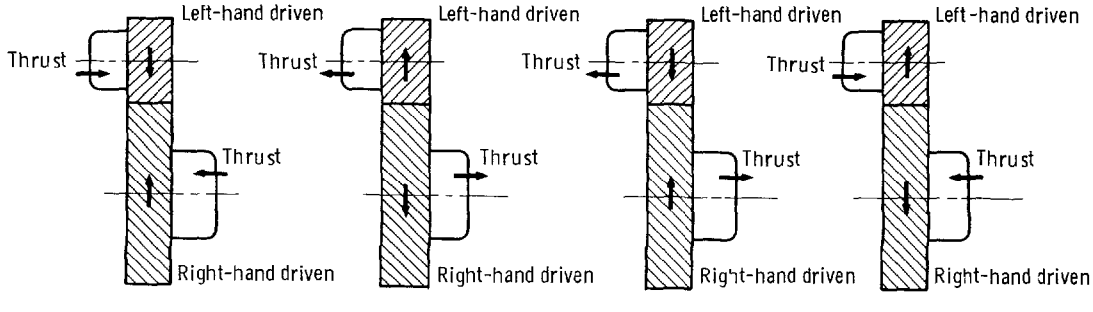

Figure 8.—Direction of axial thrust load for helical gears on parallel shafts.

and in other dimensions such as the center distance. Such inaccuracies can cause stress concentrations on the edges and tips of the gear teeth. To prevent this edge loading, the radii are made slightly unequal and are struck from different centers. Although this slight mismatch decreases the stress concentrations, the contact surface area is also reduced and this amplifies the Hertzian contact stress. The resultant contact stresses depend on the helix angle.

As a historical note, in early designs thermal expansion in gearcases and shafts was sufficient to affect the gear pair center distances, increasing the contact stresses and leading to early failure (ref. 22).

As was discussed for involute gearing, a constant velocity ratio exists for spur gear tooth pairs at every angular position because the teeth "roll" over each other. However, with conformal gearing, there is only one angular position where a tooth is in contact with its opposite number. Immediately before and after that point there is no contact. To achieve a constant velocity ratio, the teeth must run in a helical form across the gear, and an overlap must be achieved from one tooth pair to the next as the contact area shifts across the gear, from one side to the other, during meshing (ref. 21). The sweep velocity of the contact area across the face width is often thought of as being a pure rolling action, as no physical translation of the metal occurs in this direction. However, there is a small sliding component acting along the tooth. If the pitch surfaces of the mating gears are considered, the length of the meshing helices would be the same on both the pinion and the gear. But the conformal system uses an all-addendum pinion and all-addendum wheel; so when the contact area traverses one axial pitch, it must sweep over a longer distance on the pinion and a shorter distance on the gear. Thus a small sliding component exists (fig. 10(a)).

The magnitude of the sliding can vary with tooth design. However, since the sliding velocity depends on the displacement from the pitch surface, the percentage of sliding will vary across the contact area (fig. 10(b)). The main sliding velocity, which occurs at the tooth contact, acts up and down the tooth height. The magnitude of this sliding component can vary up to approximately 15 percent of the pitch helix sweep velocity. Thus the slide-to-roll ratio seems to indicate why slightly lower power losses than with involute gears can be attained by using conformal gears (ref. 21).

2.2 Intersecting-Shaft Gears

Several types of gear system can be used for power transfer between intersecting shafts. The most common of these are straight-bevel gears and spiral-bevel gears. In addition, there are special bevel gears that accomplish the same or similar results and are made with special geometrical characteristics for economy. Among these

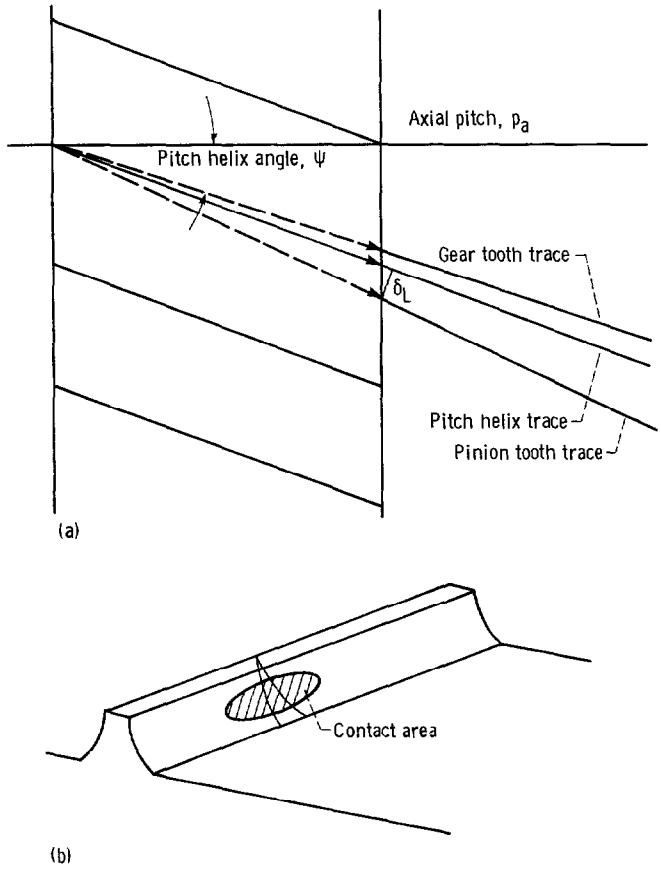

(a) Sliding components in rolling direction.
(b) Relative sliding velocities in contact area.

Figure 10.—Tooth contact trace diagram.

are Zerol[1] gears, Coniflex[1] gears, Formate[1] gears, Revacycle[1] gears, and face gears. For the most part the geometry of spiral-bevel gears is extremely complex and does not lend itself to simplified formulas or analyses. The gear tooth geometry is dictated by the machine tool used to generate the gear teeth and the machine tool settings.

Straight-bevel gears.—Bevel gears can be arranged in various ways (fig. 11(a)). A cutaway drawing of a straight-bevel gear (fig. 11(b)) shows the terminology and important physical dimensions. Straight-bevel gears are used generally for relatively low-speed applications with pitch-line velocities to 5.08 m/s (1000 ft/min) and where vibration and noise are not important criteria. However, with carefully machined and ground straight-bevel gears it may be possible to achieve speeds to 76.2 m/s (15 000 ft/min).

Bevel gears are mounted on intersecting shafts at any desired angle, although 90° is most common. They are designed and manufactured in pairs and as a result are not always interchangeable. One gear is mounted on the

[1]Registered trademark. The Gleason Works, Rochester, N.Y.

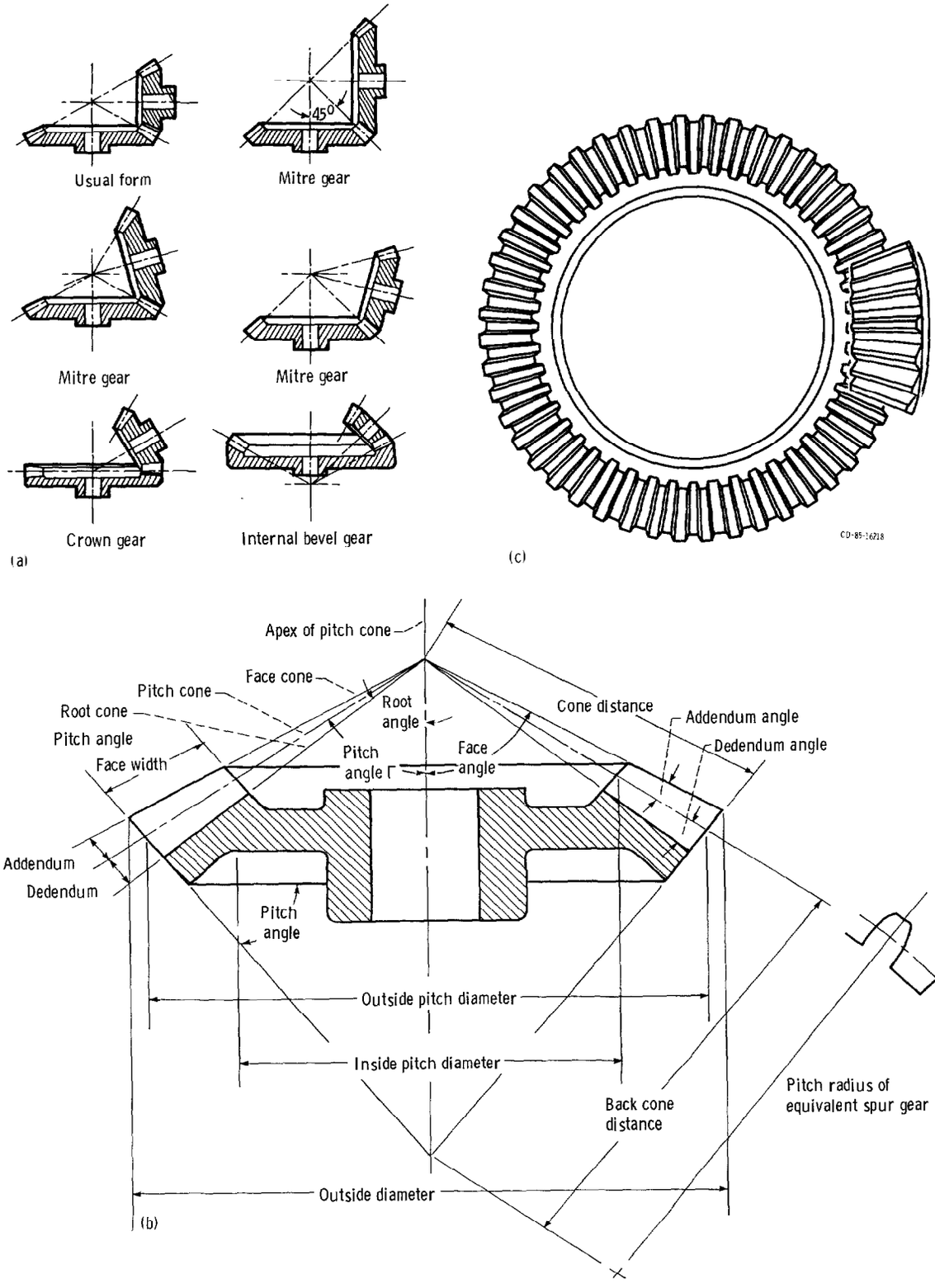

(a) Gear arrangements.
(b) Gear terminology.
(c) Gear pair.

Figure 11.—Straight-bevel gear.

cantilevered, or outboard, end of the shaft. Because of the outboard mounting the deflection of the shaft where the gear is attached can be rather large. This would result in the teeth at the small end moving out of mesh. The load would thus be unequally distributed, with the larger ends of the teeth taking most of the load. To reduce this effect, the tooth face width is usually made no greater than one-third of the cone distance.

Bevel gears are usually classified according to their pitch angle. A bevel gear having a pitch angle of 90° and a plane for its pitch surface is known as a crown gear. When the pitch angle of a bevel gear exceeds 90°, it is called an internal bevel gear. Internal bevel gears cannot have a pitch angle very much greater than 90° because of problems incurred in manufacturing such gears. These manufacturing difficulties are the main reason why internal bevel gears are rarely used. Bevel gears with pitch angles less than 90° are the type most commonly used. When two meshing bevel gears have a shaft angle of 90° and have the same number of teeth, they are called mitre gears. In other words, mitre gears have a speed ratio of 1. Each of the two gears has a 45° pitch angle.

The relationship (Tregold's approximation) between the actual number of teeth for the bevel gear, the pitch angle, and the virtual or equivalent number of teeth is given by

$$N_e = \frac{N}{\cos \Gamma} \tag{22}$$

where Γ is the pitch angle. The back cone distance becomes the pitch radius for the equivalent spur gear.

Face gears have teeth cut on the flat face of the blank. The face gear meshes at right angles with a spur or helical pinion. When the shafts intersect, the face gear is known as an "on center" face gear. These gears may also be offset to provide a right-angle nonintersecting shaft drive.

Coniflex gears are straight-bevel gears whose teeth are crowned in the lengthwise direction to accommodate small shaft misalignments.

Formate gears have the gear member of the pair with nongenerated teeth, usually with straight tooth profiles. The pinion member of the pair has generated teeth that are conjugate to the rotating gear.

Revacycle gears are straight-bevel gears generated by a special process, with a special tooth form.

Spiral-bevel gears.—The teeth of spiral-bevel gears (fig. 12(a)) are curved and oblique. These gears are suitable for pitch-line velocities to 61 m/s (12 000 ft/min). Ground teeth extend this limit to 125 m/s (25 000 ft/min). Spiral-bevel gears differ according to the methods of generating the gear tooth surfaces. Among these methods are the Gleason method, the Klingelnberg system, and the Oerlikon system. These companies have developed specified and detailed directions for the design of spiral-bevel gears that are related to the respective method of manufacture. However, some general considerations, such as the concept of pitch cones, generating gears, and conditions of force transmission, are common for the generation of all types of spiral-bevel gear (fig. 12(b)). The actual tooth gear geometry is dictated by the machine tool settings supplied by the respective manufacturers.

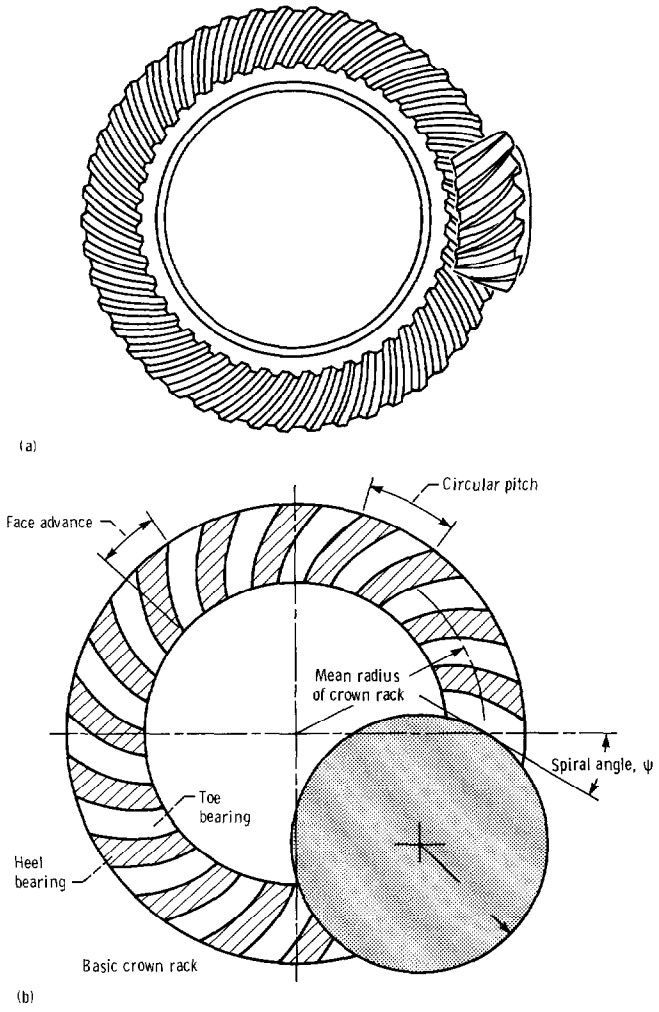

(a) Gear pair.
(b) Cutting spiral gear teeth on basic crown rack.

Figure 12.—Spiral-bevel gear.

The standard pressure angle φ for spiral-bevel gears is 20° although 14.5° and 16° angles are used. The usual spiral angle ψ is 35°. Because spiral-bevel gears are much stronger than similar-sized straight-bevel or Zerol[1] gears (fig. 13), they can be used for large-speed-reduction-ratio applications at a reduced overall installation size. The hand of the spiral should be selected so as to cause the

[1]Registered trademark, The Gleason Works, Rochester, N.Y.

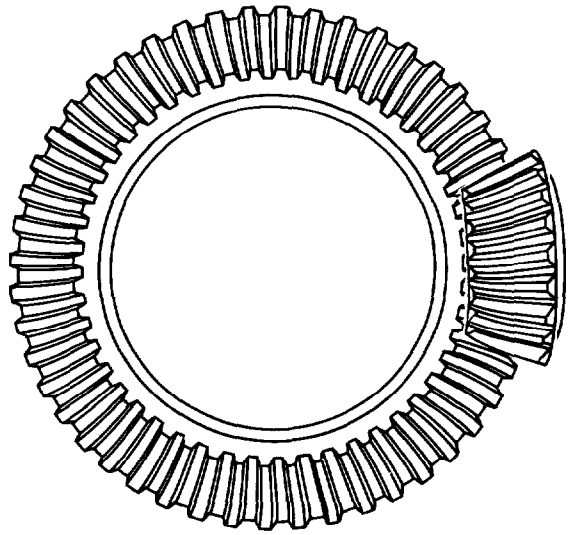

Figure 13.—Zerol gear.

gears to separate from each other during rotation and not to force them together, which might cause jamming.

Thrust loads produced in operation with spiral-bevel gears are greater than those produced with straight-bevel gears. An analogy for the relationship that exists between straight- and spiral-bevel gears is that existing between spur and helical gears. Localized tooth contact is also achieved. This means that some mounting and load deflections can occur without a resultant load concentration at the ends of the teeth.

The total force W_N acting normal to the pinion tooth and assumed to be concentrated at the average radius of the pitch cone can be divided into three perpendicular components. These are the transmitted, or tangential, load W_t; the axial, or thrust, component W_x; and the separating, or radial, component W_r. The force W_t can, of course, be computed from

$$W_t = \frac{T}{r_{av}} \tag{23}$$

where

T input torque

r_{av} radius of pitch cone measured at midpoint of tooth

The forces W_x and W_r depend on the hand of the spiral and the direction of rotation. Thus there are four possible cases to consider. For a right-hand pinion spiral with clockwise pinion rotation or for a left-hand spiral with counterclockwise rotation, the equations are

$$W_x = \frac{W_t}{\cos \psi} (\tan \varphi_n \sin \Gamma - \sin \psi \cos \Gamma) \tag{24}$$

$$W_r = \frac{W_t}{\cos \psi} (\tan \varphi_n \cos \Gamma + \sin \psi \sin \Gamma) \tag{25}$$

where

ψ spiral angle

Γ pinion pitch angle

φ_n normal tooth pressure angle

The other two cases are a left-hand spiral with clockwise rotation and a right-hand spiral with counterclockwise rotation. For these two cases the equations are

$$W_x = \frac{W_t}{\cos \psi} (\tan \varphi_n \sin \Gamma + \sin \psi \cos \Gamma) \tag{26}$$

$$W_r = \frac{W_t}{\cos \psi} (\tan \varphi_n \cos \Gamma - \sin \psi \sin \Gamma) \tag{27}$$

and the rotation is observed from the input end of the pinion shaft.

Equations (24) to (27) give the forces exerted by the gear on the pinion. A positive sign for either W_x or W_r indicates that the load is directed away from the cone center. The forces exerted by the pinion on the gear are equal and opposite. Of course, the opposite of an axial pinion load is a radial gear load, and the opposite of a radial pinion load is an axial gear load.

Zerol bevel gears are used for much the same applications as straight-bevel gears. The suggested minimum number of teeth is 14, one or more teeth should always be in contact, and the basic pressure angle is 20°, although angles of 22.5° or 25° are sometimes used to eliminate undercutting.

2.3 Nonparallel-Nonintersecting-Shaft Gears

Nonparallel, nonintersecting shafts lie in parallel planes and can be skewed at any angle between zero and 90°. Among the gear systems used to transfer power between nonparallel, nonintersecting shafts are hypoid gears, crossed-helical gears, worm gears, Cone-Drive[2] worm gears, face gears, Spiroid[3] gears, Planoid[3] gears, Helicon[3] gears, and Beveloid[4] gears.

Hypoid gears.—Hypoid gears (fig. 14) are very similar to spiral-bevel gears. The main difference is that their pitch surfaces are hyperboloids rather than cones. As a result their pitch axes do not intersect: the pinion axis being above or below the gear axis. In general, hypoid gears are most desirable for those applications involving

[2]Registered trademark, Michigan Tool Co., Detroit, Michigan.
[3]Registered trademark, Illinois Tool Works, Chicago, Illinois.
[4]Registered trademark, Vinco Corporation, Detroit, Michigan.

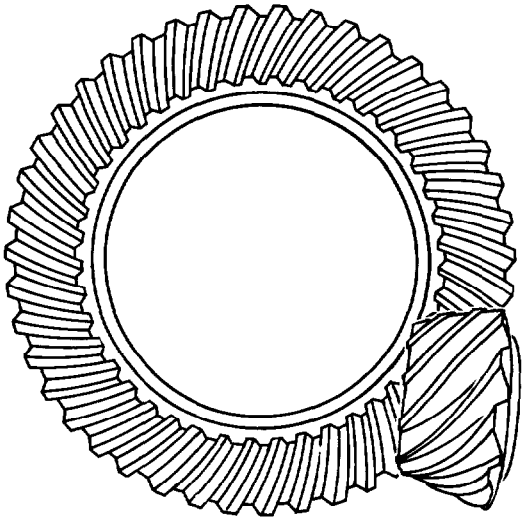

Figure 14.—Hypoid gear.

large speed-reduction ratios, those involving nonintersecting shafts, and those requiring great smoothness and quietness of operation. Hypoid gears are almost universally used for automotive applications, allowing the drive shaft to be located underneath the passenger compartment floor. They operate more smoothly and quietly than spiral-bevel gears and are stronger for a given ratio. Because the two supporting shafts do not intersect, bearings can be mounted on both sides of the gear to provide extra rigidity. The pressure angles usually range between 19° and 22.5°. The suggested minimum number of teeth is eight for speed ratios greater than 6 and six for smaller ratios. High-reduction hypoids permit ratios between 10 and 120 and even as high as 360 in fine pitches.

Crossed-helical gears.—Crossed-helical gears (fig. 15) are also known as spiral gears. They are in fact ordinary helical gears used in nonparallel-shaft applications. They transmit relatively small amounts of power because of their sliding action and limited tooth contact area. However, they permit a wide range of speed ratios without change of center distance or gear size. They can be used at angles other than 90°.

For two helical gears to operate as crossed-helical gears they must have the same normal diametral pitch P_n and normal pressure angle φ_n. The gears do not need to have the same helix angle or be of opposite hand. In most crossed-helical gear applications the gears have the same hand. The relationship (fig. 16) between the helix angles of the gears and the angle between the shafts on which the gears are mounted is given by

$$\Sigma = \Psi_1 + \Psi_2 \tag{28}$$

for gears having the same hand and by

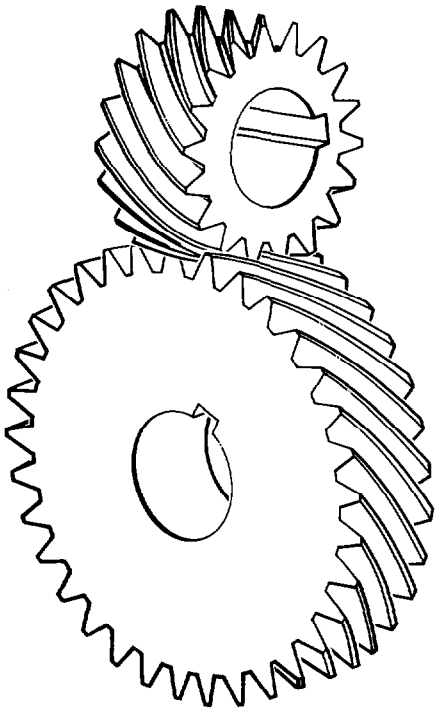

Figure 15.—Crossed-helical gear.

$$\Sigma = \Psi_1 - \Psi_2 \tag{29}$$

for gears having opposite hands, where Σ is the shaft angle. For crossed-helical gears where the shaft angle is 90° the helical gears must be of the same hand.

The center distance between the gears is given by

$$C = \frac{1}{2P_n}\left(\frac{N_1}{\cos \Psi_1} + \frac{N_2}{\cos \Psi_2}\right) \tag{30}$$

The sliding velocity v_s acts at the pitch point tangentially along the tooth surface (fig. 16), where by the law of cosines

$$v_s = \left(v_1^2 + v_2^2 - 2v_1 v_2 \cos \Sigma\right)^{1/2} \tag{31}$$

where

$v_1 = \omega_1 r_{p,1}$

$v_2 = \omega_2 r_{p,2}$

For a shaft angle of 90° the sliding velocity is given by

$$v_s = \frac{v_1}{\cos \Psi_2} = \frac{v_2}{\cos \Psi_1} \tag{32}$$

The direction of the thrust load for crossed-helical gears can be determined from figure 17. The forces on the crossed-helical gears (fig. 16) are as follows:

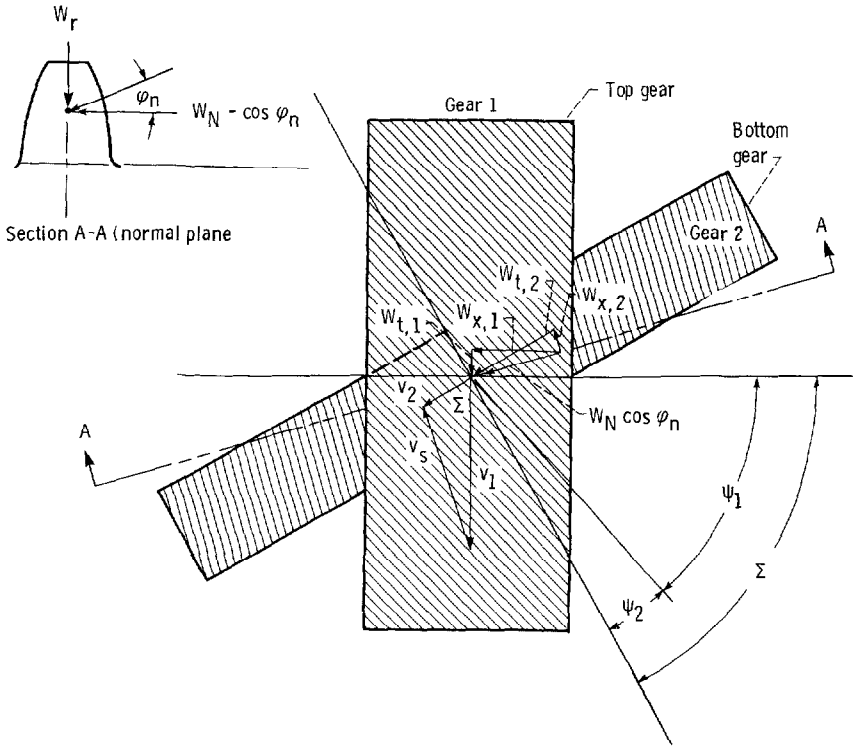

Figure 16.—Meshing crossed-helical gears showing relationship between helix angles, shaft angle, and load and velocity vectors.

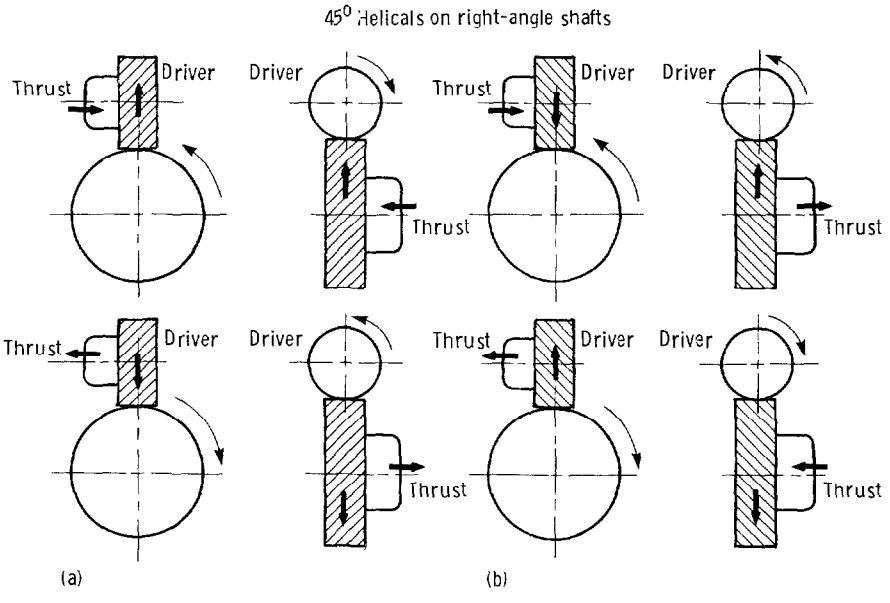

(a) Both gear and pinion left hand.
(b) Both gear and pinion right hand.

Figure 17.—Direction of thrust load for two meshing crossed-helical gears mounted on shafts oriented 90° to each other.

Transmitted force:

$$W_t = W_N \cos \varphi_n \cos \Psi \tag{33}$$

Axial thrust load:

$$W_x = W_N \cos \varphi_n \sin \Psi \tag{34}$$

Radial or separating force:

$$W_r = W_N \sin \varphi_n \tag{35}$$

where φ_n is the normal pressure angle.

The pitch circle diameter D is obtained from the equation

$$D = \frac{N}{P_n \cos \Psi} \tag{36}$$

where

N number of teeth
P_n normal diametral pitch
Ψ helix angle

Since the pitch diameters are not directly related to the number of teeth, they cannot be used to obtain the angular velocity ratio. This ratio must be obtained from the ratio of the number of teeth.

Worm gears.—The worm gearset (fig. 18) comprises a worm, which resembles a screw, and a worm wheel, which is a helical gear. The shafts on which the worm and wheel are mounted are usually 90° apart. Because of the screw action of worm gear drives they are quiet and vibration free and produce a smooth output. On a given center distance much higher ratios can be obtained through a worm gearset than with other conventional types of gearing. The contact (Hertz) stresses are lower with worm gears than with crossed-helical gears. Although there is a large component of sliding motion in a worm gearset (as in crossed-helical gears), a worm gearset will have a higher load capacity than a crossed-helical gearset.

Worm gearsets may be either single or double enveloping. In a single-enveloping set (fig. 19) the worm wheel has its width cut into a concave surface, thus partially enclosing the worm when in mesh. The double-enveloping set, in addition to having the helical gear width cut concavely, has the worm length cut concavely. The result is that both the worm and the gear partially enclose each other. A double-enveloping set will have more teeth in contact and will have area rather than line contact, thus permitting greater load transmission.

All worm gearsets must be carefully mounted to ensure proper operation. The double-enveloping, or cone, type is much more difficult to mount than the single-enveloping type.

The relationships to define the worm gearset (figs. 18 and 19) are as follows: the lead angle of the worm is

$$\lambda_W = \arctan \frac{L_W}{\pi D_W} \tag{37}$$

This is the angle between a tangent to the pitch helix and the plane of rotation. If the lead angle is less than 5°, a rotation worm gearset cannot be driven backwards or, in other words, is self-locking. The pitch diameter is D_W. The lead is the number of teeth or threads multiplied by the axial pitch of the worm or

$$L_W = N_W p_{a,W} \tag{38}$$

The lead and helix angles of the worm and worm wheel are complementary

$$\lambda_W + \Psi_W = 90° \tag{39}$$

where Ψ_W is the helix angle of the worm. Also

$$\lambda_G + \Psi_G = 90° \tag{40}$$

and for 90° shaft angles

$$\lambda_W = \Psi_G \tag{41}$$

The center distance is given by

$$C = \frac{D_W + D_G}{2} \tag{42}$$

where D_G is the pitch diameter of the gear wheel.

The American Gear Manufacturers Association (AGMA) recommends that the following equation be used to check the magnitude of D_W:

$$D_W \geq \frac{C^{0.875}}{2.2} \approx 3 p_G \tag{43}$$

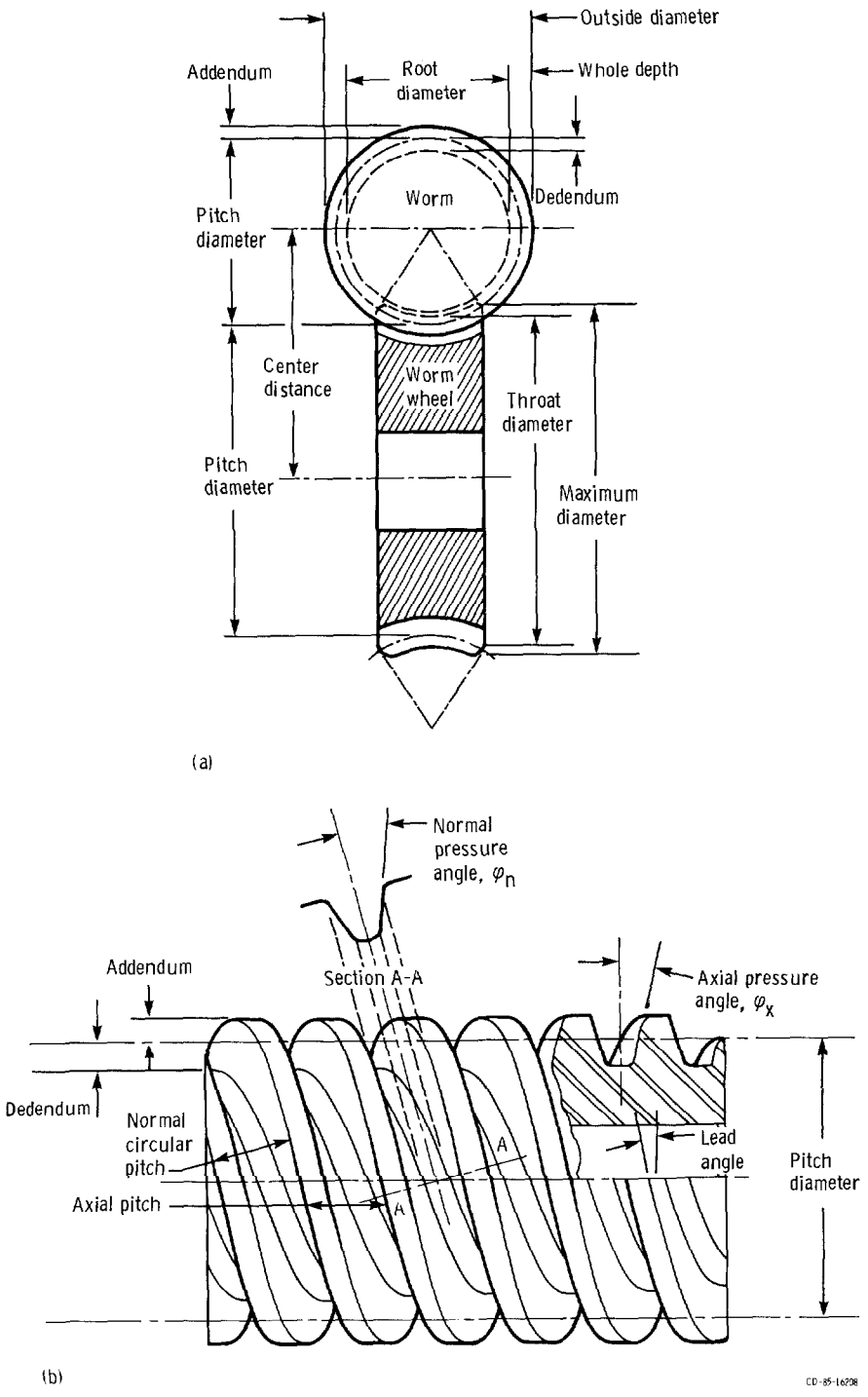

(a) Worm and wheel.
(b) Worm.

Figure 18.—Worm gearset nomenclature.

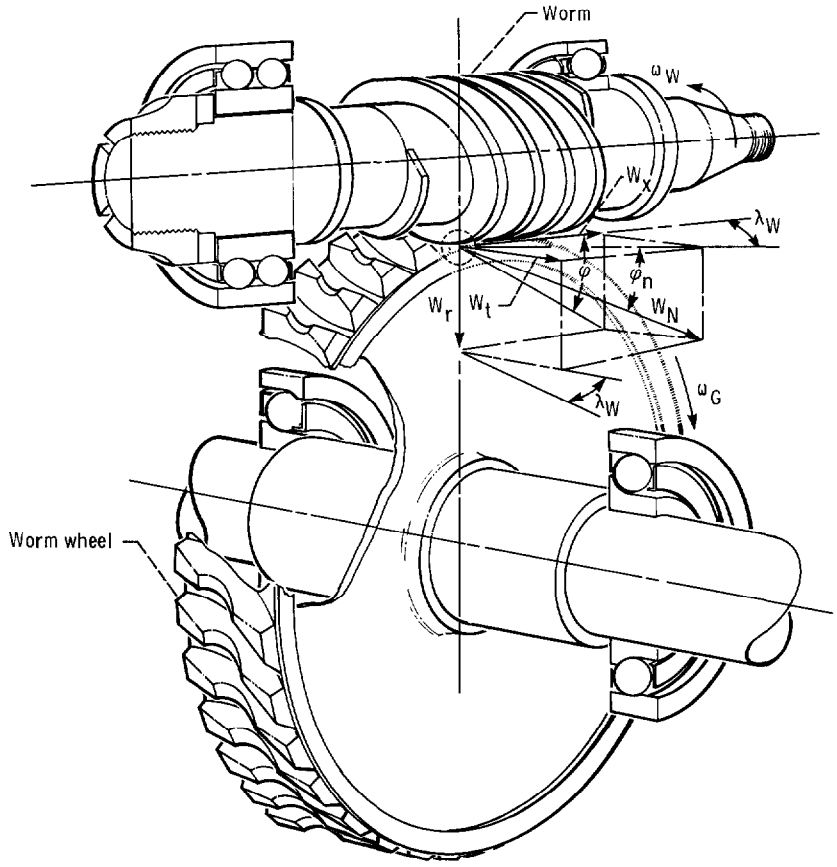

Figure 19.—Worm gearset showing load vectors.

where p_G is the circular pitch of the worm wheel. The gear ratio is given by

$$m_G = \frac{\omega_W}{\omega_G} = \frac{N_G}{N_W} = \frac{\pi D_G}{L_W} \tag{44}$$

If friction is neglected, the forces acting on the tooth surface (fig. 18) are as follows:

(1) Transmitted force, which is tangential to the worm and axial to the worm wheel

$$W_t = W_N \cos \varphi_n \sin \lambda_W \tag{45}$$

(2) Axial thrust load on the worm and tangential or transmitted force on the worm wheel

$$W_x = W_N \cos \varphi_n \cos \lambda_W \tag{46}$$

(3) Radial or separating force

$$W_r = W_N \sin \varphi_n \tag{47}$$

The directions of the thrust loads for worm gearsets are given in figure 20.

3.0 Processing and Manufacture

3.1 Materials

A wide variety of gear materials are available today for the gear designer. The designer can choose from wood, plastics, aluminum, magnesium, titanium, bronze, brass, gray cast iron, nodular and malleable iron, and a whole variety of low-, medium-, and high-alloy steels. In addition, there are many ways of modifying or processing the materials to improve their properties or to reduce the cost of manufacture. These include reinforcements for plastics, coating and processing for aluminum and titanium, and hardening and forging for many of the iron-based (or ferrous) gear materials.

When selecting a gear material for an application, the gear designer will first determine the requirements for the gears being considered. The design requirements for a gear in a given application will depend on such conditions as accuracy, load, speed, material, and noise limitations. The more stringent these requirements are, the more costly the gear will become. For instance, a gear requiring high accuracy because of speed or noise limitations may require several processing operations in its manufacture. Each operation will add to the cost. Machined gears,

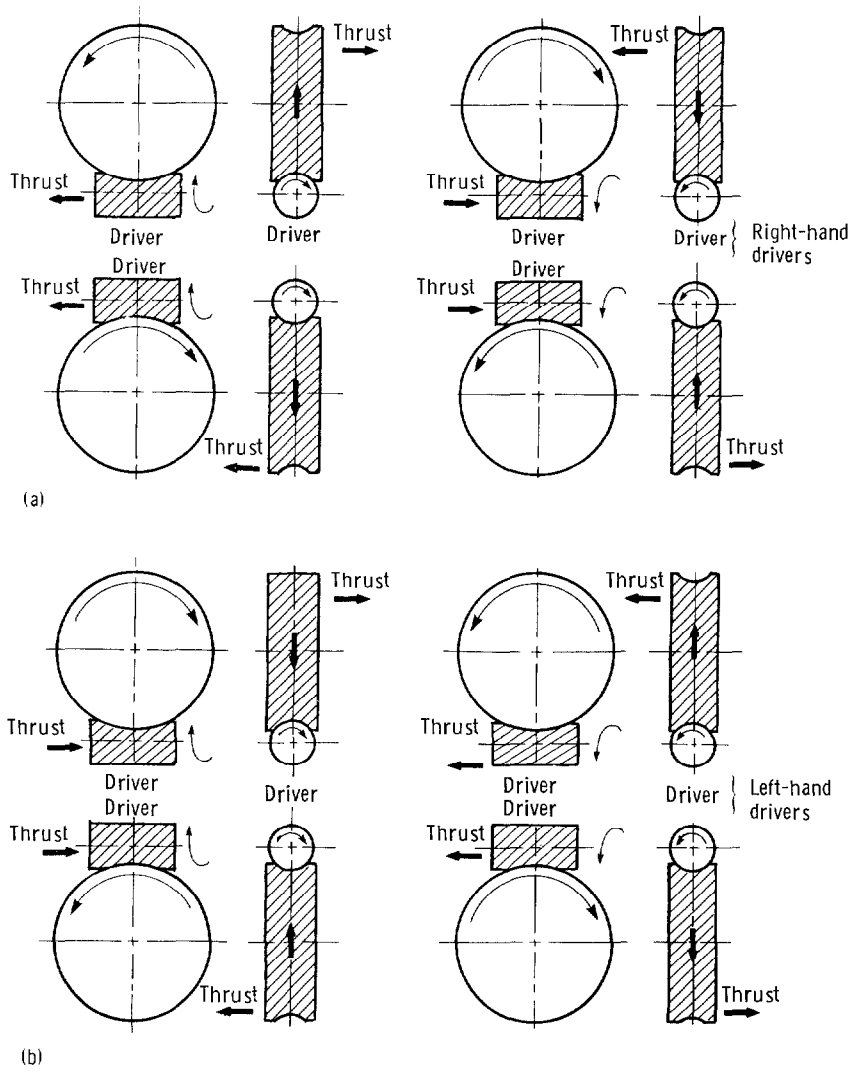

(a) Right-hand drivers.
(b) Left-hand drivers.

Figure 20.—Direction of thrust load for worm gearset.

which are the most accurate, can be made from materials with good strength characteristics. However, these gears are very expensive. The cost is further increased if hardening and grinding are required as in applications where noise limitation is a critical requirement. Machined gears should be a last choice for a high-production gear application because of cost.

Some of the considerations in the choice of a material include allowable bending and Hertz stress, wear resistance, impact strength, water and corrosion resistance, manufacturing cost, size, weight, reliability, and lubrication requirements. Steel, under proper heat treatment, meets most of these qualifications. Where wear is relatively severe, as with worm gearing, a high-quality chill-cast nickel bronze may be used for rim material. The smaller worm gears may be entirely of nickel bronze.

In aircraft applications, such as helicopter, V/STOL, and turboprops, the dominant factors are reliability and weight. Cost is of secondary importance. Off-the-road vehicles, tanks, and some actuators may be required to operate at extremely high loads with a corresponding reduction in life. These loads can produce bending stresses in excess of 1.03 GPa (150 000 psi) and Hertz stresses in excess of 2.76 GPa (400 000 psi) for portions of the duty cycle. This may be acceptable because of the relatively short life of the vehicle and a deemphasis on reliability. (In contrast, aircraft gearing typically operates at maximum bending stresses of 0.45 GPa (65 000 psi) and maximum Hertz stresses of 1.24 GPa (180 000 psi)).

Plastics.—There has always been a need for a light-weight, low-cost gear material for light-duty applications. In the past, gears were made from wood or phenolic-resin-impregnated cloth. However, in recent years, with

the development of many new polymers, many gears are made of various "plastic" materials (table 3). The most common molded plastic gears are the acetate and nylon resins. These materials are limited in strength, temperature resistance, and accuracy. The nylon and acetate resins have a room-temperature yield strength of approximately 69 MPa (10 000 psi). This is reduced to approximately 28 MPa (4000 psi) at their upper temperature limit of 121 °C (250 °F). Nylon resin is subject to considerable moisture absorption, which reduces its strength and causes considerable expansion. Larger gears are made with a steel hub that has a plastic tire for better dimensional control. Plastic gears can operate for long periods in adverse environments, such as dirt, water, and corrosive fluids, where other materials would tend to wear excessively. They can also operate without lubrication or can be lubricated by the processed material as in the food industry. The cost of plastic gears can be as low as a few cents per gear for a simple gear on a high-volume production basis. This is probably the most economical gear available. Often a plastic gear is run in combination with a metal gear to give better dimensional control, low wear, and quiet operation.

Polyimide is a more expensive plastic material than nylon or acetate resin, but it has an operating temperature limit of approximately 316 °C (600 °F). This makes the polyimides suitable for many adverse applications that might otherwise require metal gears. Polyimides can be used effectively in combination with a metal gear without lubrication because of polyimide's good sliding properties (refs. 23 to 25). However, in addition to the greater material cost, polymide gears are more expensive than other plastic gears because they are more difficult to mold.

Nonferrous metals.—Several grades of wrought and cast aluminum alloys are used for gearing. The wrought alloy 7075-T6 is stronger than 2024-T4 but is also more expensive. Aluminum does not have good sliding and wear properties. However, it can be anodized with a thin, hard surface layer that will give it better operating characteristics. Anodizing gives aluminum good corrosion protection in saltwater applications, but the coating is thin and brittle and may crack under excessive load.

Magnesium is not considered a good gear material because of its low elastic modulus and other poor mechanical properties.

Titanium has excellent mechanical properties, approaching those of some heat-treated steels, with a density nearly half that of steel. However, because of its poor sliding properties, which produce high friction and wear, it is not generally used as a gear material. Several attempts have been made to develop a wear-resistant coating, such as chromium plating, iron coating, or nitriding for titanium (refs. 26 to 29). Titanium would be an excellent gear material if a satisfactory coating or alloy could be developed to provide improved sliding and wear properties.

Several alloys of zinc, aluminum, magnesium, brass, and bronze are used as die-cast materials. Many prior die-cast applications now use less-expensive plastic gears. The die-cast materials have higher strength properties, are not affected by water, and will operate at higher temperatures than the plastics. As a result they still have a place in moderate-cost, high-volume applications. Die-cast gears are made from copper or lower cost zinc or aluminum alloys. The main advantage of die casting is that it completely eliminates or drastically reduces the requirement for machining. The high fixed cost of the dies makes low production runs uneconomical. Some of the die-cast alloys used for gearing are listed in references 30 and 31.

Copper alloys.—Several copper alloys are used in gearing. Most are the bronze alloys containing varying amounts of tin, zinc, manganese, aluminum, phosphorus, silicon, lead, nickel, and iron. The brass alloys contain primarily copper and zinc with small amounts of aluminum, manganese, tin, and iron. The copper alloys are most often used in combination with an iron or steel gear to give good wear and load capacity especially in worm gear applications, where there is a high sliding component. In these cases the steel worm drives a bronze gear. Bronze gears are also used where corrosion and water are a problem. Several copper alloys are listed in table 4. The bronze alloys are either aluminum bronze, manganese bronze, silicon bronze, or

TABLE 3.—PROPERTIES OF PLASTIC GEAR MATERIALS

Property	ASTM	Acetate	Nylon	Polyimide
Yield strength, MPa (psi)	D 638	69 (10 000)	81 (11 800)	72 (10 500)
Shear strength, MPa (psi)	D 732	66 (9510)	66 (9600)	81 (11 900)
Impact strength (Izod), N-m (ft-lb)	D 256	1.9 (1.4)	1.2 (0.9)	1.2 (0.9)
Elongation at yield, percent	D 638	15	5	6.5
Modulus of elasticity, GPa (psi)	D 790	2.8 (410 000)	2.8 (410 000)	3.2 (460 000)
Coefficient of linear thermal expansion, cm/cm °C (in/in °F)	D 696	8.8×10^{-5} (4.5×10^{-5})	8.1×10^{-5} (4.5×10^{-5})	5.04×10^{-5} (2.8×10^{-5})
Water absorption (24 hr), percent	D 570	0.25	1.5	0.32
Specific gravity	D 792	1.425	1.14	1.43
Temperature limit, °C (°F)	-----	121 (250)	121 (250)	315 (600)

TABLE 4.—PROPERTIES OF COPPER ALLOY GEAR MATERIALS

Material	Modulus of elasticity		Yield strength		Ultimate strength	
	GPa	psi	MPa	psi	MPa	psi
Yellow brass	104	15×10^6	345	50×10^3	414	60×10^3
Naval brass	104	15	310	45	483	70
Phosphorous bronze	104	15	276	40	518	75
Aluminum bronze	131	19	345	50	690	100
Manganese bronze	110	16	310	45	352	80
Silicon bronze	104	15	207	30	414	60
Nickel-tin bronze	104	15	173	25	345	50

phosphorous bronze. These bronze alloys have yield strengths of 138 to 414 MPa (20 000 to 60 000 psi) and all have good machinability.

Cast iron.—Cast iron is used extensively in gearing because of its low cost, good machinability, and moderate mechanical properties. Many gear applications can use gears made from cast iron because of its good sliding and wear properties, which are in part a result of its free graphite and porosity. There are three basic cast irons, which are distinguished by the structure of graphite in the ferrite matrix: (1) gray cast iron, where the graphite is in flake form; (2) malleable cast iron, where the graphite consists of uniformly dispersed, fine, free-carbon particles or modules; and (3) ductile iron, where the graphite is in the form of tiny balls or spherules. The malleable iron and ductile iron have more shock and impact resistance. The cast irons can be heat treated to give improved mechanical properties. The bending strength of cast iron ranges from 34 to 172 MPa (5000 to 25 000 psi) (ref. 32), and the surface fatigue strength ranges from 345 to 793 MPa (50 000 to 115 000 psi) (ref. 33). In many worm gear drives the bronze gear can be replaced with a cast iron gear at a lower cost because of the sliding properties of the cast iron.

Sintered powder metals.—Sintering of powder metals is one of the more common methods used in high-volume, low-cost production of medium-strength gears with fair dimensional tolerance (ref. 34). In this method a fine metal powder of iron or other material is placed in a high-pressure die and formed into the desired shape and density under very high pressure. The unsintered (green) part has no strength as it comes from the press. It is then sintered in a furnace under a controlled atmosphere to fuse the powder together for greater strength and toughness. Usually an additive (such as copper in iron) is used in the powder for added strength. The sintering temperature is then set at the melting temperature of the copper to fuse the iron powder together for a stronger bond than would be obtained with the iron powder alone. The parts must be properly sintered to give the desired strength.

Several materials with a wide range of properties are available for sintered powder-metal gears. Table 5 lists properties of some of the more commonly used gear

TABLE 5.—PROPERTIES OF SINTERED POWDER-METAL ALLOY GEAR MATERIALS

Composition	Ultimate tensile strength		Apparent hardness, Rockwell	Comment
	GPa	psi		
1 to 5Cu-0.6C-94Fe	414	60×10^3	B-60	Good impact strength
7Cu-93Fe	221	32	B-35	Good lubricant impregnation
15Cu-0.6C-84Fe	587	85	B-80	Good fatigue strength
0.15C-98Fe	359	52	A-60	Good impact strength
0.5C-96Fe	345	50	B-75	Good impact strength
2.5Mo-0.3C-1.7N-95Fe	897	130	C-35	High strength, good wear
4Ni-1Cu-0.25C-94Fe	828	120	C-40	Carburized and hardened
5Sn-95Cu	138	20	H-52	Bronze alloy
10Sn-87Cu-0.4P	207	30	H-75	Phosphorous bronze alloy
1.5Be-0.25Co-98Cu	552	80	B-85	Beryllium alloy

materials; other materials are available. The cost for volume production of sintered powder-metal gears is an order of magnitude lower than that for machined gears.

A process that has been more recently developed is the hot-forming powder-metals process (refs. 35 and 36). In this process a powder-metal preform is made and sintered. The sintered powder-metal preformed part is heated to forging temperature and finished forged. The hot-formed parts have strengths and mechanical properties approaching the ultimate mechanical properties of the wrought materials. A wide choice of materials is available for the hot-forming powder-metals process. Since this is a fairly new process, there will undoubtedly be improvements in the materials made from this process and reductions in the cost. Several promising high-temperature, cobalt-base alloy materials are being developed.

Because additional processes are involved, hot-formed powder-metal parts are more expensive than those formed by the sintered powder-metal process. However, either process is more economical than machining or conventional forging while producing the desired mechanical properties. This makes the hot-forming powder-metals process attractive for high-production parts where high strength is needed, such as in the automotive industry. The accuracy of the powder-metal and hot-forming processes is generally in the AGMA class 8 range. Although accuracy can be improved with special precautions if die wear is limited, this tends to increase the cost. Figure 21 shows the relative cost of some of the materials or processes for high-volume, low-cost gearing.

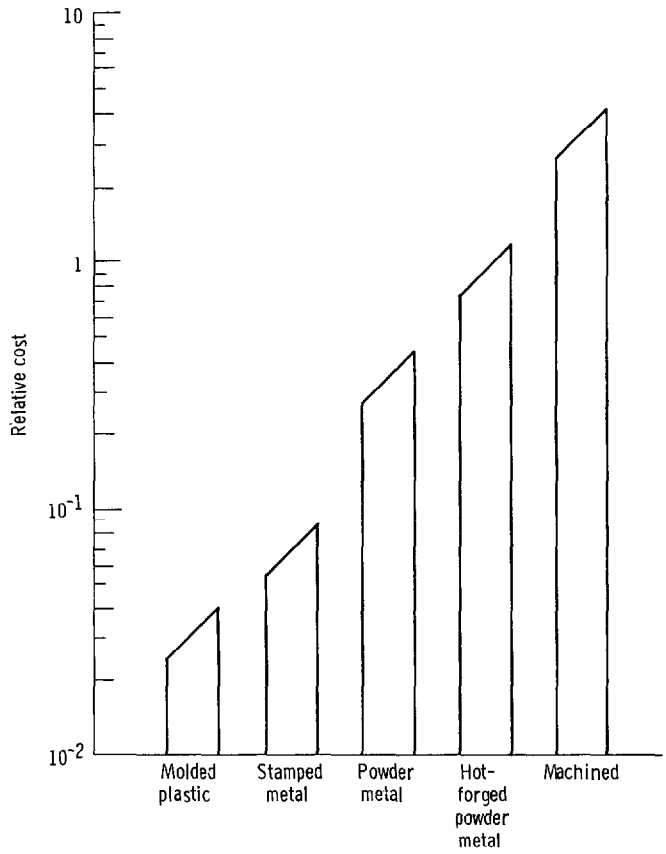

Figure 21.—Relative costs of gear materials.

Hardened steels.—A large variety of iron or steel alloys are used for gearing (table 6). The choice of which material to use is based on a combination of operating conditions such as load, speed, lubrication system, and temperature plus the cost of producing the gears. When operating conditions are moderate, such as medium loads with ambient temperatures, a low-alloy steel can be used without the added cost of heat treatment and additional processing. The low-alloy material in the non-heat-treated condition can be used for bending stresses in the 138-MPa (20 000-psi) range and surface durability Hertz stresses of approximately 586 MPa (85 000 psi). As the operating conditions become more severe, it becomes necessary to harden the gear teeth for improved strength and to case harden the gear tooth surface by case carburizing or case nitriding for longer pitting fatigue life, better scoring resistance, and better wear resistance. Several medium-alloy steels can be hardened to give good load-carrying capacity with bending stresses of 345 to 414 MPa (50 000 to 60 000 psi) and contact stresses of 1.1 to 1.24 GPa (160 000 to 180 000 psi). The higher alloy steels are much stronger and must be used in heavy-duty applications. AISI 9310, AISI 8620, Nitralloy N, and Super Nitralloy are good materials for these applications and can operate with bending stresses of 483 MPa (70 000 psi) and maximum contact (Hertz) stresses of 1.38 GPa (200 000 psi). These high-alloy steels should be case carburized (AISI 8620 and 9310) or case nitrided (Nitralloy) for a hard, wear-resistant surface.

Gears that are case carburized will usually require grinding after the hardening operation because of distortion during heat treatment. The nitrided materials offer the advantage of much less distortion during nitriding and therefore can be used in the as-nitrided condition without additional finishing. This is very helpful for large gears with small cross sections, where distortion can be a problem. Since case depth for nitriding is limited to approximately 0.051 cm (0.020 in), case crushing can occur if the load is too high.

Gear surface fatigue strength and bending strength can be improved by shot peening (refs. 37 and 38). The 10-percent surface fatigue life of the shot-peened gears was 1.6 times that of the standard ground gears (ref. 37).

The low- and medium-alloy steels have a limiting operating temperature above which they begin to lose their hardness and strength. Above this temperature, usually around 149 °C (300 °F), the materials are tempered and early bending failures, surface pitting failures, or scoring will occur. To avoid this condition, a material is needed that has a higher tempering temper-

TABLE 6.—PROPERTIES OF STEEL ALLOY GEAR MATERIALS

Material	Tensile strength		Yield strength		Elongation in 5 cm (2 in), percent
	MPa	psi	MPa	psi	
Cast iron	310	45×10^3	----	-------	----
Ductile iron	552	80	414	60×10^3	3
AISI 1020	552	80	483	70	20
AISI 1040	690	100	414	60	27
AISI 1066	828	120	621	90	19
AISI 4146	667	140	883	128	18
AISI 4340	932	135	828	120	16
AISI 8620	1173	170	966	140	14
AISI 8645	1450	210	1242	180	13
AISI 9310	1277	185	1104	160	15
AISI 440C	759	110	499	65	14
AISI 416	1104	160	966	140	19
AISI 304	759	110	518	75	35
Nitralloy 135M	932	135	690	100	16
Super Nitralloy	1450	210	1311	190	15
CBS 600	1532	222	1242	180	15
CBS 1000M	1463	212	1201	174	16
Vasco X-2	1711	248	1553	225	6.8
EX-53	1180	171	973	141	16
EX-14	1166	169	794	115	19

ature and that maintains its hardness at high temperatures. The generally accepted minimum hardness required at operating temperature is Rockwell C-58. In recent years several materials have been developed that maintain a Rockwell C-58 hardness at temperatures from 232 to 315 °C (450 to 600 °F) (ref. 39). Several materials have shown promise of improved life at normal operating temperature. The hot-hardness data indicate that they will also provide good fatigue life at higher operating temperatures.

AISI M-50 has been used successfully for several years as a rolling-element bearing material for temperatures to 315 °C (600 °F) (refs. 40 to 44). It has also been used for lightly loaded accessory gears for aircraft applications at high temperatures. However, the standard AISI M-50 material is generally considered too brittle for more heavily loaded gears. AISI M-50 is considerably better as a gear material when forged with integral teeth. The grain flow from the forging process improves the bending strength and impact resistance of the AISI M-50 considerably (ref. 45). The AISI M-50 material can also be ausforged with gear teeth to give good bending strength and better pitting life (refs. 46 and 47). However, around 760 °C (1400 °F) the ausforging temperature is so low that forging gear teeth is difficult and expensive. As a result ausforging for gears has had considerably limited application (ref. 46). Test results show that the forged and ausforged gears can give lives approximately three times those of the standard AISI 9310 gears (ref. 46).

Nitralloy N is a low-alloy nitriding steel that has been used for several years as a gear material. It can be used for applications requiring temperatures of 204 to 232 °C (400 to 450 °F). A modified Nitralloy N called Super Nitralloy or 5Ni-2Al Nitralloy was used in the U.S. supersonic aircraft program for gears. It can be used for gear applications requiring temperatures to 260 °C (500 °F). Table 7 gives relative surface fatigue data for Super Nitralloy.

Two materials that were developed for case-carburized, tapered roller bearings but also show promise as high-temperature gear materials are CBS 1000M and CBS 600 (refs. 48 and 49). These materials are low- to medium-alloy steels that can be carburized and hardened to give a hard case of Rockwell C-60 with a core of

TABLE 7.—RELATIVE SURFACE PITTING FATIGUE FOR VAR AISI 9310 STEEL AND AIRCRAFT-QUALITY GEAR STEELS (ROCKWELL 59-62)

Steel[a]	Ten-percent relative life
VAR AISI 9310	1
VAR AISI 9310 (shot peened)	1.6
VAR Carpenter EX-53	2.1
CVM CBS 600	1.4
VAR CBS 1000	2.1
CVM VASCO X-2	2.0
CVM Super Nitralloy (5Ni-2Al)	1.3
VIM-VAR AISI M-50 (forged)	3.2
VIM-VAR AISI M-50 (ausforged)	2.4

[a]VAR = vacuum arc remelting.
CVM = consumable-electrode vacuum remelt.
VIM-VAR = vacuum induction melting-vacuum arc remelting.

Rockwell C-38. Surface fatigue test results for CBS 600 and AISI 9310 are also shown in table 7. The CBS 600 has a medium fracture toughness that can cause fracture failures after a surface fatigue spall has occurred.

Two other materials that have recently been developed as advanced gear materials are EX-53 and EX-14. Reference 50 reports that the fracture toughness of EX-53 is excellent at room temperature and improves considerably as temperature increases. The EX-53 surface fatigue results show a 10-percent life that is twice that of the AISI 9310.

Vasco X-2 is a high-temperature gear material (ref. 51) that is currently being used in advanced CH-47 helicopter transmissions. This material has an operating temperature limit of 315 °C (600 °F) and has been shown to have good gear load-carrying capacity when properly heat treated. The material has a high chromium content (4.9 percent) that oxidizes on the surface and can cause soft spots when the material is carburized and hardened. A special process has been developed that eliminates these soft spots when the process is closely followed (ref. 52). Several groups of Vasco X-2 with different heat treatments were surface fatigue tested in the NASA gear test facility. All groups except the group with the special processing gave poor results (ref. 53). Vasco X-2 has a lower fracture toughness than AISI 9310 and is subject to tooth fractures after a fatigue spall.

3.2 Metallurgical Processing Variables

Research reported in the literature on gear metallurgical processing variables is not as extensive as that for rolling-element bearings. However, an element of material in a Hertz stress field does not recognize whether it is in a bearing or a gear. It only recognizes the resultant shearing stress acting on it. Consequently the behavior of the material in a gear will be much like that in a rolling-element bearing. The metallurgical processing variables to be considered are

(1) Melting practice, such as air, vacuum induction, consumable-electrode vacuum remelt (CVM), vacuum degassing, electroslag (electroflux) remelt, and vacuum induction melting-vacuum arc remelting (VIM-VAR);

(2) Heat treatment to give hardness, differential hardness, and residual stress

(3) Metalworking, consisting of thermomechanical working and fiber orientation

These variables can significantly affect gear performance. Other factors that can also significantly affect gear fatigue life and that have some meaningful documentation are not included. These are trace elements, retained austenite, gas content, and inclusion type and content. Although any of these factors can exercise some effect on gear fatigue life, they are, from a practical standpoint, too difficult to measure or control by normal quality control procedures.

Heat treatment procedures and cycles, per se, can also affect gear performance. However, at present no controls, as such, are being exercised over heat treatment. The exact thermal cycle is left to the individual producer with the supposition that a certain grain size and hardness range be met. Hardness is discussed in some detail in reference to gear life. Lack of definitive data precludes any meaningful discussion of grain size.

Melting practice.—Sufficient data and practical experience exist to suggest that the use of vacuum-melted materials, and specifically CVM, can increase gear surface pitting fatigue life beyond that obtainable with air-melted materials (refs. 54 to 59). Since, in essentially all critical applications such as gears for helicopter transmissions and turboprop aircraft, vacuum-melted material is specified, a multiplication factor can be introduced into the life estimation equation.

Life improvements over air-melted steels to 13 times by CVM processing (refs. 41 to 44) and to 100 times by VIM-VAR processing (ref. 59) are indicated in the literature. However, it is recommended that conservative estimates of life improvements be considered, such as a factor of 3 for CVM processing and a factor of 10 for VIM-VAR processing. Although these levels may be somewhat conservative, the confidence factor for achieving this level of improvement is high. Consequently the extra margin of reliability desired in critical gear applications will be inherent in the life calculations. Data available on other melting techniques such as vacuum induction, vacuum degassing, and electroslag remelting indicate that the life improvement approaches or equals that with the CVM process. However, it is also important to differentiate between CVM (consumable-electrode vacuum melting) and CVD (carbon vacuum degassing). The CVM process yields cleaner and more homogeneous steels than CVD.

Heat treatment.—Gears are heat treated by furnace hardening, carburizing, induction hardening, or flame hardening (ref. 14). Gears are case hardened, through hardened, nitrided, or precipitation hardened for the proper combination of toughness and tooth hardness. Using high-hardness, heat-treated steels permits smaller gears for a given load. Also, hardening can significantly increase service life without increasing size or weight. But the gear must have at least the accuracies associated with softer gears and, for maximum service life, even greater precision.

Heat treatment distortion must be minimized for longer service life. Several hardening techniques have proven useful. For moderate service life increases the gears are hardened but kept within the range of machinability so that distortion produced by heat treating can be machined away. Where maximum durability is required, surface hardening is necessary.

Carburizing, nitriding, and induction hardening are generally used. However, precision gearing (quality 10 or

better) can only be ensured by finishing after hardening. Full-contour induction hardening is an economical and effective method for surface-hardening gears. The extremely high but localized heat allows small sections to come to hardening temperatures while the balance of the gear dissipates heat. Thus major distortions are eliminated.

Although conventional methods such as flame hardening reduce wear by hardening the tooth flank, gear strength is not necessarily improved. In fact, stresses built up at the juncture of the hard and soft materials may actually weaken the tooth. Induction hardening provides a hardened tooth contour with a heat-treated core to increase both surface durability and tooth strength. The uniformly hardened tooth surface extends from the flank, around the tooth, to the flank. No stress concentrations are developed to impair gear life.

Nitriding is a satisfactory method of hardening small and medium-size gears. Distortion is minimal because furnace temperatures are comparatively low. The hardening pattern is uniform, but the depth of hardness is limited. Best results are achieved when special materials suited to nitriding are specified. Most gear manufacturing specifications do not designate heat treatment, but rather call for material characteristics (i.e., hardness and grain size) that are controlled by the heat treatment cycle. Hardness is the most influential heat-treatment-induced variable (refs. 60 to 62). It is recommended that Rockwell C-58 be considered the minimum hardness for critical gear applications.

A relationship has been proposed in reference 42 that approximates the effect of hardness on surface fatigue life:

$$\frac{L_2}{L_1} = e^{0.1(R_{C,2} - R_{C,1})} \tag{48}$$

where L_1 and L_2 are 10-percent fatigue lives at gear hardnesses $R_{C,1}$ and $R_{C,2}$, respectively. Although this relationship was obtained for AISI 52100, it can be extended to other steels. The life-hardness curve in figure 22 represents equation (48) with the relative life at Rockwell C-60 equal to 1.0. These hardness-temperature curves indicate the decrease in hardness with increased temperature for various initial room-temperature material hardnesses.

To use the nomograph (fig. 22), first determine the gear operating temperature and then follow a horizontal line to the appropriate room-temperature hardness curve. Next move vertically to the life-hardness curve and read the relative life at that point. See the dashed-line example for 149 °C (300 °F) operating temperature and Rockwell

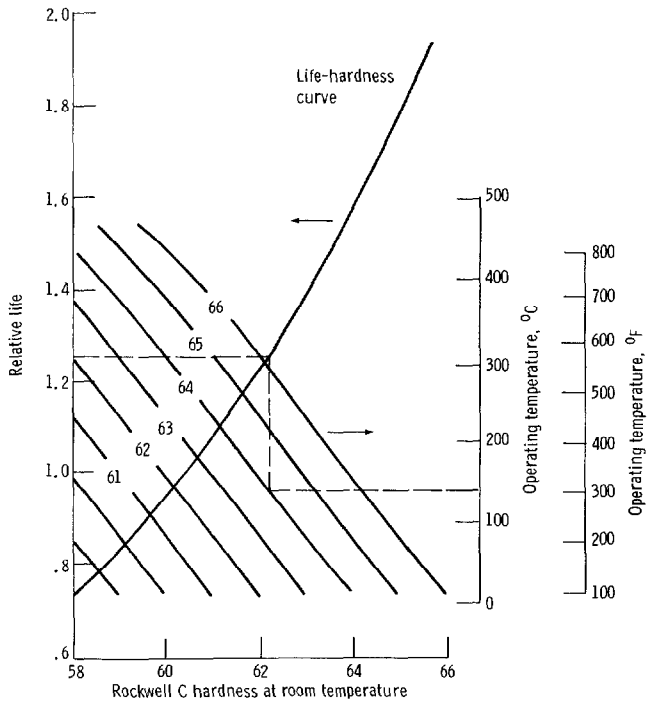

Figure 22.—Nomograph for determining relative life at operating temperature as a function of room-temperature hardness.

C-64 room-temperature hardness. Relative life for this example is approximately 1.3.

Another concept to be considered is the effect of differences in hardness between the pinion and the gear (refs. 63 and 64). Evidence exists that hardness differences between the mating components can affect system life positively by inducing compressive residual stresses during operation (ref. 64). Differential hardness ΔH is defined as the hardness of the larger of two mating gears minus the hardness of the smaller of the two. It appears that a ΔH of 2 points Rockwell C may be an optimum for maximum life. For critical applications, as a practical matter, it would be advisable to match the hardness of the mating gears to ensure a ΔH of zero and at the same time ensure that the case hardness of the gear teeth at room temperature is the maximum attainable. This will allow for maximum elevated operating temperature and maximum life. The ΔH effect has been verified experimentally for rolling-element bearings, but there is no similar published work for gears.

As previously discussed, residual stresses can be induced by the heat-treatment process, differential hardness, or shot peening. There is no analytical method to predict the amount of residual stress in the subsurface region of gear tooth contact. However, these residual stresses can be measured in test samples by x-ray diffraction methods. The effect of these residual stresses

on gear pitting fatigue life can be determined by the following equation (ref. 37):

$$\text{Life} \propto \left(\frac{1}{\tau_{\max} - \frac{S_{r,y}}{2}} \right)^9 \tag{49}$$

where

$\tau_{\max}$ maximum shear stress (45° plane)

$S_{r,y}$ measured compressive residual stress below surface at location of $\tau_{\max}$

Metalworking.—Proper grain flow or fiber orientation can significantly extend pitting fatigue life (refs. 65 and 66) and may improve the bending strength of gear teeth. Proper fiber orientation can be defined as grain flow parallel to the gear tooth shape. Standard forging of gears with integral gear teeth as opposed to machining teeth in a forged disk is one way of obtaining proper fiber orientation (ref. 46). A controlled-energy-flow forming technique (CEFF) can be used for this purpose. This is a high-velocity metalworking procedure that has been a production process for several years.

AISI M-50 steel is a through-hardened material often used for rolling-element bearings in critical applications. Test gears forged from AISI M-50 steel yielded approximately five times the fatigue life of machined vacuum-arc-remelted (VAR) AISI 9310 gears (ref. 46). Despite its excellent fatigue life AISI M-50 is not recommended for gears. Its low fracture toughness makes gears prone to sudden catastrophic tooth fracture after a surface fatigue spall has begun rather than to the gradual failure and noisy operation typical of surface pitting. It is expected that forged AISI 9310 (VAR) gears would achieve similar life improvement while retaining the greater reliability of the tougher material.

Ausforging, a thermomechanical fabrication method, has potential for improving the strength and life of gear teeth. Rolling-element tests with AISI M-50 steel (not recommended for gears—see above) show that 75- to 80-percent work (reduction of area) produces the maximum benefit (refs. 67 to 69). The suitability of candidate steels to the ausforging process must be individually evaluated. AISI 9310 is not suitable because of its austenite-to-martensite transformation characteristic. Tests reported in reference 46 found no statistically significant difference in lives of ausforged and standard forged AISI M-50 gears. The lack of improvement in the ausforged gears is attributed to the final machining required, which removes some material with preferential grain flow. Reference 46 also reports a slightly greater tendency to tooth fracture in ausforged gears. This tendency is attributed to poorer grain flow than in standard forged gears. The energy required limits the ausforging process to gears no larger than 90 mm (3.5 in) in diameter.

3.3 Manufacturing

Gears can be formed by various processes that can be classified under the general headings of milling, generating, and molding.

Milling.—Almost any tooth form can be milled. However, only spur, helical, and straight-bevel gears are usually milled. The surface finish can be held to 3.18 μm (125 μin) rms.

Generating.—In the generating process teeth are formed in a series of passes by a generating tool shaped somewhat like a mating gear. Either hobs or shapers can be used. Hobs resemble worms that have cutting edges ground into their teeth. Hobbing can produce almost any external tooth form except bevel gear teeth, which are generated with face-mill cutters, side-mill cutters, and reciprocating tools. Hobbing closely controls tooth spacing, lead, and profile. Surface finishes as fine as 1.6 μm (63 μin) rms can be obtained. Shapers are reciprocating pinion- or rack-shaped tools. They can produce external and internal spur, helical, herringbone, and face gears. Shaping is limited in the length of cut it can produce. Surface finishes as fine as 1.6 μm (63 μin) rms are possible.

Molding.—Large-volume production of gears can often be achieved by molding. Injection molding is used for light gears of thermoplastic material. Die-casting is a similar process using molten metal. Zinc, brass, aluminum, and magnesium gears are die-cast. Sintering is used in making small, heavy-duty gears for instruments and pumps; iron and brass are the materials most used. Investment casting and shell molding are used for medium-duty iron and steel gears for rough applications.

Gear finishing.—Shaving gears improves accuracy and finish while removing only a small amount of surface metal. A very hard mating gear with many small cutting edges is run with the gear to be shaved. The surface finish can be as fine as 0.81 μm (32 μin) rms.

Lapping corrects minute heat treatment distortion errors in hardened gears. The gear is run in mesh with a gear-shaped lapping tool or another mating gear. An abrasive lapping compound is used between them. Lapping improves tooth contact but does not increase the accuracy of the gear. Finish is of the order of 0.81 μm (32 μin) rms.

Grinding is the most accurate tooth-finishing process. Profiles can be controlled or altered to improve tooth contact. For example, barreling or crowning the flanks of teeth promotes good contact at the center, where the tooth is strong, and minimizes contact at the edge and corner, where the tooth is unsupported. Surface finishes as fine as 0.41 μm (16 μin) rms or better can be obtained. However, at surface finishes better than 0.41 μm (16 μin) rms, tooth errors can be induced that may affect gear tooth dynamic loading and as a result nullify the advantage of the improved surface finish.

4.0 Stresses and Deflections

There are several approaches to determining the stresses and deflections in gears. The one used most commonly for determining the bending stress and deflection is a modified form of the Lewis equation (ref. 8). This approach considers the gear tooth to be a cantilevered beam or plate. Modifying factors based on geometry or type of application are then used to amend the calculated stress and allowed design strength. It is now known that the calculated stress may not accurately represent the true stress. But since a large amount of experience has accrued across the gearing industry, data on compatible "allowed stress" have been compiled, and the modified Lewis equation is used successfully to design gears. The Lewis method should be thought of as a means of comparing a proposed new gear design for a given application with successful operation of similar designs. If the computed stress is less than the computed allowable stress, the design will be satisfactory.

The American Gear Manufacturers Association has published a standard (AGMA 218.01) (ref. 70) for calculating the bending strength of spur and helical gears, as well as many other standards for gear design and applications. A second method of calculating stresses and deflections comes from classical theory on elasticity. Several examples of such methods are found in the literature (refs. 71 to 73). The methods involve the use of complex variable theory to map the shape of the gear tooth onto a semi-infinite space in which the stress equations are solved. The methods have the advantage of computing accurate stresses in the regions of stress concentration. Although for practical use they require a computer, the computation times are fast enough that the methods can be used in everyday design. They do, however, seem limited to plane stress problems. Therefore they will not work for bevel or helical gears, where the effects of the wide teeth and distributed tooth load are important.

The most powerful method for determining accurate stress and deflection information is the finite-element method. However, the method is too expensive and cumbersome to use in an everyday design situation. Although at first the method would seem to answer all problems of computational accuracy, it does not. Research is continuing in this promising area (refs. 74 to 79). The versatility of the finite-element method introduces other questions of how best to use the method. These questions include (1) the number of elements and the most efficient arrangement of elements in the regions of stress concentrations; (2) how to represent the boundary support conditions; and (3) how to choose the aspect ratios of the solid brick element in three-dimensional stress problems. Pre- and postprocessors specifically for gears have been developed (ref. 79). Various studies have been conducted around specific questions such as the effect of rim thickness on critical stress in lightweight gears (refs. 80 and 81). It is expected that methods such as the finite-element method and the classical theory of elasticity will continue to be used in a research mode, with research results being used to supply application factors and stress-modifying factors for the modified Lewis (AGMA) method. One such approach has been suggested for the effect of the ratio of rim thickness to gear tooth height (ref. 82).

Experimental methods and testing of all proposed gear applications cannot be overemphasized. The foregoing discussion has centered around the bending fatigue strength of the gear teeth, where the failure-causing stress is at the gear tooth fillet between the tooth profile and the root of the gear. Surface pitting fatigue and scoring failures are discussed in another section and are also likely modes of failure. Experimental testing of gear prototype designs will reveal any weakness in the design that could not be anticipated by conventional design equations, such as where special geometry factors will cause the failure-causing stress to appear at locations other than the tooth fillet.[5] In critical applications such as aircraft, full-scale testing of every prototype gearbox is done in ground-based test rigs, and every piece of the flight-hardware gearbox assembly is tested in a "green run" transmission test rig as a distinct step in the production process for the completed assembly. An experimental verification of a proposed gear design is essential to a complete design process.

4.1 Lewis Equation Approach for Bending Stress Number (Modified by AGMA)

For a gear tooth loaded by the transmitted tangential load W_t, which is assumed to act at the tip of the tooth (fig. 23), the Lewis formula for the stress at the fillet

[5]Ref. 82 shows that for thin-rimmed internal gears the maximum tensile stress occurs several teeth away from the loaded tooth. Ref. 79 shows that for thin-rimmed external gears the bending stress in the root can be higher than the fillet stress. These observations emphasize the need for care in applying conventional design equations with a cavalier confidence in their universal applicability.

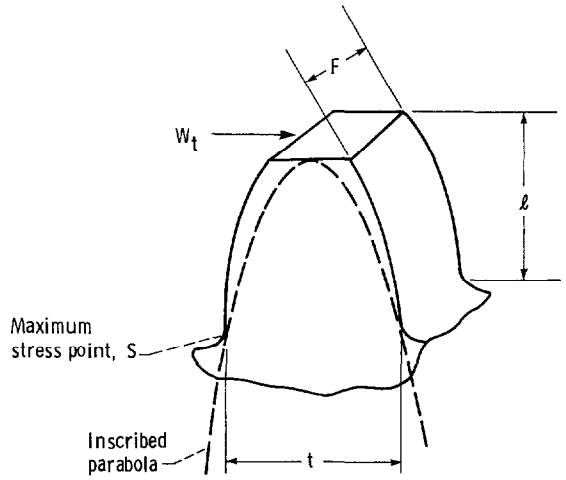

Figure 23.—Gear tooth load.

follows the simple strength-of-materials formula for bending stress in a beam:

$$S_b = \frac{Mc}{I} = \frac{(W_t l)t/2}{Ft^3/12} = \frac{6W_t l}{Ft^2} \tag{50}$$

The values for the tooth thickness at the critical section and the beam length are obtained from inscribing a parabola inside the tooth, tangent to the fillet, with the apex at the point of load application. The procedure is based a parabolic-shaped beam being a beam of constant bending stress.

For a family of geometrically similar tooth forms a dimensionless tooth form factor Y is defined as follows:

$$Y = \frac{t^2 P}{6l} \tag{51}$$

where P is the diametral pitch. From the form factor the tooth bending stress is calculated by

$$S_b = \left(\frac{W_t}{F}\right)\left(\frac{P}{Y}\right) \tag{52}$$

where

W_t transmitted tangential load
F face width

The assumptions for which the preceding equation was derived are as follows:

(1) The radially directed load was neglected.

(2) Only one tooth carried the full transmitted load.

(3) There was uniform line contact between teeth, causing a uniform load distribution across the face width.

(4) The effect of stress concentration at the fillet was neglected.

A more comprehensive equation has been defined by AGMA as follows:

$$S_b = \left(\frac{W_t}{F}\right)\left(\frac{P}{J}\right)\left(\frac{K_a K_S K_m}{K_V}\right) \tag{53}$$

where

S_b bending stress, MPa (psi)
K_a application factor
K_S size factor
K_m load distribution factor
K_V dynamic load factor or velocity factor
J geometry factor

The *application factor* K_a is intended to modify the calculated stress according to the type of service the gear will see. Some of the pertinent application influences include type of load, type of prime mover, acceleration rates, vibration, shock, and momentary overloads. Application factors are established after considerable field experience has been gained with a particular type of application. The designer should establish application factors based on past experience with actual designs that have run successfully. If the designer is unable to do this, suggested factors from experience (table 8) may be used.

The *size factor* K_S reflects the influence of non-homogeneous materials. From the weakest-link theory we can expect a large section of material to be weaker than a small section because of the greater probability of the presence of a "weak" link. The size factor K_S corrects the stress calculation to account for the known fact that larger parts are more prone to fail. At present, a size factor of $K_S = 1$ is recommended for spur and helical gears by the AGMA; for bevel gears The Gleason Works recommends

TABLE 8.—SUGGESTED APPLICATION FACTORS K_a FOR SPEED-INCREASING AND -DECREASING DRIVES[a]

Power source	Load on driven machine		
	Uniform	Moderate shock	Heavy shock
	K_a		
Uniform	1.00	1.25	≥1.75
Light shock	1.25	1.50	≥2.00
Medium shock	1.50	1.75	≥2.25

[a]For speed-increasing drives of spur and bevel gears (but not helical and herringbone gears), add 0.01 (N_2/N_1), where N_1 is the number of pinion teeth and N_2 is the number of gear teeth.

$$K_S = P^{-0.25} \qquad P < 16$$
$$K_S = 0.5 \qquad P > 16 \qquad (54)$$

The *load distribution factor* K_m is intended to account for the effects of possible misalignments in the gear that will cause uneven loading and a magnification of the stress above the uniform case. If possible, the ratio of face width to pitch diameter should be kept small (<2) for less sensitivity to misalignment and uneven load distribution due to load-sensitive deflections. A second rule of thumb is to keep the face width between three and four times the circumferential pitch. Often gear teeth are crowned or edge relieved to diminish the effect of misaligned axes on tooth stresses. Normally the range of this factor is approximately 1 to 2. A factor larger than 2 should be used for gears mounted with less than full face contact. When more precision is desired and enough detail of the proposed design is in hand to make the necessary calculations, consult the AGMA standards. For most preliminary design calculations use the data in table 9 for spur and helical gears and those in figure 24 and table 10 for bevel gears.

The *dynamic load factor* K_V is intended to correct for the effects of the speed of rotation and the degree of precision on gear accuracy. A first approximation for K_V can be taken from the chart in figure 25. This chart is intended only to account for the effect of tooth inaccuracies. It should not be used for lightly loaded, lightly damped gears or for resonant conditions. If the gear system approaches torsional resonance, or if the gear blank is near resonance, computerized numerical methods such as those presented in references 83 and 84 must be used. The chart in figure 26 shows the reciprocal of the dynamic factor as a function of speed for a certain

TABLE 9.—LOAD DISTRIBUTION FACTORS K_m FOR SPUR AND HELICAL GEARS

Condition of support	Face width, F, cm (in)							
	≤5 (2)		15 (6)		23 (9)		31 (16)	
	Spur	Helical	Spur	Helical	Spur	Helical	Spur	Helical
Accurate mounting, low bearing clearances, minimum elastic deflection, precision gears	1.3	1.2	1.4	1.3	1.5	1.4	1.8	1.7
Less rigid mountings, less accurate gears, contact across full face	1.6	1.5	1.7	1.6	1.8	1.7	2.0	2.0
Accurate and mounting such that less than full face contact exists			Over 2.0					

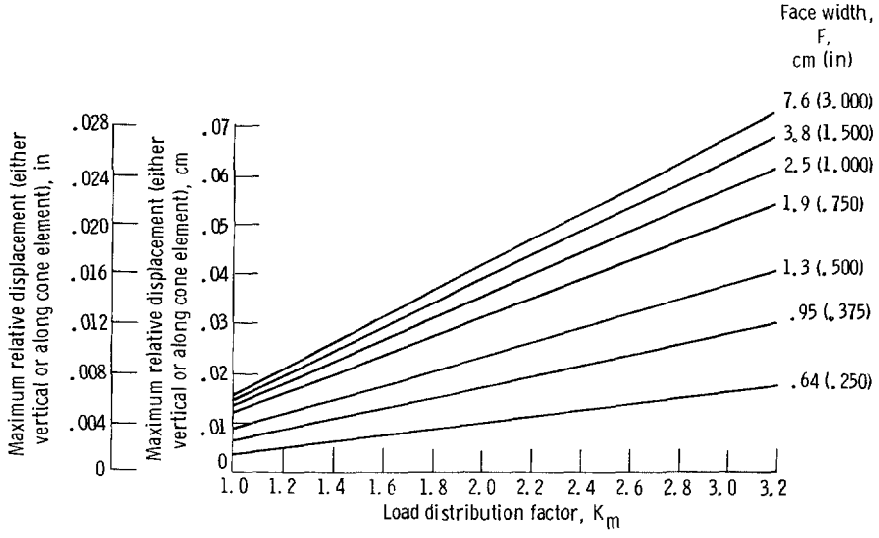

Figure 24.—Load distribution factor for bevel gears.

TABLE 10.—LOAD DISTRIBUTION FACTORS K_m FOR BEVEL GEARS

Application	Both members straddle mounted	One member straddle mounted	Neither member straddle mounted
	K_m		
General industrial	1.00 to 1.10	1.10 to 1.25	1.25 to 1.40
Automotive	1.00 to 1.10	1.10 to 1.25	----------
Aircraft	1.00 to 1.25	1.10 to 1.40	1.25 to 1.50

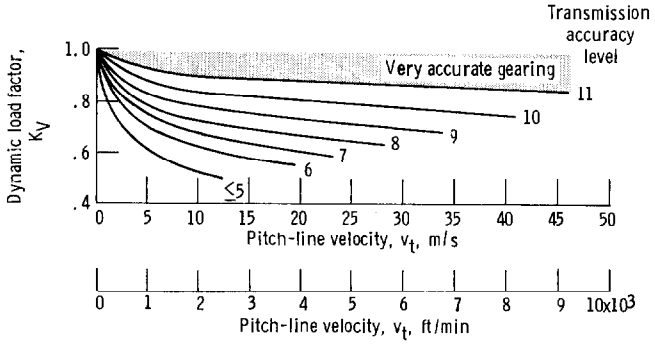

Figure 25.—Dynamic load factor. (Transmission accuracy level number specifies the AGMA class for accuracy of manufacture.)

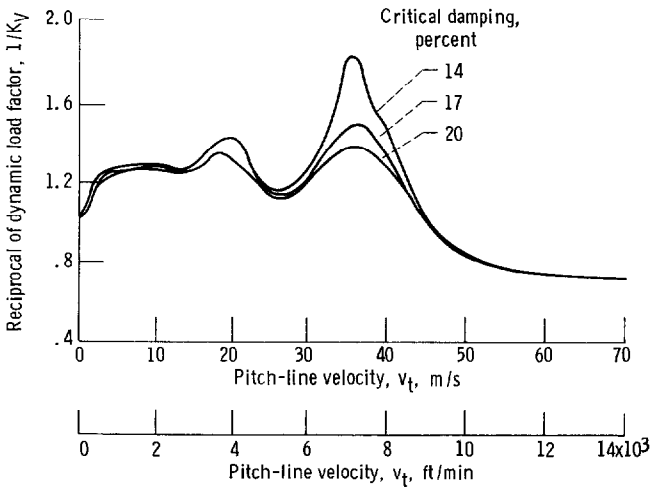

Figure 26.—Dynamic load factor as a function of damping ratio. Gear ratio, m_G, 1; number of teeth, N, 28; diametral pitch, P, 8.

specific design for three values of damping. No comprehensive data for a broad range of parameters are yet available. However, the computer programs TELSGE (Thermal Elastohydrodynamic Lubrication of Spur Gears) and GRDYNSING (Gear Dynamic Analysis for Single Mesh) are available from the NASA computer program library.[6]

[6]Available from the Computer Software Management and Information Center (COSMIC), Computing and Information Services, 112 Barrow Hall, The University of Georgia, Athens, Georgia 30602.

The *geometry factor J* is a modification of the form factor Y to account for three more influences: stress concentration, load sharing between the teeth, and changing the load application point to the highest point of single-tooth contact. The form factor Y can be found from a geometrical layout of the Lewis parabola within the gear tooth outline (fig. 23). The load-sharing ratio can be worked out by using a statistically indeterminate analysis of the pairs of teeth in contact that considers their flexibilities. Stress concentration factors from the work of Dolan and Broghammer (ref. 85) can be applied to get J. The J factors have already been computed for a wide range of standard gears and are available in the AGMA standards. For many gear applications the charts presented in figures 27 to 32 for spur, helical, and bevel gears can be used.

The transmitted tooth load W_t is equal to the torque divided by the pitch radius for spur and helical gears. For bevel gears the calculation should use the large-end pitch cone radius.

A rim thickness factor K_b that multiplies the stress computed by the AGMA formula (eq. (53)) has been proposed in reference 82. The results in figure 33 show that for thin-rimmed gears the calculated stress should be adjusted by a factor K_b if the backup ratio is less than 2. For spiral-bevel gears a stress correction factor has been

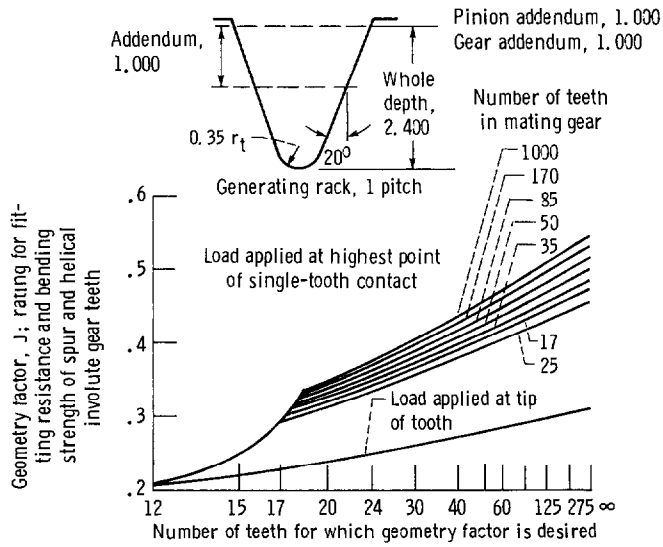

Figure 27.—Geometry factor for 20° spur gear. Standard addendum.

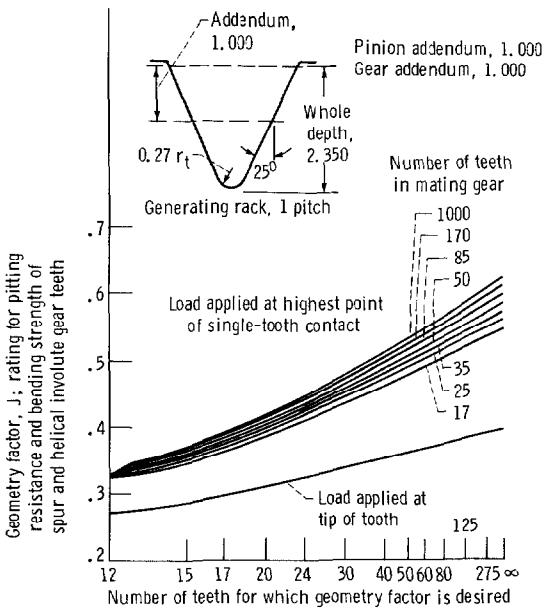

Figure 28.—Geometry factor for 25° spur gear. Standard addendum.

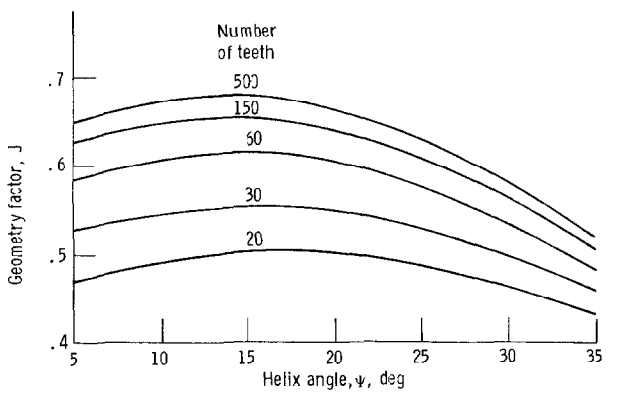

Figure 31.—Geometry factor for spiral-bevel gears with 20° pressure angle, 35° spiral angle, and 90° shaft angle.

Figure 29.—Geometry factor for 20° normal-pressure-angle helical gear. Standard addendum; full fillet hob.

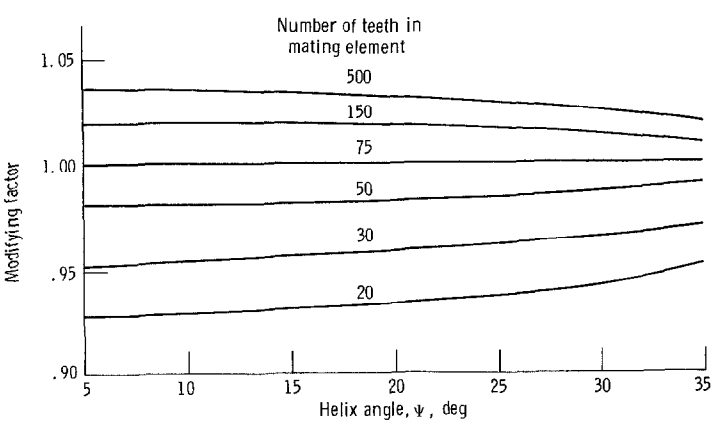

Figure 30.—Geometry factor multipliers for 20° normal-pressure-angle helical gear. (Modifying factor can be applied to J factor when other than 75 teeth are used in mating element.)

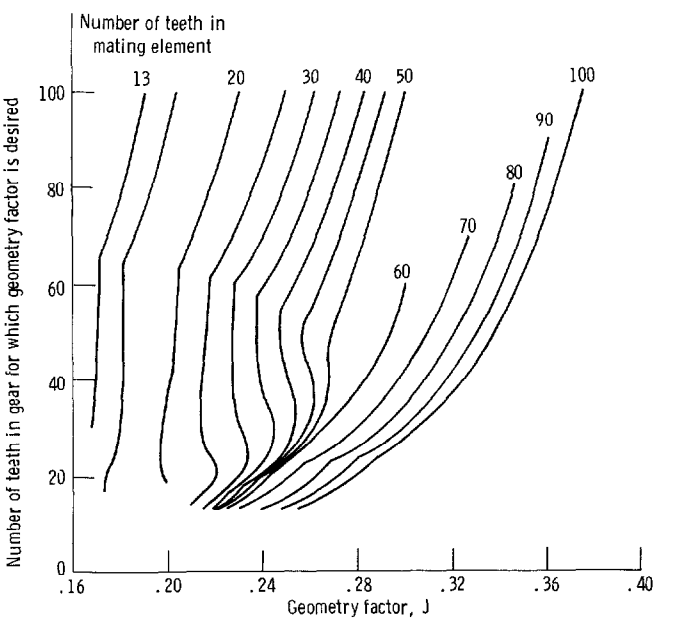

Figure 32.—Geometry factor for straight bevel gears with 20° pressure angle and 90° shaft angle.

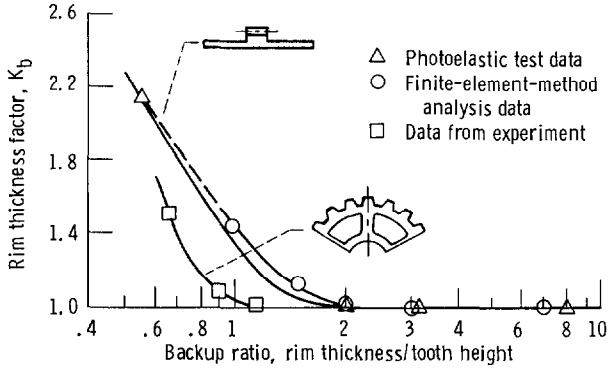

Figure 33.—Rim thickness factor.

given by Gleason to account for the effects of cutter radius curvature, which is a measure of the tooth lengthwise curvature. The Gleason equation for cutter radius factor is

$$K_X = 0.2111\left(\frac{r_c}{A}\right)^{\frac{0.2788}{\log \sin \psi}} + 0.7889 \tag{55}$$

where

A gear mean cone distance

ψ gear mean spiral angle

r_c cutter radius

Normally r_c/A ranges from 0.2 to 1 and ψ from 10° to 50°, giving a K_X range of 1 to 1.14. Recommended practice is to select the next larger nominal cutter that has a radius given by

$$r_c = 1.1\, A \sin \psi \tag{56}$$

The cutter radius factor should be entered in the denominator of the stress equation (eq. (53)).

4.2 Allowable Bending Stress Number

The previous section has presented a consistent method for calculating a bending stress index number. The stresses calculated by equation (53) may be much less than stresses measured by strain gauges or calculated by other methods such as finite-element methods. However, there is a large body of allowable stress data available in the AGMA standards that is consistent with the calculation procedure of equation (53). If the calculated stress S is less than the allowable tensile stress $S_{a,t}$ the design should be satisfactory. The equation is

$$S \leq S_{a,t}\left(\frac{K_L}{K_T K_R}\right) \tag{57}$$

where the K factors modify the allowable stress to account for the effects that alter the basic allowed stress in bending. Table 11 shows the basic allowable stress in bending fatigue for 10^7 stress cycles for single-direction bending. Use 70 percent of these values for reverse bending such as in an idler gear. If there are momentary overloads, the design should be checked against the possibility of exceeding the yield strength and causing permanent deformation of the gear teeth. For through-hardened steel the allowable yield strength is dependent on Brinell hardness H_B according to the following empirical equation:

$$S_{a,y} = (482\, H_B - 69 \text{ kPa})$$

$$= (482\, H_B - 32\,800 \text{ psi}) \tag{58}$$

The *life factor* K_L can be selected from table 12 and is used to adjust the allowable stress for the effect of designing to lives other than 10^7 stress cycles.

The *temperature factor* K_T is used to derate the strength in order to account for loss of basic material strength at high temperature. For temperatures to 121 °C (250 °F) the factor is unity. For higher temperatures strength is lost from the tempering effect, and in some materials at over 177 °C (350 °F), K_T must be greater than unity. One alternative method that is used widely is to form the K_T factor

$$K_T = \frac{460 + °\text{C}}{620} = \frac{460 + °\text{F}}{620} \tag{59}$$

where the temperature range is between 71 and 149 °C (160 and 300 °F). Operation at temperatures above 149 °C (300 °F) is normally not recommended.

The *reliability factor* K_R is used to adjust for desired reliability levels either less or greater than 99 percent, which is the level for the allowable bending strength data in table 11. If statistical data on the strength distribution of the gear material are in hand, a suitable K_R factor can be selected. In lieu of this, use the values from table 13.

4.3 Other Methods

There is no available methodology that applies to all gear types for stress and deflection analysis. However, some selected methods that have a limited application are practical for design use and for gaining some insight into the behavior of gears under load.

TABLE 11.—ALLOWABLE BENDING STRESS NUMBER $S_{a,t}$ FOR 10^7 STRESS CYCLES

Material	AGMA class	Commercial designation	Heat treatment	Minimum hardness surface	Core	Spur and helical gear		Bevel gear	
						MPa	ksi	MPa	ksi
Steel	A-1 to A-5	ASTM 100-70-03	Through hardened and tempered	180 BHN	------	173-228	25-33	97	14
				240 BHN	------	210-280	31-41	---	----
				300 BHN	------	250-320	36-47	131	19
				360 BHN	------	280-360	40-52	---	----
				400 BHN	------	290-390	42-56	---	----
			Flame- or induction-hardened section	50-54 HRC	------	310-380	45-55	---	----
				55 HRC (min)	------	------	-----	207	30
			Flame- or induction-hardened section		------	150	22	93	13.5
			Carburized and case hardened	55 HRC	------	380-450	55-65	190	27.5
				60 HRC	------	380-480	55-70	207	30
		AISI 4140	Nitrided	48 HRC	300 BHN	230-310	34-45	140	20
		AISI 4340		46 HRC	300 BHN	250-325	36-47	---	----
		Nitralloy 135M		60 HRC	300 BHN	260-330	38-48	---	----
		2.5 Percent chromium		54-60 HRC	350 BHN	380-450	55-65	---	----
Cast iron	20		As cast	--------	------	35	5	20	2.7
	30		As cast	175 BHN	------	60	8.7	32	4.6
	40		As cast	200 BHN	------	90	13	50	7.0
Nodular (ductile) iron	A-7-a	ASTM 60-40-18	Annealed	140 BHN	------	104	15	55	8.0
	A-7-c	ASTM 80-55-06	Quenched and tempered	180 BHN	------	140	20	76	11
	A-7-d	ASTM 100-70-03	Quenched and tempered	230 BHN	------	180	26	97	14
	A-7-e	ASTM 120-90-02	Quenched and tempered	270 BHN	------	207	30	130	18.5
Malleable iron (pearlitic)	A-8-c	45007	----------	165 BHN	------	70	10	---	----
	A-8-e	50005	----------	180 BHN	------	90	13	---	----
	A-8-f	53007	----------	195 BHN	------	110	16	---	----
	A-8-i	80002	----------	240 BHN	------	145	21	---	----
Bronze	Bronze 2	AGMA 2C	Sand cast	Tensile strength (min), 275 MPa (40 000 psi)	------	40	5.7	21	3
	Al/Br$_3$	ASTM B-148-52 (alloy 9C)	Heat treated	Tensile strength (min), 620 MPa (90 000 psi)	------	163	23.6	83	12

TABLE 12.—LIFE FACTOR K_l

Number of cycles	Spur, helical, and herringbone gears				Bevel gears (case carburized[a])
	160 BHN	250 BHN	450 BHN	Case carburized[a]	
	K_l				
Up to 1000	1.6	2.4	3.4	2.7	4.6
10 000	1.4	1.9	2.4	2.0	3.1
100 000	1.2	1.4	1.7	1.5	2.1
1 million	1.1	1.1	1.2	1.1	1.4
10 million	1.0	1.0	1.0	1.0	1.0
100 million and over	1.0–0.8	1.0–0.8	1.0–0.8	1.0–0.8	4.6

[a]Rockwell C-55 (min).

TABLE 13.—RELIABILITY FACTOR K_R

Requirements of application	K_R	Reliability
Fewer than one failure in 10 000	1.50	0.9999
Fewer than one failure in 1000	1.25	.999
Fewer than one failure in 100	1.00	.99
Fewer than one failure in 10	[a].85	.9

[a]At this value, plastic flow might occur rather than pitting.

A method for determining the stress in bending has been successfully applied to spur gears (ref. 86). The stress is calculated by the following equation:

$$S_t = \frac{W_N \cos \varphi'_L}{F}\left[1+0.26\left(\frac{t_s}{2r}\right)^{0.7}\right]\left[\frac{6l'_s}{t_s^2}+\left(\frac{0.72}{t_s l_s}\right)^{1/2} \times \left(1+\frac{t_L}{t_s}\nu \tan \varphi'_L\right)-\frac{\tan \varphi'_L}{t_s}\right] \quad (60)$$

where

S_t root fillet tensile stress at location indicated in fig. 34

F tooth face width measured parallel to gear axis

W_N instantaneous force that is normal to tooth surface and transmitted by tooth

ν Poisson's ratio

and the remaining quantities in equation (60) are defined in figure 34. Angle γ in figure 34 defines the area where the root fillet tensile stress is calculated by equation (60). Cornell (ref. 86) provides an equation for the value of γ that locates the position of the maximum root stress:

$$\tan \gamma_{i+1} = \frac{\left(1+0.16A_i^{0.7}\right)A_i}{B_i\left(4+0.416A_i^{0.7}\right)-\left(\frac{1}{3}+0.016A_i^{0.7}\right)A \tan \varphi'_L} \quad (61)$$

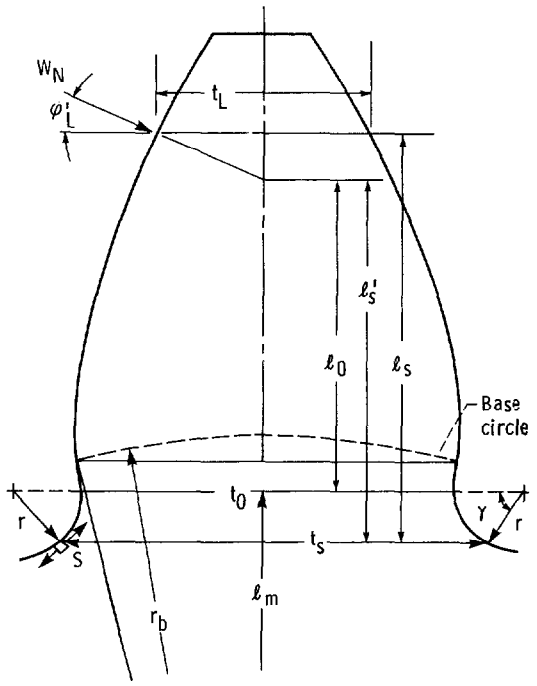

Figure 34.—Tooth geometry for evaluation of root bending stress formula parameters.

where

$$A_i = \frac{t_0}{r} + 2(1 - \cos \gamma_i) \quad (62)$$

and

$$B_i = \frac{l_0}{r} + \sin \gamma_i \quad (63)$$

where t_0 and l_0 are defined in figure 34 and subscripts i and $i+1$ denote that the transcendental equation (61) can be solved iteratively for γ, with i standing for the steps in the iteration procedure. Once the angle γ is determined, the dimension t_s shown in figure 34 also is determined by the formula

$$t_s = t_0 + 2r(1 - \cos \gamma) \quad (64)$$

Deflections of gear teeth at the load contact point are important in determining the correct amount of tip relief to minimize dynamic loads. A finite-element study has been done for a gear with a fully backed tooth (thick rim) (ref. 84). Figure 35 shows the results. The ordinate is the dimensionless deflection $\delta EF/W_N$, where δ is deflection, W_N/F is the load per unit of face width, and E is Young's modulus. The dimensionless deflection depends only on the load position and the tooth/gear blank configuration and not on the size of the gear. The loading positions are numbered 1 to 10 with the pitch point being loading

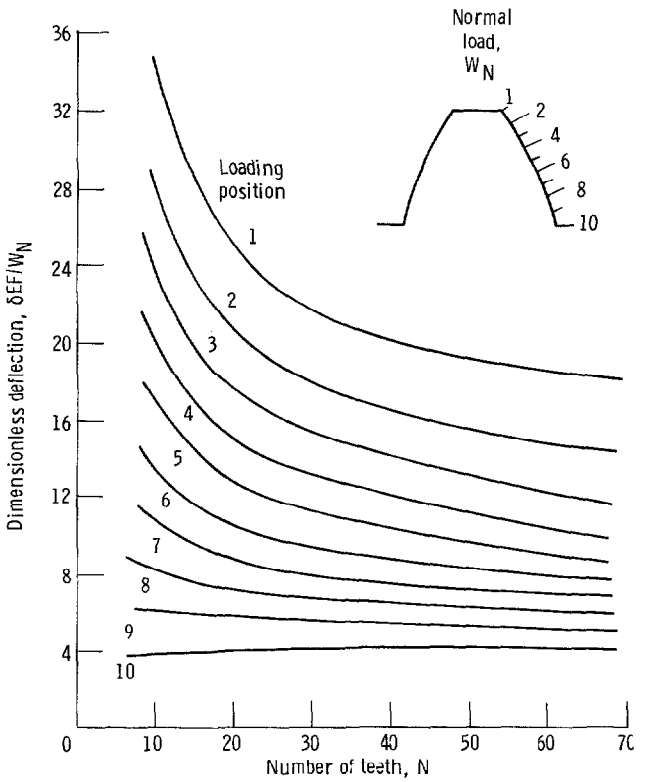

Figure 35.—Dimensionless deflection as a function of number of gear teeth and loading position.

position 5.5. These deflection values are also useful in the construction of a mathematical model of torsional vibration in the gear train.

The methods presented in reference 86 allow study of the separate effects contributing to gear tooth deflection. The method is based on beam deflection theory with corrections included to account for Hertz deflection, shear deformation, and the flexibility effects of the gear blank itself. The results of the method applied to a 8.9-cm (3.5-in) pitch diameter gear with 28 teeth, a diametral pitch of 8, a face width of 0.64 cm (0.25 in), and a solid gear blank are shown in figure 36. This figure gives an idea of the relative contributions of individual flexibility effects to the total deflection. The Hertz deflection is approximately 25 percent of the total. The gear blank deflection is approximately 40 percent. The beam bending effect of the tooth is approximately 35 percent of the total. Beam bending affects three regions: the fillet; the region of blending between the fillet and the involute profile (labeled "undercut" in fig. 36); and the tooth proper (labeled "involute" in fig. 36). Figure 36 shows deflection as a function of load position on the tooth. The discontinuities in slope are the points where the load sharing changes from single tooth-pair contact to double tooth-pair contact.

5.0 Gear Life Predictions

Gears in operation are subjected to repeated cycles of contact stress. Even if the gears are properly designed to have acceptable bending stresses for the avoidance of bending fatigue failure, there remains the likelihood of failure by surface contact fatigue. Contact fatigue is unlike bending fatigue in that there is no endurance limit for contact fatigue failure. Eventually a pit will form when the gear has been stressed by enough repeated load cycles. This section shows how to use the method that was developed at NASA for predicting the surface fatigue life of gears (refs. 87 to 91). The method is based on the assumption that pitting fatigue failures for gears and

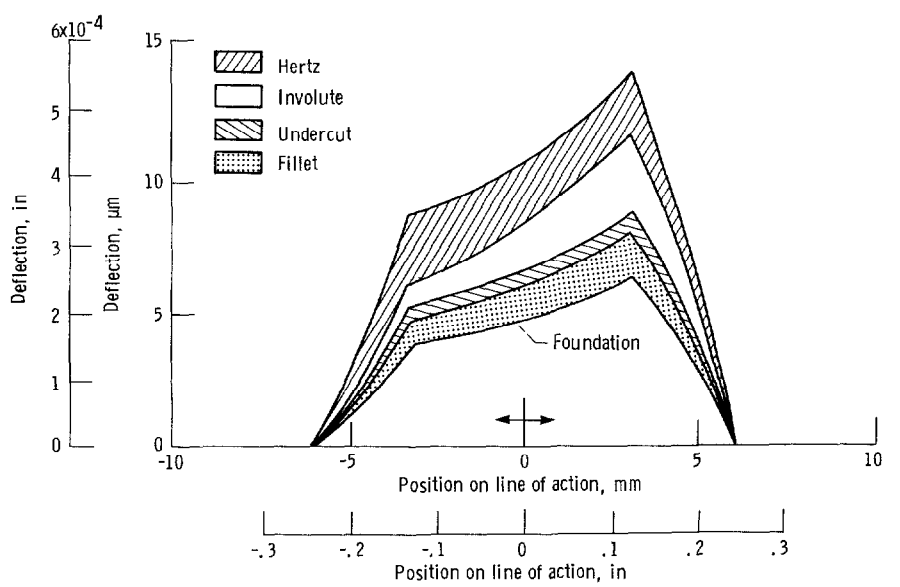

Figure 36.—Tooth deflection calculated by method of Cornell.

bearings are similar. The theoretical basis of the life prediction formulas is esplained briefly in this section.

5.1 Theory of Gear Tooth Life

The fatigue life model proposed in 1947 by Lundberg and Palmgren (ref. 92) is the commonly accepted theory for the determination of the fatigue life of rolling-element bearings. The probability of survival as a function of stress cycles is expressed as

$$\log \frac{1}{\mathrm{S}} \propto \frac{\tau_o^c \eta^e V}{z^h} \tag{65}$$

Hence, if the probability of survival S is specified, the life η in millions of stress cycles for the required reliability S can be considered a function of the stressed volume V, the maximum critical shear stress τ_o, and the depth to the critical shear stress z. As a result, the proportionality can be written as

$$\eta \propto \frac{z^{h/e}}{\tau_o^{c/e} V^{1/e}} \tag{66}$$

This formula reflects the idea that greater stress shortens life. The depth below the surface z at which the critical shear stress occurs is also a factor. A microcrack beginning at a point below the surface requires time to work its way to the surface. Therefore we expect that life varies by the power of z. The stressed volume V is also an important factor. Pitting begins near any small stress-raising imperfection in the material. The larger the stressed volume, the greater will be the likelihood of fatigue failure. By the very nature of the fatigue failure phenomenon, it is the repetitive application of stress that causes cumulative damage to the material. The greater the number of stress cycles, the greater will be the probability of failure. Experience shows that the failure distribution follows the Weibull model, with $e=2.5$ for gears. Experiments have determined that the exponents c and h equal 23.25 and 2.75, respectively. The following formulas, based on direct application of statistical fundamentals and the Hertz stress equations, enable the straightforward calculation of fatigue life for spur gears. The expression for reliability as a function of stress cycles on a single gear tooth is

$$\log \frac{1}{\mathrm{S}} = \left(\frac{\eta}{T_{10}}\right)^e \log \left(\frac{1}{0.9}\right) \tag{67}$$

where

S probability of survival

T_{10} life corresponding to a 90-percent reliability, millions of stress cycles

The dispersion or scatter parameter e (Weibull exponent) based on NASA fatigue tests is equal to 2.5. The single-tooth life T_{10} is determined from

$$T_{10} = C_{10} W_N^{-4.3} F_e^{3.9} \Sigma\rho^{-5.0} l^{-0.4} \tag{68}$$

where C_{10} is 6.44×10^9 for newtons and millimeters or 9.18×10^{18} for pounds and inches.

W_N normal load, N (lb)

F_e loaded or effective face width, mm (in)

l loaded profile length, mm (in)

$\Sigma\rho$ curvature sum, mm^{-1} (in^{-1})

The curvature sum is given by

$$\Sigma\rho = \left(\frac{1}{r_{p,1}} + \frac{1}{r_{p,2}}\right) \frac{1}{\sin\varphi} \tag{69}$$

where

$r_{p,1}$, $r_{p,2}$ pitch circle radii, m(in)

φ pressure angle, deg

The factor 9.18×10^{18} is an experimentally obtained constant based on NASA gear fatigue tests of aircraft-quality gears made of AISI 9310 (VAR) steel. If another material with a known fatigue life expectancy relative to the AISI 9310 material is selected, the life calculated by equation (68) for T_{10} should be multiplied by an appropriate factor. The relative lives for several steels based on NASA gear fatigue data (table 7) can be used as life adjustment factors. A similar treatment of life adjustment factors was made for rolling-element bearings for the effects of material, processing, and lubrication variables (ref. 93). As is always true, the designer should base his/her life calculations on experimental life data whenever possible. An alternative procedure for estimating life is given by the American Gear Manufacturers Association (AGMA) standard 218.01 (ref. 70). The method is based on allowable stress, which may be corrected for certain application and geometry effects. Because standard 218.01 is widely available, the method will not be repeated here. The AGMA method, unlike the Lundberg and Palmgren (ref. 92) approach presented herein, includes neither the stressed volume directly nor the depth to critical stress sensitivities.

Example problem.—A gear is to be made of an experimental steel that has a known life three times that of AISI 9310 (based on experimental surface fatigue results for a group of specimens). The gear has a pressure angle of 20°, a pitch of 8 (module of 3.18 mm/tooth), 28 teeth, a face width of 9.52 mm (0.375 in), and a standard addendum. The gear is to mesh with an identical gear. Determine the expected life at the 90- and 99-percent

reliability levels for a single tooth if the mesh is to carry 149 kW (200 hp) at 10 000 rpm.

Solution.—First, the necessary geometry and loading must be worked out. The pitch radius from equations (1) and (5) is

$$r_{p,1} = r_{p,2} = \frac{1}{2}(28 \text{ teeth})(3.18 \text{ mm/tooth}) = 44.5 \text{ mm}$$

$$r_{p,1} = r_{p,2} = \frac{1}{2} \times \frac{28 \text{ teeth}}{8 \text{ teeth/inch of pitch diameter}} = 1.75 \text{ in}$$

Also, the base circle radius is

$$r_{b,1} = r_{b,2} = r_p \cos \varphi = (44.5 \text{ mm}) \cos (20°)$$

$$= 41.8 \text{ mm } (1.646 \text{ in})$$

The load normal on the gear tooth surface is determined from the power. The torque is

$$T = \frac{149 \text{ kW}}{10\,000 \text{ rpm}} \times \frac{60 \text{ s}}{1 \text{ min}} \times \frac{1}{2\pi} = 142.3 \text{ N-m } (1259 \text{ lb-in})$$

The normal load is

$$W_N = \frac{T}{r_p \cos \varphi} = \frac{T}{r_b} = \frac{142.3 \text{ N-m}}{41.8 \text{ mm}} = 3.40 \text{ kN } (765 \text{ lb})$$

The standard addendum gear tooth has an addendum radius of $r_a = r_p + 1/P$ (note that $1/P$ = module). Therefore the addendum radius is 47.6 mm (1.875 in). The contact ratio is defined as the average number of tooth pairs in contact. It can be calculated by dividing the contact path length by the base pitch. The length of the contact path along the line of action from equation (8) is

$$Z = 2[(47.6 \text{ mm})^2 - (41.8 \text{ mm})^2]^{1/2} - 2(44.5 \text{ mm}) \sin (20°)$$

$$= 15.10 \text{ mm } (0.595 \text{ in})$$

The base pitch is

$$p_b = 2\pi\left(\frac{r_b}{N}\right) = 2\pi\left(\frac{41.8 \text{ mm}}{28}\right) = 9.38 \text{ mm } (0.369 \text{ in})$$

Therefore, the contact ratio is 1.61, which means that the gear mesh alternates between having one pair of teeth and two pairs of teeth in contact at any instant. Thus the load is shared for a portion of the time. Since the loading is most severe with a single pair of teeth in contact, the loaded profile length corresponds to the profile length for a single tooth-pair contact. If the contact ratio is greater than 2.0, two separate zones of double tooth-pair contact contribute to the loaded profile length. For the current example with identical gears in mesh, the pinion roll angle from the base of the involute to where the load begins (lowest point of double tooth-pair contact) is

$$\epsilon_c \frac{(r_{p,1} + r_{p,2}) \sin \varphi - (r_{a,2}^2 - r_{b,2}^2)^{1/2}}{r_{b,1}}$$

$$\epsilon_c = \frac{(44.5 \text{ mm} + 44.5 \text{ mm}) \sin 20° - [(47.6 \text{ mm})^2 - (41.8 \text{ mm})^2]^{1/2}}{41.8 \text{ mm}}$$

$$= 0.1835 \text{ rad}$$

The pinion roll angle increment for the double tooth-pair contact (light load zone) is

$$\epsilon_L = \frac{Z - p_b}{r_{b,1}} = \frac{15.10 \text{ mm} - 9.38 \text{ mm}}{41.8 \text{ mm}} = 0.1368 \text{ rad}$$

The pinion roll angle increment for single tooth-pair contact (heavy load zone) is

$$\epsilon_H = \frac{2p_b - Z}{r_{b,1}} = \frac{2(9.38 \text{ mm}) - 15.10 \text{ mm}}{41.8 \text{ mm}} = 0.0876 \text{ rad}$$

The length of involute corresponding to the single tooth-pair contact is

$$l_1 = r_{b,1}\epsilon_H\left(\epsilon_c + \epsilon_L + \frac{\epsilon_H}{2}\right)$$

$$l_1 = (41.8 \text{ mm})(0.0876)\left(0.1835 + 0.1368 + \frac{0.0876}{2}\right)$$

$$l_1 = 1.333 \text{ mm } (0.0525 \text{ in})$$

The curvature sum from equation (69) is

$$\sum \rho = \left(\frac{1}{44.5 \text{ mm}} + \frac{1}{44.5 \text{ mm}}\right) \frac{1}{\sin (20°)}$$

$$= 0.1314 \text{ mm}^{-1} \ (3.34 \text{ in}^{-1})$$

Finally the tooth life is obtained as follows from equation (68):

$$T_{10} = (6.44 \times 10^9)(3400)^{-4.3}(9.52)^{3.9} \times (0.1314)^{-5.0}(1.333)^{-0.4}$$

$$= 627 \text{ million stress cycles}$$

In hours, the life is

$$T_{10} = (627 \times 10^6 \text{ cycles})\left(\frac{1 \text{ rev}}{1 \text{ cycle}}\right) \times \left(\frac{1}{10\,000 \text{ rpm}}\right)\left(\frac{1 \text{ hr}}{60 \text{ min}}\right)$$

$$= 1045 \text{ hr}$$

Conversion to 99-percent reliability by using equation (67) yields

$$T_1 = \left[\frac{\log\left(\frac{1}{0.99}\right)}{\log\left(\frac{1}{0.90}\right)}\right]^{1/2.5} (1045 \text{ hr}) = 408 \text{ hr}$$

5.2 Gear Life

From basic probability notions the gear life is based on the survival probabilities of the individual teeth. For a simple gear with N teeth meshing with another gear the gear life corresponding to the tooth life at the same reliability level is given by the following relation:

$$G_{10} = T_{10} N^{-1/e} \text{ (simple gear)} \tag{70}$$

where

e Weibull slope (2.5)

G_{10} 10-percent gear life

T_{10} 10-percent single-tooth life as determined by previous equations

N number of teeth

When the power is transferred from an input gear to an output gear through an idler gear, both sides of the tooth are loaded once during each revolution of the idler gear. This is equivalent to a simple gear with twice the number of teeth. Therefore the life of an idler gear with N teeth is approximately

$$G_{10} = T_{10}(2N)^{-1/e} \text{ (idler gear)} \tag{71}$$

when it meshes with gears of equal face width. The life of a power-collecting (bull) gear with N teeth where there are u identical pinions transmitting equal power to the bull gear is

$$G_{10} = \frac{T_{10}}{u}(N)^{-1/e} \text{ (bull gear)} \tag{72}$$

5.3 Gear System Life

From probability theory it can be shown that the life of two gears in mesh is given by

$$L = (L_1^{-e} + L_2^{-e})^{-1/e} \tag{73}$$

where L_1 and L_2 are the gear lives. This equation can be generalized to n gears, in which case

$$L = \left(\sum_{i=1}^{n_1} L_i^{-e}\right)^{-1/e} \tag{74}$$

If the power transmission system has rolling-element bearings, the system life equations must be solved with different values for the Weibull scatter parameter or slope. For cylindrical or tapered bearings $e = 3/2$ and for ball bearings $e = 10/9$. The probability distribution for the total power transmission is obtained from the following equation (95) (ref. 94).

$$\log\left(\frac{1}{S_T}\right) = \log\left(\frac{1}{0.9}\right)\left[\left(\frac{L}{L_1}\right)^{e_1} + \left(\frac{L}{L_2}\right)^{e_2} + \left(\frac{L}{L_3}\right)^{e_3} + \ldots\right] \tag{75}$$

where L_1, L_2, L_3, etc., are the component lives corresponding to 90-percent reliability.

Example problem.—A gearbox has been designed and the component lives have been determined (table 14). Find the system life at the 95-percent reliability level.

Solution.—Iterating the following equation

$$\log\left(\frac{1}{0.95}\right) = \left(\log\frac{1}{0.9}\right) \times \left[\left(\frac{L}{1200}\right)^{10/9} + \left(\frac{L}{1500}\right)^{10/9} + \left(\frac{L}{1300}\right)^{3/2} + \left(\frac{L}{1700}\right)^{3/2} + \left(\frac{L}{1000}\right)^{2.5} + \left(\frac{L}{1900}\right)^{2.5}\right]$$

TABLE 14.—COMPONENT LIVES FOR EXAMPLE PROBLEM

Bearing	Weibull slope, e	Bearing life, B_{10}, hr	Gear	Weibull slope, e	Gear life, G_{10}, hr
1 (ball)	10/9	1200	1 (pinion)	2.5	1000
2 (ball)	10/9	1500	2 (gear)	2.5	1900
3 (roller)	3/2	1300			
4 (roller)	3/2	1700			

on a programmable calculator yields

$L = 249$ hr

for the life at the 95-percent reliability level. This result is surprisingly low and emphasizes the need for highly reliable components if the required system reliability and life are to be met.

5.4 Helical Gear Life

The calculation of helical gear teeth life is presented in this section. The approach is to think of the helical gear as a modified spur gear, with the tooth profile in the plane normal to the gear axis being preserved but with the spur tooth being sliced like a loaf of bread and wrapped around the base circle along a helix of angle Ψ. The helical tooth life can be obtained as a "corrected" spur tooth life. Adjustment factors for each of the factors that influence life in the previous equations are given as follows (ref. 88):

Load adjustment:

$$W_{\text{helical}} = \frac{W_{\text{spur}} p_b}{0.95\, Z \cos \Psi} \tag{76}$$

Curvature sum adjustment:

$$\Sigma\rho_{\text{helical}} = \left(\Sigma\rho_{\text{spur}}\right) \cos \Psi \tag{77}$$

Face-width-in-contact adjustment:

$$F_{\text{helical}} = F_{\text{spur}} \sec \Psi \tag{78}$$

No adjustment factor for involute length l is recommended. These adjustment factors are recommended for helical gears with axial contact ratios above 2. For lesser axial contact ratios the life should be calculated as if the gear were a spur gear.

Example problem.—Calculate the tooth life at 90-percent reliability level for a gear with a 3410-N (767-lb) force transmitted along the pitch line. The gear has the following properties:

Transverse pressure angle, φ_t, deg	20
Helix angle, Ψ, deg	45
Diametral pitch, P, in^{-1}	8
Module, $1/P$, mm/tooth	3.18
Number of teeth, N	28
Face width, F, mm (in)	25.4 (1.000)
Addendum	Standard
Material	AISI 9310

(The properties in the transverse plane are taken from the previous example for spur gear tooth life.)

Solution.—From the previous example problem, the transverse base pitch is 9.38 mm (0.369 in) and the length of the contact path is 15.10 mm (0.595 in). The axial pitch is calculated as follows:

$$p_a = \frac{p_b}{\tan \Psi} = \frac{9.38 \text{ mm}}{\tan 45^\circ} = 9.38 \text{ mm } (0.369 \text{ in})$$

Also the axial contact ratio can be evaluated.

$$\text{Axial contact ratio} = \frac{F \tan \Psi}{p_a}$$

$$= \frac{(25.4 \text{ mm}) \tan (45^\circ)}{9.38 \text{ mm}} = 2.71$$

Since the axial contact ratio is greater than 2, the adjustment factors in equations (76) to (78) should be used.

$$W_{\text{helical}} = \frac{(3400 \text{ N})(9.38 \text{ mm})}{0.95\,(15.10 \text{ mm}) \cos (45^\circ)} = 3.14 \text{ kN } (706 \text{ lb})$$

$$\Sigma\rho_{\text{helical}} = (0.1314 \text{ mm}^{-1}) \cos (45^\circ)$$

$$= 0.0929 \text{ mm}^{-1} \ (2.36 \text{ in}^{-1})$$

$$F_{\text{helical}} = (25.4 \text{ mm}) \sec (45^\circ) = 35.9 \text{ mm } (1.414 \text{ in})$$

These adjusted values can now be substituted into the tooth life equation (68), to determine the 90-percent life.

$$T_{10} = (6.44 \times 10^9)(3140)^{-4.3}(35.9)^{3.9} \times (0.0929)^{-5.0}(1.333)^{-0.4}$$

$$= 8.85 \times 10^{11} \text{ stress cycles}$$

In hours, the life is

$$T_{10} = (8.85 \times 10^{11} \text{ cycles})\left(\frac{1 \text{ rev}}{1 \text{ cycle}}\right) \times \left(\frac{1}{10\,000 \text{ rpm}}\right)\left(\frac{1 \text{ hr}}{60 \text{ min}}\right)$$

$$= 1.48 \times 10^6 \text{ hr}$$

5.5 Bevel and Hypoid Gear Life

For bevel and hypoid gears the contact pattern can be determined from a tooth contact analysis (TCA). The TCA is done with a computer program developed by The Gleason Works (ref. 95). The mathematics is very complicated (refs. 96 and 97), but the needed parameters

for a life analysis are simply the surface curvatures and the path of contact (from which the Hertz stress can be calculated).

Assuming that the result from a TCA analysis is available, the bevel or hypoid tooth life is calculated by the following formulas, which are adapted from reference 98. An alternative method of assessing surface durability is presented in reference 99.

$$T_{10} = \left(\frac{D_{10} Z^{7/3}}{\tau^{31/3} V} \right)^{1/2.5} \tag{79}$$

where D_{10} is 1.429×10^{35} for newtons and millimeters or 3.58×10^{56} for pounds and inches and $V = wzl$.

$$\Sigma\rho = \frac{1}{\rho_{1,x}} + \frac{1}{\rho_{2,x}} + \frac{1}{\rho_{1,y}} + \frac{1}{\rho_{2,y}} \qquad \text{curvature sum} \tag{80}$$

$$\Delta\rho = \frac{\left(\frac{1}{\rho_{1,x}} + \frac{1}{\rho_{2,x}} \right) - \left(\frac{1}{\rho_{1,y}} + \frac{1}{\rho_{2,y}} \right)}{\Sigma\rho}$$

curvature difference (81)

From table 15, get the values of a^*, b^*, and Υ

TABLE 15.—CONTACT STRESS PARAMETERS

$\Delta\rho$	a^*	b^*	Υ
0	1	1	1.2808
.1075	1.0760	.9318	1.2302
.3204	1.2623	.8114	1.1483
.4795	1.4556	.7278	1.0993
.5916	1.6440	.6687	1.0701
.6716	1.8258	.6245	1.0517
.7332	2.011	.5881	1.0389
.7948	2.265	.5480	1.0274
.83495	2.494	.5186	1.0206
.87366	2.800	.4863	1.0146
.90999	3.233	.4499	1.00946
.93657	3.738	.4166	1.00612
.95738	4.395	.3830	1.00376
.97290	5.267	.3490	1.00218
.983797	6.448	.3150	1.00119
.990902	8.062	.2814	1.000608
.995112	10.222	.2497	1.000298
.997300	12.789	.2232	1.000152
.9981847	14.839	.2070	1.000097
.9989156	17.974	.18822	1.000055
.9994785	23.55	.16442	1.000024
.9998527	37.38	.13050	1.000006
1	∞	0	1.000000

$$a = a^* \sqrt[3]{\frac{3 W_N}{2\Sigma\rho} \left(\frac{1 - \nu_1^2}{E_1} + \frac{1 - \nu_2^2}{E_2} \right)} \tag{82}$$

$$b = b^* \sqrt[3]{\frac{3 W_N}{2\Sigma\rho} \left(\frac{1 - \nu_1^2}{E_1} + \frac{1 - \nu_2^2}{E_2} \right)} \tag{83}$$

$$S_c = \frac{3 W_N}{2\pi a b} \tag{84}$$

$$\tau_o = \frac{(2\Upsilon - 1) S_c}{2\Upsilon(\Upsilon + 1)} \tag{85}$$

$$z = \frac{b}{(\Upsilon + 1)(2\Upsilon - 1)^{1/2}} \tag{86}$$

Example problem.—A TCA study showed the contact path on the bevel pinion to be approximately 7.6 mm (0.3 in) in length. At the central point of the contact path the principal radii of curvature are as follows (concave negative):

Pinion	Gear
$\rho_{1,x} = 50.8$ mm (2.00 in)	$\rho_{2,x} = \infty$
$\rho_{1,y} = 101.6$ mm (4.00 in)	$\rho_{2,y} = -127.0$ mm (-5.00 in)

The load normal to the tooth surface is 3.11 kN (700 lb). Estimate the tooth life for the pinion.

Solution.—First, using equation (80), calculate the curvature sum.

$$\Sigma\rho = \frac{1}{50.8\,\text{mm}} + \frac{1}{\infty} + \frac{1}{101.6\,\text{mm}} - \frac{1}{127.0\,\text{mm}}$$

$$= 0.0217\ \text{mm}^{-1}\ (0.550\ \text{in}^{-1})$$

Next determine the nondimensional curvature difference from equation (81).

$$\Delta\rho = \frac{\left(\frac{1}{50.8\,\text{mm}} + \frac{1}{\infty} \right) - \left(\frac{1}{101.6\,\text{mm}} - \frac{1}{127.0\,\text{mm}} \right)}{0.0217\ \text{mm}^{-1}}$$

$$= 0.816$$

Using the curvature difference and interpolating from table 15 yields the following values:

$a^* = 2.386$
$b^* = 0.5325$
$\Upsilon = 1.024$

Now, determine the dimensions of the Hertz ellipse by using equations (82) and (83). Assume the material properties of steel: $E = 207$ GPa (30.0×10^6 psi); $\nu = 0.25$.

$$\left[\frac{3W_N}{2\Sigma\rho}\left(\frac{1-\nu_1^2}{E_1}+\frac{1-\nu_2^2}{E_2}\right)\right]^{1/3}$$

$$= \left[\frac{3(3110\text{ N})}{2(0.0217\text{ mm}^{-1})}(2)\left(\frac{1-0.25^2}{207\times 10^3\text{N/mm}^2}\right)\right]^{1/3}$$

$$= 1.249\text{ mm (0.0492 in)}$$

$$a = (2.386)(1.249\text{ mm}) = 2.98\text{ mm (0.1174 in)}$$

$$b = (0.5325)(1.249\text{ mm}) = 0.665\text{ mm (0.0262 in)}$$

Calculate the maximum Hertz compression stress by using equation (84).

$$S_c = \frac{3(3110\text{ N})}{2\pi(2.98\text{ mm})(0.665\text{ mm})} = 749\text{ MPa (108.7 ksi)}$$

Evaluate the maximum subsurface orthogonal reversing shear stress and the depth below the surface at which it occurs by using equations (85) and (86), respectively.

$$\tau_o = \frac{[2(1.024)-1](749\text{ MPa})}{2(1.024)[1.024+1]} = 182.8\text{ MPa (26.5 ksi)}$$

$$z = \frac{0.5325}{(1.024+1)[2(1.024)-1]^{1/2}} = 0.321\text{ mm (0.0126 in)}$$

Assume that the semiwidth of the Hertzian contact ellipse is representative of the width of the contact path across the tooth, and calculate the stressed volume as follows:

$$V = wzl \approx azl = (2.98\text{ mm})(0.321\text{ mm})(7.6\text{ mm})$$

$$= 7.27\text{ mm}^3\ (444\times 10^{-6}\text{ in}^3)$$

Finally calculate the tooth life at 90-percent reliability by using equation (79).

$$T_{10} = \left[\frac{(1.429\times 10^{35})(0.321\text{ mm})^{7/3}}{(182.8\text{ N/mm}^2)^{31/3}(7.27\text{ mm}^3)}\right]^{1/2.5}$$

$$= 8080\text{ million stress cycles}$$

6.0 Lubrication

In gear applications fluid lubrication serves four functions:

(1) It provides a separating film between rolling and sliding contacting surfaces and thus prevents wear.

(2) It acts as a coolant to maintain proper gear temperature.

(3) It protects the gear from dirt and other contaminants.

(4) It prevents corrosion of gear surfaces.

The first two lubrication functions are not necessarily separable. The degree of surface separation affects the friction mode and the magnitude of friction force. These in turn influence frictional heat generation and gear temperatures.

Until the last two decades the role of lubrication between surfaces in rolling and sliding contacts was not fully appreciated. Metal-to-metal contact was assumed to occur in all applications, with attendant required boundary lubrication. An excessive quantity of lubricant sometimes generated excessive gear tooth temperatures and caused thermal failure. The development of the elastohydrodynamic lubrication theory showed that lubricant films of thicknesses of the order of microinches and tens of microinches occur in rolling contacts. Since surface finishes are of the same order of magnitude as the lubricant film thickness, the significance of gear tooth finish to gear performance became apparent.

6.1 Lubricant Selection

The useful bulk temperature limits of several classes of fluid lubricants in an oxidative environment are given in table 16 (ref. 100). Grease lubricants are listed in table 17 (ref. 100). The heat transfer requirements of gears dictate whether a grease lubricant can be used. Grease lubrication permits the use of simplified housing and seals.

The most commonly used lubricant is mineral oil, both in liquid and grease form (table 18; ref. 100). As a liquid, mineral oil usually contains an antiwear or extreme-pressure (EP) additive, an antifoam agent, and an oxidation inhibitor. In grease the antifoam agent is not required.

Synthetic lubricants have been developed to overcome some of the harmful effects of lubricant oxidation. However, synthetic lubricants should not be selected over readily available and invariably less-expensive mineral oils if operating conditions do not require them. It is usually easier to incorporate synthetic lubricants in a new design than to convert an existing machine to their use.

TABLE 16.—LUBRICANTS

Type	Specification	Bulk temperature limit in air	
		°C	°F
Mineral oil	MIL-L-6081	93+	200+
Diester	MIL-L-7808	149+	300+
Type II ester	MIL-L-23699	218	425
Triester	MIL-L-9236B	218	425
Superrefined and synthetic mineral oils	----------	218	425
Fluorocarbon[a]	----------	288	550
Polyphenyl ether[a]	----------	315	600

[a]Not recommended for gears.

6.2 Elastohydrodynamic Film Thickness

Rolling elements, under which category gear teeth can be considered to fall, are separated by a highly compressed, extremely thin lubricant film of thickness h. Because of the presence of high pressures in the contact zone the lubrication process is accompanied by some elastic deformation of the contact surface. Accordingly this process is referred to as elastohydrodynamic (EHD) lubrication. Ertel (ref. 101) and later Grubin (ref. 102) were among the first to identify this phenomenon. Hamrock and Dowson (ref. 103) have derived a simplified approach to calculating the EHD film thickness as follows:

$$H_{\min} = 3.63\, U^{0.68} G^{0.49} W^{-0.073} (1 - e^{-0.68k}) \qquad (87)$$

In this equation the most dominant exponent occurs on the speed parameter U, and the exponent on the load parameter W is very small and negative. The materials parameter G also carries a significant exponent, although

TABLE 17.—GREASES

Type	Specification	Recommended temperature range		General composition
		°C	°F	
Aircraft(high speed; ball and roller bearing)	MIL-G-38220	−40 to 204	−40 to 400	Thickening agent and fluorocarbon
Aircraft (synthetic; extreme pressure)	MIL-G-23827	−73 to 121	−100 to 250	Thickening agent, low-temperature synthetic oils, or mixtures of EP additive
Aircraft (synthetic; molybdenum disulfide)	MIL-G-21164	−73 to 121	−100 to 250	Similar to MIL-G-23827 plus MoS_2
Aircraft (general purpose; wide temperature range)	MIL-G-81322	−54 to 177	−65 to 350	Thickening agent and synthetic hydrocarbon
Helicopter (oscillating bearing)	MIL-G-25537	−54 to 71	−65 to 160	Thickening agent and mineral oil
Plug value (gasoline and oil resistant)	MIL-G-6032	0 to 95	32 to 200	Thickening agent, vegetable oils, glycerols, or polyesters
Aircraft (fuel and oil resistant)	MIL-G-27617	−1 to 204	−30 to 400	Thickening agent and fluorocarbon and fluorosilicone
Ball and roller bearing (extreme high temperature)	MIL-G-25013	−73 to 232	−100 to 450	Thickening agent and silicone fluid

TABLE 18.—MINERAL OIL CLASSIFICATION AND COMPARATIVE VISCOSITIES

Category	SAE number	ASTM grade[a]	AGMA gear oil	Temperature	
				38 °C (100 °F)	99 °C (210 °F)
				Approximate viscosity, cS	
------	----	32	----	2	----
	----	40	----	3-5.5	----
	----	60	----	8.5-12	----
	----	75	----	12-16	----
	----	105	----	19-24	----
	----	150	----	29-35	----
Extra light	----	215	----	42-51	----
	10W	----	1	45	4.2
	----	315	----	61-75	----
Light	20W	----	2	69	5.7
	----	465	----	90-110	----
Medium	30W	----	----	------	10
	----	----	3	128	----
	----	700	----	130-166	----
Medium heavy	40	----	----	------	13
	----	----	4	183	----
Heavy	50	----	----	------	17
	----	1000	----	194-237	18
	----	----	5	------	----
	----	1500	----	291-356	----
	----	2150	----	417-525	----
	----	----	6	------	24
	140	----	----	------	25
	----	3150	----	630-780	----
Super heavy	----	----	[b]7	------	29
	----	4650	----	910-1120	----
	----	----	[b]8	------	36
	250	----	----	------	43
	----	----	[b]8A	------	47
	----	7000	----	1370-1670	----
	----	----	9	------	97
	----	----	10	------	227
	----	----	11	------	464

[a]Grade number is equivalent to average Saybolt Universal Viscosity (SUS) at 38 °C (100 °F).
[b]Compounded with fatty oil.

the range of this variable in engineering situations is limited.

The variables related in equation (87) are from five dimensionless groupings:

Dimensionless film thickness $H = h/\rho_x$ (88)

Ellipticity parameter $k = (\rho_y/\rho_x)^{2/\pi}$ (89)

Dimensionless load parameter $W = W_N/E'\rho_x^2$ (90)

Dimensionless speed parameter $U = \mu_0 v/E'\rho_x$ (91)

Dimensionless materials parameter $G = \alpha E'$ (92)

where

E' effective elastic modulus, Pa (psi)
W_N normal applied load, N (lb)
h film thickness, m (in)
ρ_x effective radius of curvature in x (motion) direction, m (in)
ρ_y effective radius of curvature in y (transverse) direction, m (in)

v mean surface velocity in x direction, m/s (in/s)

α pressure-viscosity coefficient of fluid, m^2/N (in^2/lb)

μ_0 atmospheric viscosity, N s/m^2 (lb s/in^2)

and

$$E' = \frac{2}{\frac{1-\nu_1^2}{E_1} + \frac{1-\nu_2^2}{E_2}} \tag{93}$$

$$\frac{1}{\rho_x} = \frac{1}{\rho_{1,x}} + \frac{1}{\rho_{2,x}}$$

$$\frac{1}{\rho_y} = \frac{1}{\rho_{1,y}} + \frac{1}{\rho_{2,y}} \tag{94}$$

where

E_1, E_2 elastic modulus of bodies 1 and 2

ν_1, ν_2 Poisson's ratio of bodies 1 and 2

$\rho_{1,x}, \rho_{2,x}$ radius in x (motion) direction of bodies 1 and 2

$\rho_{1,y}, \rho_{2,y}$ radius in y (transverse) direction of bodies 1 and 2

For typical steels E' is 227.5 GPa (33×10^6 psi), and for mineral oils a typical value of α is 2.2 m^2/N (1.5×10^{-4} in^2/lb). Thus for mineral-oil-lubricated rolling elements, $G = 5000$.

For bodies in sliding or rolling contact with parallel axes of rotation, the tangential surface velocities are

$$v_1 = \omega_1 r_{1,x}$$

$$v_2 = \omega_2 r_{2,x} \tag{95}$$

where $r_{1,x}$ and $r_{2,x}$ are the radii from the centers of rotation to the contact point.

The geometry of an involute gear contact at distance s along the line of action from the pitch point can be represented by two cylinders rotating at the angular velocity of the respective gears. The distance s is positive when measured toward the pinion (member 1). Equivalent radius, from equation (94), is

$$\rho_x = \frac{(r_{p,1} \sin \varphi - s)(r_{p,2} \sin \varphi + s)}{(r_{p,1} + r_{p,2}) \sin \varphi} \tag{96}$$

Contact speeds from equation (87) are

$$v_1 = \omega_1 (r_{p,1} \sin \varphi - s)$$

$$v_2 = \varphi_2 (r_{p,2} \sin \varphi + s) \tag{97}$$

Surface topography is important to the EHD lubrication process. EHD theory is based on the assumption of perfectly smooth surfaces, that is, no interaction of surface asperities. Actually, of course, this is not the case. An EHD film of several millionths of an inch can be considered adequate for highly loaded rolling elements in a high-temperature environment. However, the calculated film might be less than the combined surface roughness of the contacting elements. If this condition exists, surface asperity contact, surface distress (in the form of surface glazing and pitting), and surface smearing or deformation can occur. Extended operation under these conditions can result in high wear, excessive vibration, and seizure of mating components. A surface roughness criterion for determining the extent of asperity contact is based on the ratio of film thickness to a composite surface roughness. The film parameter Λ is

$$\Lambda = \frac{h}{\sigma} \tag{98}$$

where composite roughness σ is

$$\sigma = \left(\sigma_1^2 + \sigma_2^2\right)^{1/2} \tag{99}$$

and σ_1 and σ_2 are the rms roughness of the two surfaces in contact. The film parameter Λ can be used as an indicator of relative life (fig. 37). Although the curve has been prepared by using the rms estimate, an arithmetic average might be used. The Λ ratio can also be used as an indicator of gear performance. At $\Lambda < 1$, surface scoring, smearing, or deformation, accompanied by wear, will occur on the gear surface. When $1 < \Lambda < 1.5$, surface distress and superficial surface pitting can occur. For $1.5 < \Lambda < 3$ some surface glazing can occur and eventually the gear will fail by classical subsurface-originated rolling-element (pitting) fatigue. At $\Lambda \geq 3$ minimal wear and extremely long life can be expected.

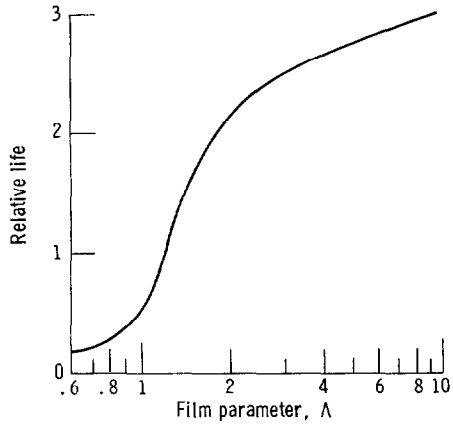

Figure 37.—Relative life as a function of film parameter.

Failure will eventually be by classical subsurface-originated rolling-element (pitting) fatigue (ref. 93).

6.3 Boundary Lubrication

Extreme-pressure lubricants can significantly increase the load-carrying capacity of gears. The extreme-pressure additives in the lubricating fluid form a film on the surfaces by a chemical reaction, adsorption, or chemisorption. These boundary films can be thinner than 0.025 μm (1 μin) or several microinches thick (ref. 104). These films are formed from the chemical reaction of sulfur (ref. 105) or from the chemisorption of iron stearate. Film thickness varies for various types of film (fig. 38, ref. 104). The films can separate the metal surfaces when the lubricant becomes thin enough for the asperities to interact. The boundary film probably lubricates by microasperity-elastohydrodynamic lubrication (ref. 104), where the asperities deform under the load. The boundary film prevents contact of the asperities and at the same time provides low-shear-strength properties that prevent shearing of the metal and reduce the friction coefficient below that of the base metal. These boundary films provide lubrication at different temperature conditions depending on the materials used. For example, some boundary films will melt at a lower temperature than others (ref. 105) and will then fail to protect the surfaces. The "failure temperature" is the temperature at which the lubricant film fails. In extreme-pressure lubrication this failure temperature is the temperature at which the boundary film melts.

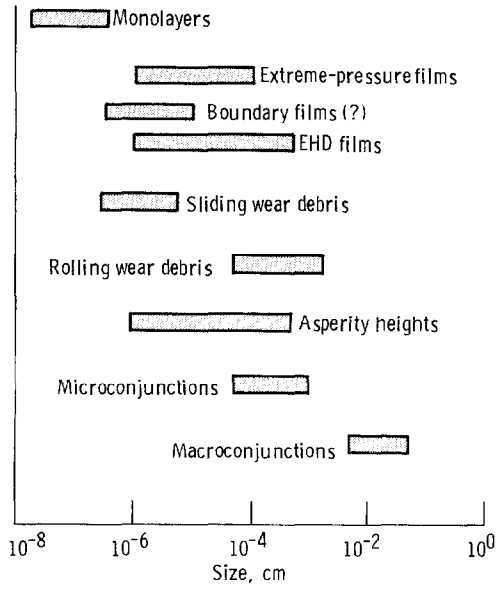

Figure 38.—Range of film thickness for various types of lubricant film, with relation to surface roughness and wear.

The melting point or thermal stability of surface films appears to be a unifying physical property governing failure temperature for a wide range of materials (ref. 105). It is based on the observation (ref. 106) that only a solid film can properly interfere with potential asperity contacts. For this reason many extreme-pressure lubricants contain more than one chemical for protection over a wide temperature range. For instance, Borsoff (refs. 107 and 108) found that phosphorous compounds are superior to chlorine and sulfur at slow speeds, but sulfur is superior at high speeds. He explains this as a result of the increased surface temperature at the higher speeds. (Most extreme-pressure additives are chemically reactive and increase their chemical activity as temperature is increased.) Horlick (ref. 109) found that some metals such as zinc and copper have to be removed from lubrication systems when using certain extreme-pressure additives.

6.4 Lubricant Additive Selection

Some of the extreme-pressure additives commonly used for gear oils contain one or more compounds of chlorine, phosphorus, or sulfur or lead soaps (ref. 110). Many chlorine-containing compounds have been suggested as extreme-pressure additives, but few have been used. Some lubricants are made with chlorine-containing molecules where the Cl_3–C linkage is used. For example, either tri (trichloroethyl) or tri (trichlortert butyl) phosphate additives have shown high load-carrying capacity. Other chlorine-containing additives are chlorinated paraffin or petroleum waxes and hexachlorethene.

The phosphorus-containing compounds are perhaps the most commonly used additives for gear oils. Some aircraft lubricants have 3 to 5 percent tricresyl phosphate or tributyl phosphite as either an extreme-pressure or antiwear agent. Other phosphorus-containing extreme-pressure agents used in percentages of 0.1 to 2.0 could be dodecyl dihydrogen phosphate, diethyl-, dibutyl-, or dicresyl-phenyl trichloroethyl phosphite and a phosphate ester containing a pentachlorphenyl radical. Most of the phosphorous compounds in gear oils also have other active elements.

The sulfur-containing extreme-pressure additives are believed to form iron sulfide films that prevent wear at high loads and speeds. However, they give higher friction coefficients and are therefore usually supplemented by other boundary-film-forming ingredients that reduce friction. The sulfur compounds should have controlled chemical activity (e.g., oils containing dibenzyl disulfide of 0.1 or more percent). Other sulfur-containing extreme-pressure additives are diamyl disulfide, dilauryl disulfide,

sulfurized oleic acid and sperm oil mixtures, and dibutylxanthic acid disulfide.

Lead soaps have been used in lubricants for many years. They resist the wiping and sliding action in gears and help prevent corrosion of steel in the presence of water. Some of the lead soaps used in lubricants are lead oleate, lead fishate, lead-12-hydroxystearate, and lead naphthenate. Lead naphthenate is used most often used because of its solubility. Lead soaps are used in concentrations of 5 to 30 percent.

Other additive compounds contain combinations of these elements. Most extreme-pressure lubricants contain more than one extreme-pressure additive. Needless to say, the selection of a proper extreme-pressure additive is a complicated process. The word "susceptibility" is frequently used with reference to additives in oils to indicate the ability of the oil to accept the additive without deleterious effects. Such properties as solubility, volatility, stability, compatibility, load-carrying capacity, and cost must be considered. Many gear oil compounds depend on the use of proprietary, or package, extreme-pressure additives. As a result, the lubricant manufacturer does not evaluate the additives' effectiveness. Because of this, any selection of extreme-pressure additives should be supported by an evaluation program to determine their effectiveness for a given application. However, a few firms have considerable background in the manufacture and use of extreme-pressure additives for gear lubrication, and their recommendations are usually accepted without question by users of gear oils.

6.5 Jet Lubrication

For most noncritical gear applications where cooling the gear teeth is not an important criterion, splash or mist lubrication is more than adequate to provide acceptable lubrication. However, in critical applications such as helicopter transmission systems and turboprop aircraft gearboxes, heat rejection becomes important. Hence jet lubrication is used. It is important to have the oil penetrate into the dedendum region of the gear teeth in order to provide cooling and lubrication. Failure to do so can result in premature gear failure, primarily by scoring and wear. Methods of oil jet lubrication were analytically determined and experimentally verified by Akin and Townsend (refs. 111 to 117).

Out of mesh.—An analysis of out-of-mesh jet lubrication of spur gears along with experimental results is given in references 111 and 114. The analysis determined the impingement depth for both gear and pinion when the jet is pointed at the out-of-mesh location and directed at the pitch points of the gear and pinion. Figure 39 shows the oil jet as it clears the gear tooth and

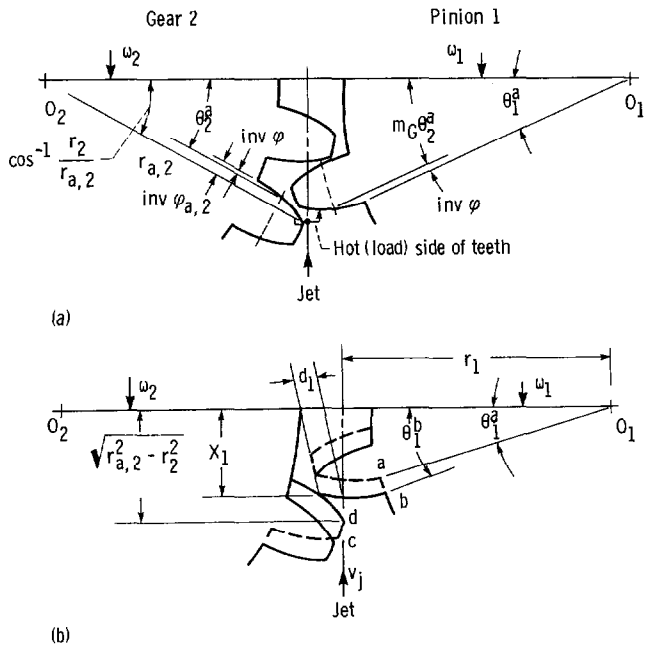

(a) Gear tooth at position where oil jet is just clearing gear tooth and begins flight toward pinion tooth. Pinion shown in position a.
(b) Moving jet from point c on gear to point d on pinion, the rotates pinion from position a to b.

Figure 39.—Model for out-of-mesh jet lubrication.

impinges on the pinion tooth and also gives the nomenclature for the equations. The time of flight for the oil jet to clear the gear tooth and impinge on the pinion tooth must equal the time of rotation of the gears and is given by the following equation:

Time of rotation = Time of flight

$$W_1^{-1}\left[\tan^{-1}\frac{x_1}{r_{p,1}} + \text{inv}\left(\frac{\cos^{-1} r_{b,1}}{(r_{p,1}^2 + x_1^2)^{1/2}}\right) - m_g \times \left(\cos^{-1}\frac{r_{p,2}}{r_{a,2}} - \text{inv}\,\varphi_{a,2} + \text{inv}\,\varphi\right) - \text{inv}\,\varphi\right] = \frac{(r_{a,2}^2 - r_{p,2}^2)^{1/2} - x_1}{v_j} \qquad (100)$$

where

$$\text{inv}\,\varphi = \tan\varphi - \varphi$$

This equation must be solved iteratively for x_1 and substituted into the following equation to determine the pinion impingement depth.

$$d_1 = r_{a,1} - \left(r_1^2 + x_1^2\right)^{1/2} \qquad (101)$$

A similar equation is used to determine the time of flight and the time of rotation of the gears for impingement on the unloaded side of the gear tooth.

$$W_2^{-1}\left(\frac{\tan^{-1}x_2}{r_2}+\text{inv}\left\{\cos^{-1}\left[r_{b,2}\left(r_{p,2}^2+x_2^2\right)^{1/2}\right]\right\}-\frac{\cos^{-1}(r_{p,y}r_{a,1})-\text{inv}\,\varphi_{a,1}+\text{inv}\,\varphi}{m_g}-\text{inv}\,\varphi\right)=\left(r_{a,1}^2-r_{p,1}^2\right)^{1/2}-\frac{x_2}{v_j} \quad (102)$$

Solving for x_2 interatively and substituting in the following equation gives the impingement depth for the gear:

$$d_2=r_{a,2}-\left(r_{p,2}^2+x_2^2\right)^{1/2} \quad (103)$$

At high gear ratios it is possible for the gear to shield the pinion entirely so that the pinion would receive no cooling unless the jet direction or position were modified. The following three tests can be used to determine the condition for zero impingement depth on the pinion, when

$$\tan^{-1}\frac{x_1}{r_1}<\cos^{-1}\frac{r_1}{r_{a,1}}$$

or

$$x_1<\left(r_{a,1}^2-r_{p,1}^2\right)^{1/2}$$

and when $d_1 \leq 0$.

The pinion tooth profile is not impinged on directly for speed reducers with ratios above 1.11 to 1.23, depending on the jet velocity ratio. Gear impingement depth is also limited by leading tooth blocking at ratios above 1.25 to 1.5.

Into mesh.—For into-mesh lubrication there is an optimum oil jet velocity to obtain best impingement depth and therefore best lubrication and cooling for the gear and pinion (refs. 116 and 117). This optimum oil jet velocity is equal to the gear and pinion pitch-line velocity. When the oil jet velocity is greater or less than the pitch-line velocity, the impingement depth will be less than optimum. Also the oil jet should be pointed at the intersections of the gear and pinion outside diameters and should intersect the pitch diameters for best results. A complete analytical treatment for into-mesh lubrication is given in references 117 and 118. Into-mesh oil jet lubrication gives much better impingement depth than out-of-mesh jet lubrication. However, in many applications, considerable power is lost from oil being trapped in the gear mesh. Radial oil jet lubrication at the out-of-mesh location gives the best efficiency, lubrication, and cooling (ref. 112).

Radial oil jet lubrication.—The vectorial model from reference 114 for impingement depth when using a radially directed oil jet is shown in figure 40. The impingement depth d can be calculated to be

$$d=\frac{1.57+2\tan\varphi+B/2}{P[nD/(2977\sqrt{\Delta p})+\tan\varphi]} \quad (104)$$

where the oil jet velocity $v_j=13\sqrt{\Delta p}$ (m/s; ft/s) and Δp is the jet pressure in pascals (psig). If the required d is known, the Δp that is required to obtain that impingement depth is

$$\Delta p=\left\{\frac{ndPD}{2977[1.57+B/2+(2-dP)\tan\varphi]}\right\}^2 \quad (105)$$

High-speed motion pictures were used to determine experimentally the impingement depth for various oil pressures and gear rotational speeds. Figure 41 is a plot of calculated and experimental impingement depth versus jet nozzle pressure for gear speeds of 2560 and 4920 rpm. At both speeds there is good agreement between the calculated and experimental impingement depths at higher pressures. However, at lower pressures, there is considerable difference between the calculated and experimental impingement depths. Most of this difference in impingement depth is due to viscous losses in the nozzle with the very viscous oil used.

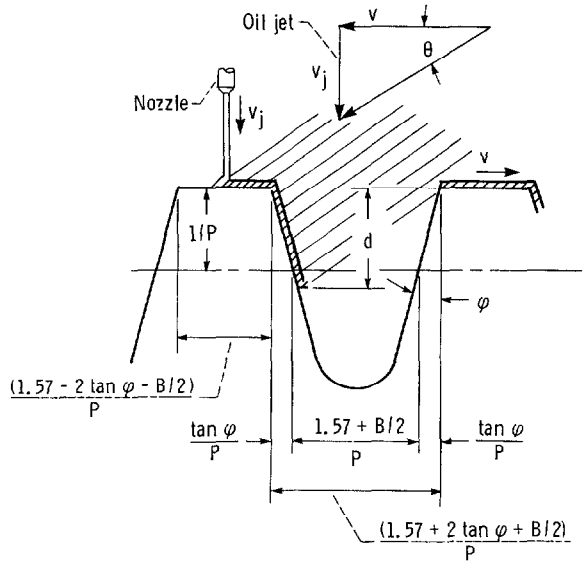

Figure 40.—Vectorial model for penetration depth.

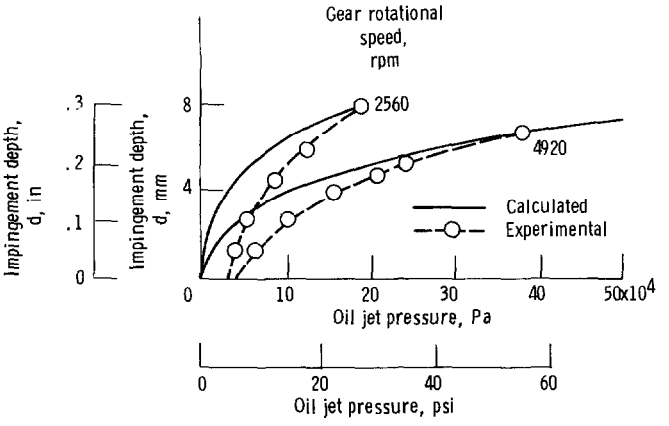

Figure 41.—Calculated and experimental impingement depth as a function of oil jet pressure at gear rotational speeds of 4920 and 2560 rpm.

6.6 Gear Tooth Temperature

A computer program to predict gear tooth temperatures was developed by using finite-element analysis (refs. 83, 84, and 118). However, this program does not include the effects of oil jet cooling and oil jet impingement depth. The program used an average surface heat transfer coefficient for surface temperature calculation that was based on the best information available at that time.

A method for predicting gear tooth temperature more accurately must be based on an analysis that allows for the use of a heat transfer coefficient for oil jet cooling coupled with a coefficient for air/oil mist cooling for that part of the time that each condition exists. Once the analysis can make use of these different coefficients, it can be combined with a method that determines the oil jet impingement depth to give a more complete gear temperature analysis program (ref. 115). However, both the oil jet and air/oil mist heat transfer coefficients are unknowns and must be determined experimentally. Once the heat generation and the oil jet impingement depth have been calculated, the heat transfer coefficients are either calculated or estimated. Then a finite-element analysis can be used to calculate the temperature profile of the gear teeth (fig. 42). The differential profiles in this figure are the temperature differences between the calculated gear tooth temperatures and the inlet cooling oil temperature. Infrared temperature measurements of the gear tooth during operation verified the accuracy of the calculated values for the gear tooth surface (refs. 112 and 115).

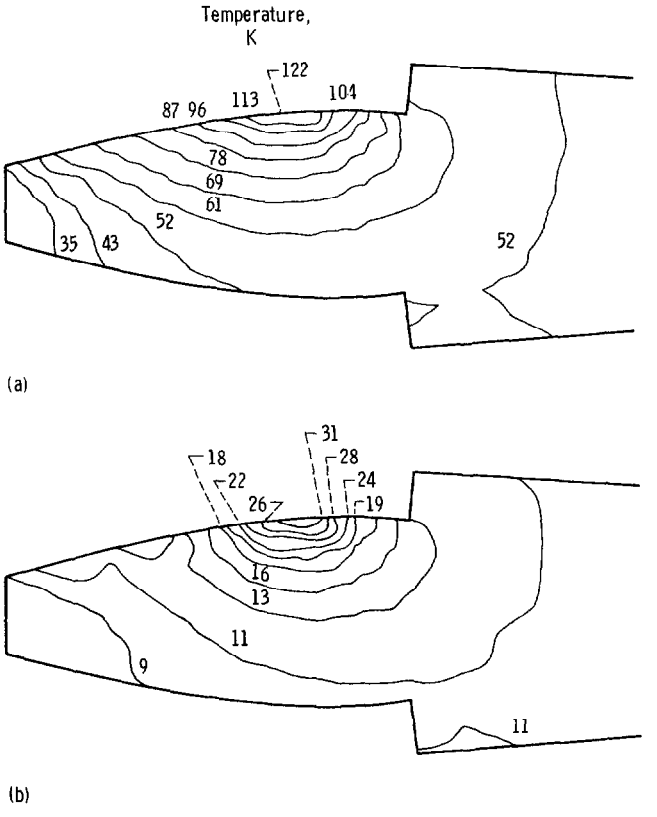

(a) Zero impingement depth.
(b) 87.5-Percent impingement depth.

Figure 42.—Calculated gear tooth temperature increase above oil inlet temperature. Gear rotational speed, 10 000 rpm; load, 5903 N/cm (3373 lb/in); pitch diameter gear, 8.9 cm (3.5 in.)

7.0 Power Loss Predictions

An experimental plot of efficiency as a function of input torque for a 236-kW (317-hp), 17-to-1 ratio helicopter transmission system comprising a spiral-bevel gear input and a three-planet system is shown in figure 43. The nominal maximum efficiency of this transmission is 98.4 percent. The power loss, 1.5 percent of 235 kW (317 hp), is highly dependent on load and almost independent of speed. Table 1 gives nominal efficiency values for various types of gear system. By multiplying the efficiency for each gear stage, the overall nominal efficiency of the gear system can be estimated. Unfortunately most transmission systems do not operate at maximum rated torque. As a result, the percentage of power loss at part load will generally be high. In addition, gear geometry can significantly influence power losses and, in turn, the efficiency of gearsets.

As an example, consider a set of spur gears with a 10-cm (4-in) pinion. A reduction in gear diametral pitch from 32 to 4 can degrade peak efficiency from 99.8 to 99.4 percent under certain operating conditions. Although this reduced efficiency may at first glance appear to be of little significance, the change does represent a 200-percent increase in power loss.

Although some analytical methods have been developed for predicting gear power losses, most of them do not conveniently account for gear mesh geometry or operating conditions. Generally these predictive

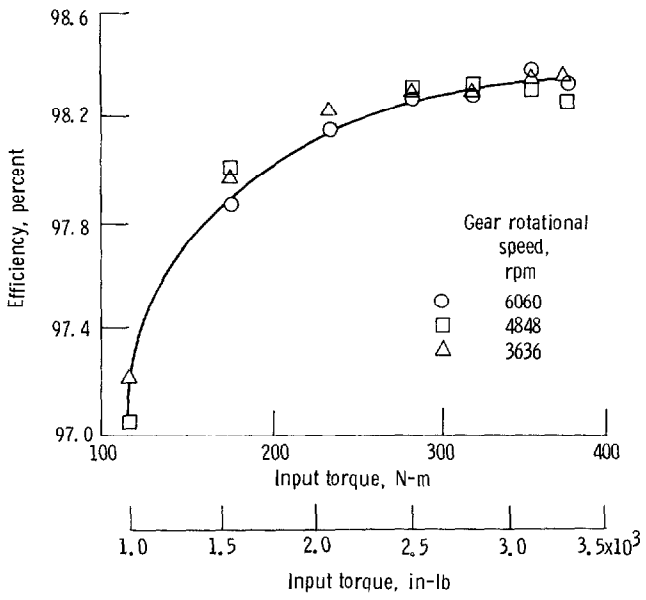

Figure 43.—Experimental efficiency as a function of input torque for three-planet (236-kW; 317-hp) helicopter transmission with spiral-bevel gear input and input-output ratio of 17.

techniques base power loss estimates on the friction coefficient at the mesh, among other parameters. Experience shows that the accuracy of these analytical tools often leaves much to be desired, especially for estimating part-load efficiency.

An evaluation of all of the power loss components as a function of torque and speed (fig. 44) shows that an unloaded gearset rotating at moderate to high speeds can account for more than half of the total power losses at full load. Although sliding loss is dominant at low operating speeds, it becomes only a moderate portion of the total gear system losses at higher speeds. Both rolling loss and support ball bearing loss increase with operating speed. Good estimates of these speed-dependent losses are vital for accurately determining the power consumption of gearboxes. Anderson and Loewenthal (refs. 119 to 122) have developed an analytical method to accurately predict power losses in spur gearsets that has been correlated with experimental data. Their method applies to spur gears that have standard tooth proportions and are jet or splash lubricated. Moreover, it considers the individual contributions of sliding, rolling, and windage to power loss at the gear mesh. Some of the power loss computations required by the method involve the use of mathematical expressions based on average operating conditions where the friction coefficient f, average sliding velocity $\bar{v}_s$, average total rolling velocity $\bar{v}_r$, and EHD film thickness $\bar{h}$ are all evaluated at the point halfway between the pitch point and the start of engagement along the line of action. The mesh losses are determined simply by summing the siding, rolling, and windage power loss components. Thus

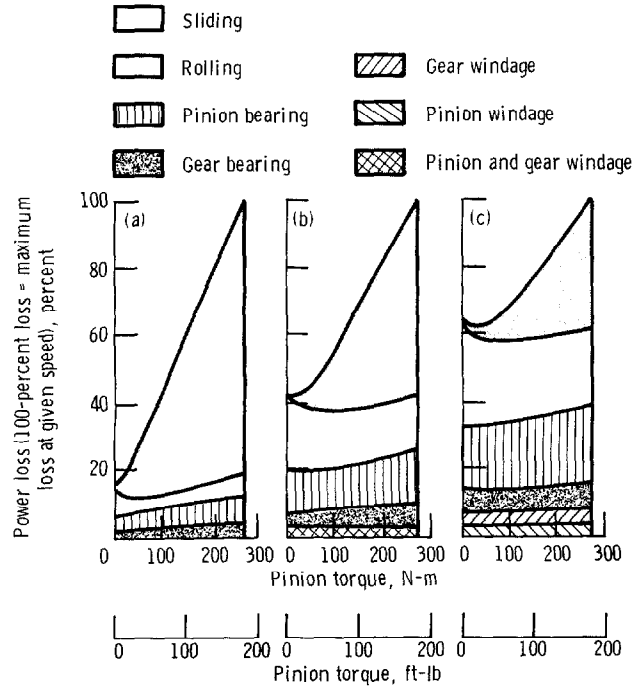

(a) Pinion speed, 250 rpm.
(b) Pinion speed, 1000 rpm.
(c) Pinion speed, 2000 rpm.

Figure 44.—Typical power loss breakdown for a gear system. Gearset parameters include pitch diameter, 15.2 cm; gear ratio, 1.66; diametral pitch, 8; ratio of pinion face width to diameter, 0.5; lubricant viscosity, 30 cP.

$$Q_m = Q_s + Q_r + Q_{w,1} + Q_{w,2} \tag{106}$$

Note that the churning loss of gears running submerged in oil is not accounted for in this analysis.

7.1 Sliding Loss

The sliding loss Q_s at the mesh results from frictional forces that develop as the teeth slide across one another. This loss can be estimated as

$$Q_s = C_1 f \bar{W}_N \bar{v}_s \tag{107}$$

where values of the constants C_1 to C_7 are given in table 19 and friction coefficient f, average normal load $\bar{W}_N$, and average sliding velocity $\bar{v}_s$ are

$$f = 0.0127 \log \left(\frac{C_6 \bar{W}_N}{F \mu \bar{v}_s \bar{v}_r^2} \right) \tag{108}$$

$$\bar{W}_N = \frac{T_1}{D_1 \cos\varphi} \tag{109}$$

TABLE 19.—CONSTANTS FOR COMPUTING GEAR MESH POWER LOSSES

Constant	Value for SI (metric) units	Value for U.S. customary units
C_1	2×10^{-3}	3.03×10^{-4}
C_2	9×10^{4}	1.970
C_3	1.16×10^{-8}	1.67×10^{-14}
C_4	0.019	2.86×10^{-9}
C_5	39.37	1.0
C_6	29.66	45.94
C_7	2.05×10^{-7}	4.34×10^{-3}

$$\bar{v}_s = \left|\underset{\sim}{\bar{v}}_2 - \underset{\sim}{\bar{v}}_1\right| \quad \text{(in the vector sense)}$$

$$= 0.0262\, n_1 \left(\frac{1+m_G}{m_G}\right) Z,\ m/s\ (ft/s) \tag{110}$$

Note that the expression for f is based on test data applied to gear sliding-loss computations involving the elastohydrodynamic (EHD) lubrication regime, where some asperity contact occurs. Such a lubrication regime generally can be considered as the common case for gearset operation. Parameter f should be limited to the range 0.01 to 0.02. For computations of $\bar{v}_s$ and f, the length of the line of action Z and the average total rolling velocity $\bar{v}_r$ are

$$Z = 0.5\left\{\left[\left(D_1 + \frac{2}{C_5 P}\right)^2 - (D_1\cos\varphi)^2\right]^{1/2} + \left[\left(D_2 + \frac{2}{C_5 P}\right)^2 - (D_2\cos\varphi)^2\right]^{1/2} - (D_1 + D_2)\sin\varphi\right\} \tag{111}$$

$$\bar{v}_r = 0.1047\, n_1\left[D_1\sin\varphi - \frac{Z_t}{4}\left(\frac{m_G - 1}{m_G}\right)\right] \tag{112}$$

7.2 Rolling Loss

Rolling loss occurs during the formation of an EHD film when oil is squeezed between the gear teeth and then pressurized. The rolling loss Q_r is a function of the EHD film thickness h and the contact ratio m_c, which denotes the average number of teeth in contact. Therefore

$$Q_r = C_2 \bar{h} \bar{v}_r F m_c \tag{113}$$

where the "central" EHD film thickness $\bar{h}$ for a typical mineral oil lubricating steel gears is

$$\bar{h} = C_7(\bar{v}_r\mu)^{0.67}\bar{W}_{\bar{N}}^{0.067}\rho_{eq}^{0.464} \tag{114}$$

and the contact ratio is

$$m_c = \frac{C_5 Z P}{\pi\cos\varphi} \tag{115}$$

The expression for $\bar{h}$ in equation (114) does not consider the thermal and starvation effects occurring at high operating speeds, generally above a pitch-line velocity of 40 m/s (8000 ft/min). These effects typically tend to constrain the film thickness to some limiting value. For computing $\bar{h}$ the equivalent-contact rolling radius is

$$\rho_{eq} = \frac{\left|D_1(\sin\varphi) + \frac{Z}{2}\right| \left|D_2(\sin\varphi) - \frac{Z}{2}\right|}{2(D_1 + D_2)\sin\varphi} \tag{116}$$

7.3 Windage Loss

In addition to sliding and rolling losses, power losses also occur from pinion and gear windage. Such losses can be estimated from expressions based on turbine-disk drag test data. Thus the pinion and gear windage losses are approximated as

$$Q_{w,1} = C_3\left(1 + 4.6\frac{F}{D_1}\right) n_1^{2.8} D_1^{4.6}(0.028\,\mu + C_4)^{0.2} \tag{117}$$

$$Q_{w,2} = C_3\left(1 + 4.6\frac{F}{D_2}\right)\left(\frac{n_2}{m_G}\right)^{2.8} \times D_2^{4.6}(0.028\,\mu + C_4)^{0.2} \tag{118}$$

These windage loss expressions apply for the air/oil atmosphere commonly found in gearboxes. The expressions assume an oil specific gravity of 0.9 and constant values for air density and viscosity at 66 °C (150 °F). To further account for the oil-rich gearbox atmosphere, both the density and viscosity of the atmosphere are corrected to reflect a 34.25-to-1 air/oil combination, which often is reported for helicopter transmissions lubricated with oil jets.

7.4 Other Losses

To determine the total gear system loss, power losses due to the support bearings should also be considered. Both hydrodynamic and rolling-element bearing losses often can equal or exceed the gear mesh losses. Bearing losses can be quantified either theoretically or by testing.

Total gear system loss is

$$Q_T = Q_m + Q_B \tag{119}$$

where

Q_m gear mesh losses

Q_B total bearing power losses

Given Q_T and input power Q_{in}, gear system efficiency in percent is predicted to be

$$\xi = \frac{Q_{in} - Q_T}{Q_{in}} \times 100 \tag{120}$$

7.5 Optimizing Efficiency

The method described for predicting spur gear power losses can also be employed in a repetitive manner for a parametric study of the various geometric and operating variables for gears. Typical results of such parametric studies are summarized by the two efficiency maps commonly called carpet plots, shown in figure 45, for light and moderate gear tooth loads. These carpet plots describe the simultaneous effects on gear mesh efficiency when the diametral pitch, pinion pitch diameter, and pitch-line velocity are varied. The computed gear mesh efficiencies do not include support-bearing losses.

In these carpet plots the three key variables are represented along orthogonal intersecting planes for three values of diametral pitch, pinion pitch diameter, and pitch-line velocity. The gear mesh efficiency accompanying any combination of these three gear parameters is represented by an intersecting point for the three planes. Efficiencies at intermediate values can be readily found by interpolating among the planes.

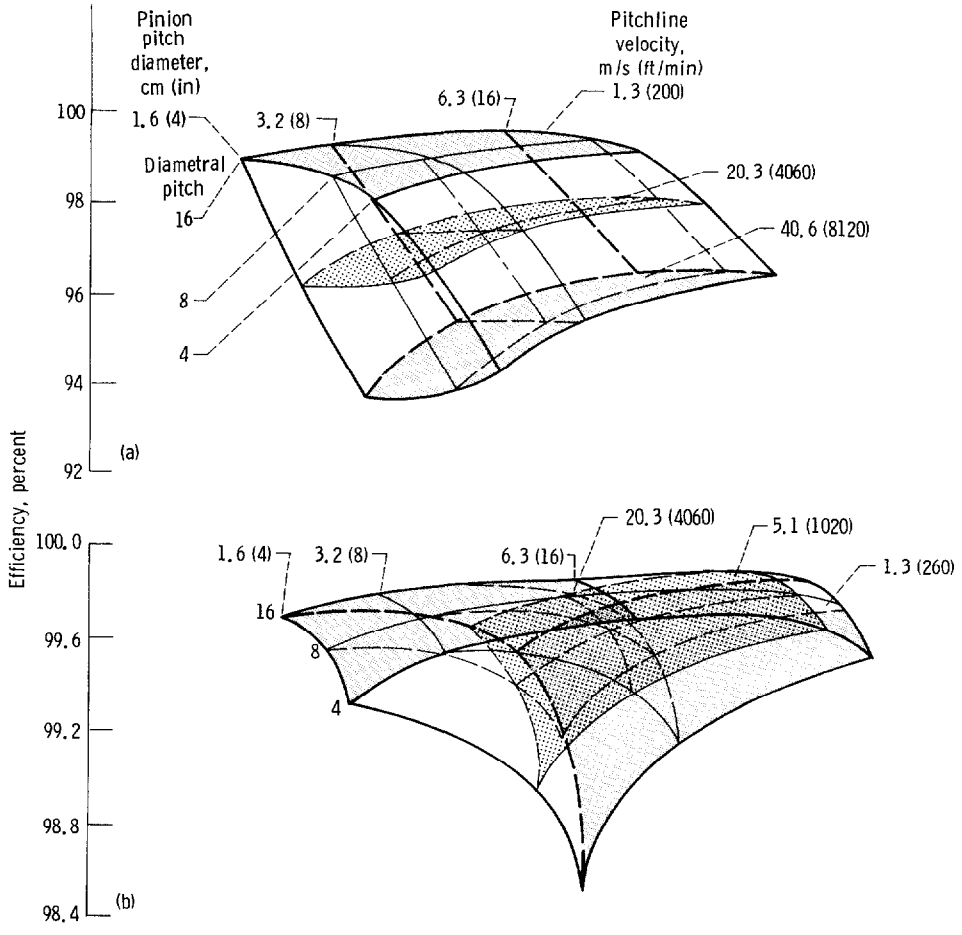

(a) Light load. $K = 70$ kPa (10 psi).
(b) Moderate load. $K = 2100$ kPa (300 psi).

Figure 45.—Parametric study for light and moderate gear loads. Gearset parameters include gear ratio, 1; ratio of pinion face width to diameter 0.5; lubricant viscosity, 30 cP.

The light and moderate spur gear loads are specified in terms of a load intensity factor, usually called a K factor. The K factor is a widely used parameter that normalizes the degree of loading on gears of different size and ratio. Essentially the K factor describes the load intensity on a gear tooth. It is evaluated as

$$K = \frac{\overline{W}_t(m_G + 1)}{FD_1 m_G} \tag{121}$$

Two carpet plots (fig. 45) were generated for light and moderate loads where K equals 69 and 2100 MPa (10 and 300 psi), respectively. Allowable K factors for spur gears generally range from about 700 MPa (100 psi) for low-hardness steel gears with generated teeth to 7000 MPa (1000 psi) for aircraft-quality, high-speed gears that are case hardened and ground. A nominal K factor for a general-purpose industrial drive with steel gears with a Brinell hardness of 300, carrying a uniform load at a pitch-line velocity of 15 m/s (3000 ft/min) or less, typically ranges from 1900 to 2200 MPa (275 to 325 psi). For light loads, increasing diametral pitch (resulting in smaller gear teeth) and decreasing pitch-line velocity tend to improve gear mesh efficiency. For moderate to heavy loads, increasing both diametral pitch and pitch-line velocity improves efficiency. The reason for this reversal in efficiency characteristics is that speed-dependent losses dominate at light loads but sliding loss is more pronounced at higher loads. Also, at higher speeds, the sliding loss is reduced because the sliding friction coefficient is lower. Essentially these two parametric studies indicate that large diameter, fine-pitch gears are most efficient when operated under appreciable load and high pitch-line velocity. Consequently, to attain best efficiency under these operating conditions, the gear geometry should be selected as noted.

8.0 Optimal Design of Spur Gear Mesh

When designing gear systems, it is cost effective to make the design efficient and long lived with a minimum weight-power ratio. This introduces the concept of optimization in the design, that is, selecting as a point of reference either minimum size (which relates also to minimum weight) or maximum strength. Although the designer is seeking to optimize some criteria index, he/she must also meet all of the basic design requirements (constraints) such as speed ratio, reliability, producibility, acceptable cost, and no failures due to wear, pitting, tooth breakage, or scoring. The design process must carefully assess all of the possible modes of failure and make adjustments in the allowable design parameters in order to achieve the optimum design. Figure 46 presents a qualitative diagram of expected

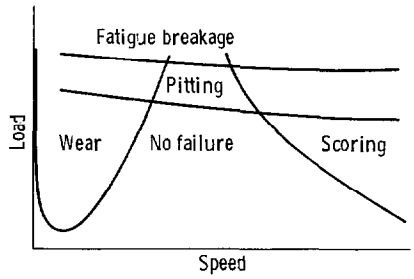

Figure 46.—Various failure regimes encountered by gear teeth.

failure modes for operation in various regimes of load and speed. The job of the designer is to anticipate the type of load and speed conditions the gears will see in service and to choose a design that will not fail and is optimum in some sense.

8.1 Minimum size

The index for optimization is often minimum size. A measure of size is center distance. A procedure for optimization based on minimum center distance has been developed (refs. 123 and 124). In the procedure the following items were the constraints: (1) an allowed maximum Hertz (normal) stress S_{max} of 1.4 GPa (200 000 psi), which affects scoring and pitting; (2) an allowed bending stess S_b of 0.4 GPa (60 000 psi), which affects tooth breakage due to fatigue; (3) a geometric constraint for no involute interference, which is contact between the teeth under the base circle or tip fouling in the case of internal gears; and (4) a ratio of tooth width to pinion pitch diameter of 0.25, which helps to keep the misalignment factor to a minimum. The results of the optimization study for a gear ratio of 1 are shown in figure 47. After all of the design parameters were considered, it was found that, for a given set of allowed stresses, gear ratios, and pressure angles, the design space could be shown on a plane, with the vertical axis being the number of teeth on the pinion and the horizontal axis being the diametral pitch. Figure 47 shows the region for designs that meet acceptable conditions, but not all of the designs resulting from those combinations of number of teeth and pitch approach a minimum-center-distance design.

The combinations of number of teeth and diametral pitch that fall on any straight line emanating from the origin will give a constant-size design. The slope of the line is directly related to the center distance. The minimum-slope line that falls into the region of acceptable designs gives the optimum choice of pitch and tooth number for an optimally small (light) design.

The data in figure 48 summarize results from a large number of plots similar to figure 47. These data can be used to select trial values of designs that can lead to optimum final designs. The value of these charts is that

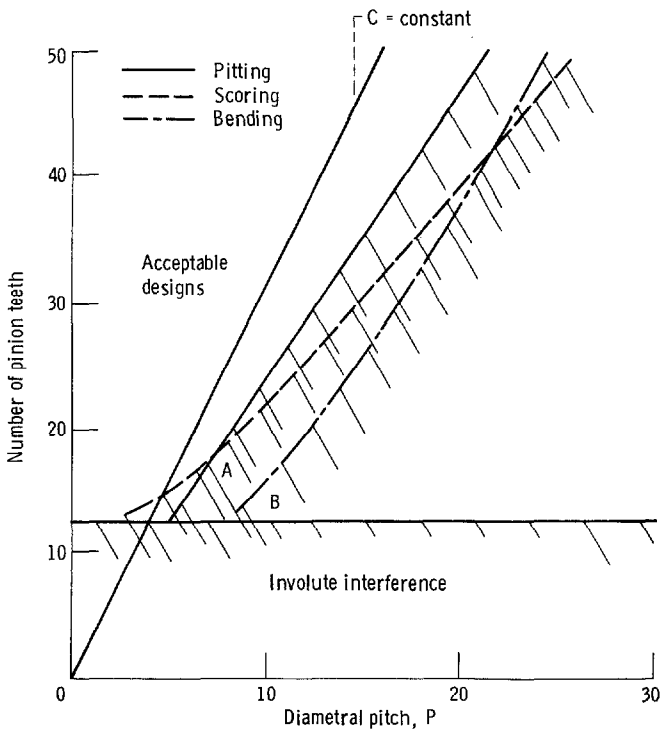

Figure 47.—External gear mesh design space. Ratio of face width to diameter of pitch circle, 0.25; pinion torque, 113 N-m (1000 in-lb); maximum Hertz stress, 1.38 GPa (200×10^3 psi); bending stress, 414 MPa (60×10^3 psi); Young modulus, 205 GPa (30×10^6 psi), Poisson's ratio, 0.25.

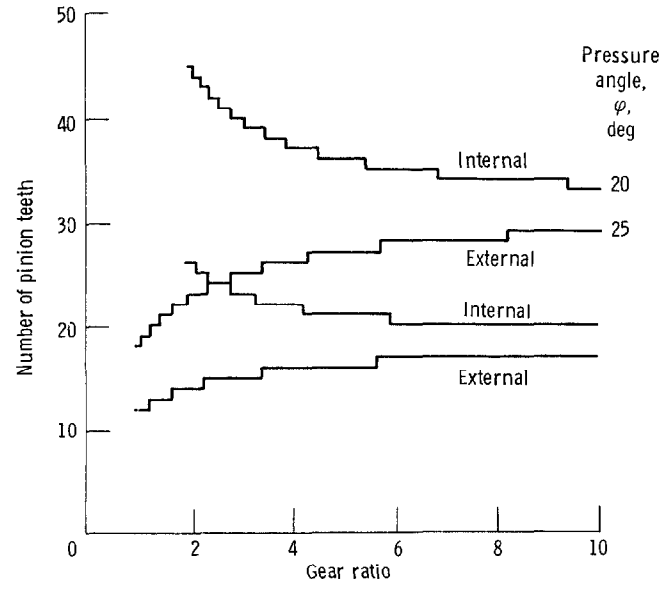

(a) Pressure angle, 20.
(b) Pressure angle, 25.

Figure 48.—Optimal number of pinion teeth.

initial designs may be quickly selected. A more detailed study of the design should then be made, using the more detailed methods for calculating bending fatigue stress, life, scoring, and efficiency previously described. Point A in figure 47 is the point nearest optimum with respect to minimum-center-distance criteria since that is the point that lies on the minimum-slope straight line through the origin and yet contains points in the regions of acceptable designs. Point B is the point that would be selected on the basis of only the bending strength criterion and kinematic conditions of no involute interference.

Hertz stress is common to both gear and pinion teeth, but the bending strength criterion was applied only to the pinion since it is the weaker element of the pinion and gear teeth.

Other approaches to optimization have included the balanced-strength approach, where the pinion was made thicker and with a shorter addendum whereas the gear was made with a longer addendum. The idea was to balance the strength of the pinion and gear teeth. In reference 125 this idea of balanced design was applied to scoring temperature index balance as well as to bending strength balance. In reference 126 long- and short-addenda gearsets were examined for their optimum tooth numbers. In reference 127 a direct-search computer algorithm was applied to the minimum-center-distance design problem.

8.2 Specific Torque Capacity

A criterion for comparing two designs has been described in the literature (ref. 21) as specific torque capacity (STC). The STC rating of a single gear is defined as the torque transmitted by that gear divided by the superficial volume of its pitch cylinder. That is, torque per unit volume is equal to

$$\frac{T}{V} = \frac{4T}{\pi D^2 F} \tag{122}$$

where

D pitch circle diameter
F face width

For a pair of gears with a ratio of 1 the same STC value attributed to each gear individually can be attributed to the pair. Thus for such a gear pair the average STC value is

$$\frac{T_1/V_1 + T_2/V_2}{2} = \frac{(4T_1/\pi D_1^2 F_1 + 4T_2/\pi D_2^2 F_2)}{2} \tag{123}$$

But if T_1 and T_2 are the torque loadings of a pinion and a wheel, $T_2 = m_G T_1$, where m_G is the gear ratio. Similarly $D_2 = m_G D_1$, but $F_2 = F_1$. Thus

$$STC_{av} = \frac{2}{\pi}\left(\frac{T_1}{D_1^2 F} + \frac{m_G^2 T_1}{m_G D_1^2 F}\right)$$

or (124)

$$STC_{av} = \left(\frac{2T_1}{\pi D_1^2 F_1}\right)\left(\frac{1+m_G}{m_G}\right)$$

But $T = W_t R/2$, where W_t is the total tangential load acting at the pitch surface. Thus

$$STC_{av} = \left(\frac{W_t}{F_1 D_1 \pi}\right)\left(\frac{1+m_G}{m_G}\right) \quad (125)$$

This expression bears a close resemblance to the AGMA K factor for contact stress, where

$$K = \left(\frac{W_t}{F_1 D_1}\right)\left(\frac{1+m_G}{m_G}\right) \quad (126)$$

Hence

$$STC_{av} = \frac{K}{\pi}$$

Thus, although K has been considered as a surface loading criterion for a gear pair, it also has a direct relationship to the basic torque capacity of a given volume of gears. It can therefore be used as a general comparator of the relative load capacity of gear pairs, without any specific association with tooth surface or root stress conditions. The STC value thus becomes a useful quantity for comparing the performance of gears that are based on completely different tooth systems, even where the factors that limit performance are not consistent.

9.0 Gear Transmission Concepts

9.1 Series Trains

Speed reducers.—The overall ratio of any reduction geartrain is the input shaft speed divided by the output speed. It is also the product of the individual ratios at each mesh, except in planetary arrangements. The ratio is most easily determined by dividing the product of the numbers of teeth of all driven gears by the product of the numbers of teeth of all driving gears. By manipulating numbers any desired ratio can be obtained, either exactly or with an extremely close approximation. In multiple-mesh series trains the forces transmitted through the gear teeth are higher at the low-speed end of the train. Therefore the pitches and face widths of the gears are usually not the same throughout the train. In instrument gears, which transmit negligible power, this variation may not be necessary (ref. 14). Table 20 gives several possible speed ratios with multiple meshes.

TABLE 20.—SPEED RATIOS WITH MULTIPLE MESHES

Type of gear	Ratios
Helical and double-helical, herringbone gears:	
Double reduction	10–75
Triple reduction	75–350
Spiral bevel (first reduction) with helical gear:	
Double reduction	9–50
Triple reduction	50–350
Worm gears (double reduction)	100–8000
Helicals with worm gears (double reduction)	50–270
Planetary gearsets:	
Simple	4–10
Compound	10–125

Speed increasers.—Speed-increasing geartrains require greater care in design, especially at high ratios. Because most gearsets and geartrains are intended for speed reduction, standards and published data in general apply to such drives. It is not safe to assume that these data can be applied without modification to a speed-increasing drive. Efficiency is sometimes lower in an increasing drive and substantial input torque is required to overcome output load; in extreme instances self-locking may occur (ref. 14). Traction and hybrid drives should be considered as reasonable alternatives to gear drives for this purpose.

Reverted trains.—When two sets of parallel-shaft gears are so arranged that the output shaft is concentric with the input, the drive is called a reverted train. The requirement of equal center distance for the two trains complicates determination of how many teeth should be

in each gear to satisfy ratio requirements with standard pitches. Helical gears provide greater design freedom through possible variation of helix angle (ref. 14).

9.2 Multispeed Gears

Sliding gears.—Speed is adjusted by sliding gears on one or more intermediate parallel shafts (fig. 49). Shifting is generally accomplished by disengaging the input shaft. Sliding-gear transmissions are usually manually shifted by means of a lever or a handwheel. A variety of shaft arrangements and mountings are available (ref. 128).

Constant mesh.—Several gears of different sizes are mounted rigidly to one shaft mesh with mating gears free to rotate on the other shaft (fig. 50). Speed is adjusted by locking different gears individually on the second shaft by means of splined clutches or sliding couplings.

Constant-mesh gears are used in numerous applications, among them heavy-duty industrial transmissions. This arrangement can use virtually any type of gearing (e.g., spur, helical, herringbone, and bevel gears). Manually shifted automotive transmissions combine two arrangements. The forward speeds are constant-mesh helical gears; the reverse speeds use sliding spur gears (ref. 129).

Idler gears.—An adjustable idler-gear speed drive consists of one shaft that carries several different-size, rigidly mounted gears (fig. 51). Speed is adjusted through an adjustable arm, which carries the idler gear, connecting with fixed or sliding gears on the other shaft.

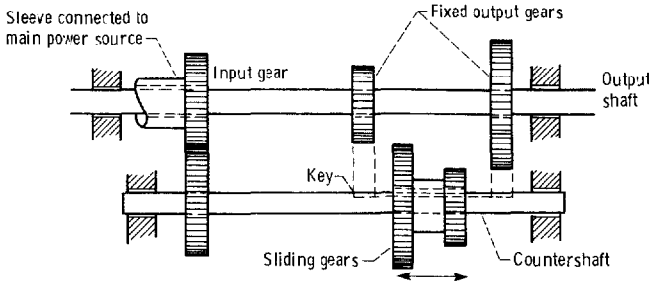

Figure 49.—Sliding gears.

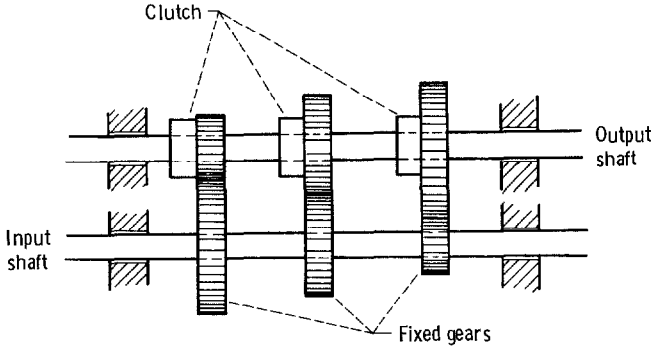

Figure 50.—Constant-mesh gears.

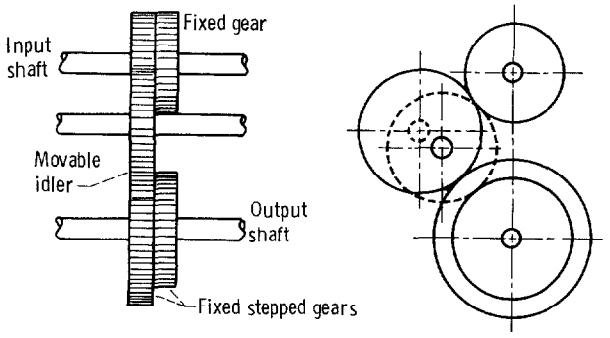

Figure 51.—Idler gear.

This arrangement is used to provide stepped speeds in small increments and is frequently found in machine tools. A transmission of this type can be connected to another multispeed train to provide an extremely wide range of speeds with constant-speed input. Shifting is usually manual. The transmission is disengaged and allowed to come to a stop before the sliding idler gear is moved to the desired setting (ref. 129).

9.3 Epicyclic Gears

An epicyclic geartrain (fig. 52) is a reverted-gear arrangement in which one or more of the gears (planets) moves around the circumference of coaxial gears that may be fixed or rotating with respect to their own axes. The planet gears have a motion consisting of rotation about their own axes and rotation about the axes of the coaxial gears (ref. 14). The arrangement shown in figure 52 consists of a central sun gear with external teeth, a ring gear with internal teeth, revolving planet pinions that engage the sun gear and the internal ring gear, and a planet carrier in which the planet pinions are supported (ref. 14). Epicyclic trains may incorporate external or internal spur or helical gears or bevel gears arranged in numerous ways for fixed-ratio or multispeed applica-

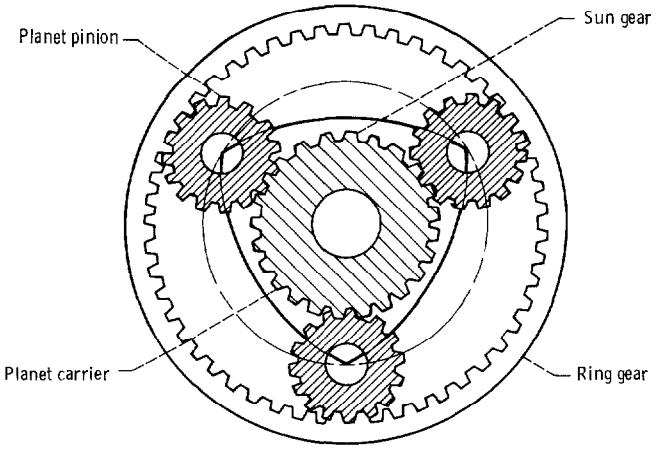

Figure 52.—Planetary gears. Epicyclic gears.

tions. A fixed-ratio, single epicyclic 373-kW (500-hp) helicopter transmission using a four-planet arrangement with a bevel gear input stage is shown in figure 53.

Epicyclic trains.—For a single epicyclic train (fig. 54(a)) the coaxial sun and ring gears are connected by a single intermediate planet gear carried by a planet carrier arm. For a compound epicyclic train (fig. 54(b)) the intermediate planet pinions are compound gears. Table 20 gives the speed ratios that can be attained.

For single planetary arrangements, to make assembly possible, $(N_R+N_S)/q$ must be a whole number, where N_R and N_S are the numbers of teeth in the ring and sun gears and q is the number of planet gears equally spaced around the sun gear (ref. 14). To make assembly possible for a compound planetary arrangement $(N_R N_{P,S} - N_S N_{P,R})/q$ must equal a whole number (ref. 14), where

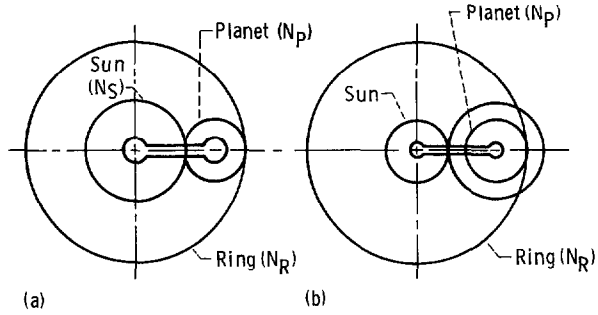

(a) Simple train.
(b) Compound train, planet gears keyed to same shaft.

Figure 54.—Epicyclic gear trains.

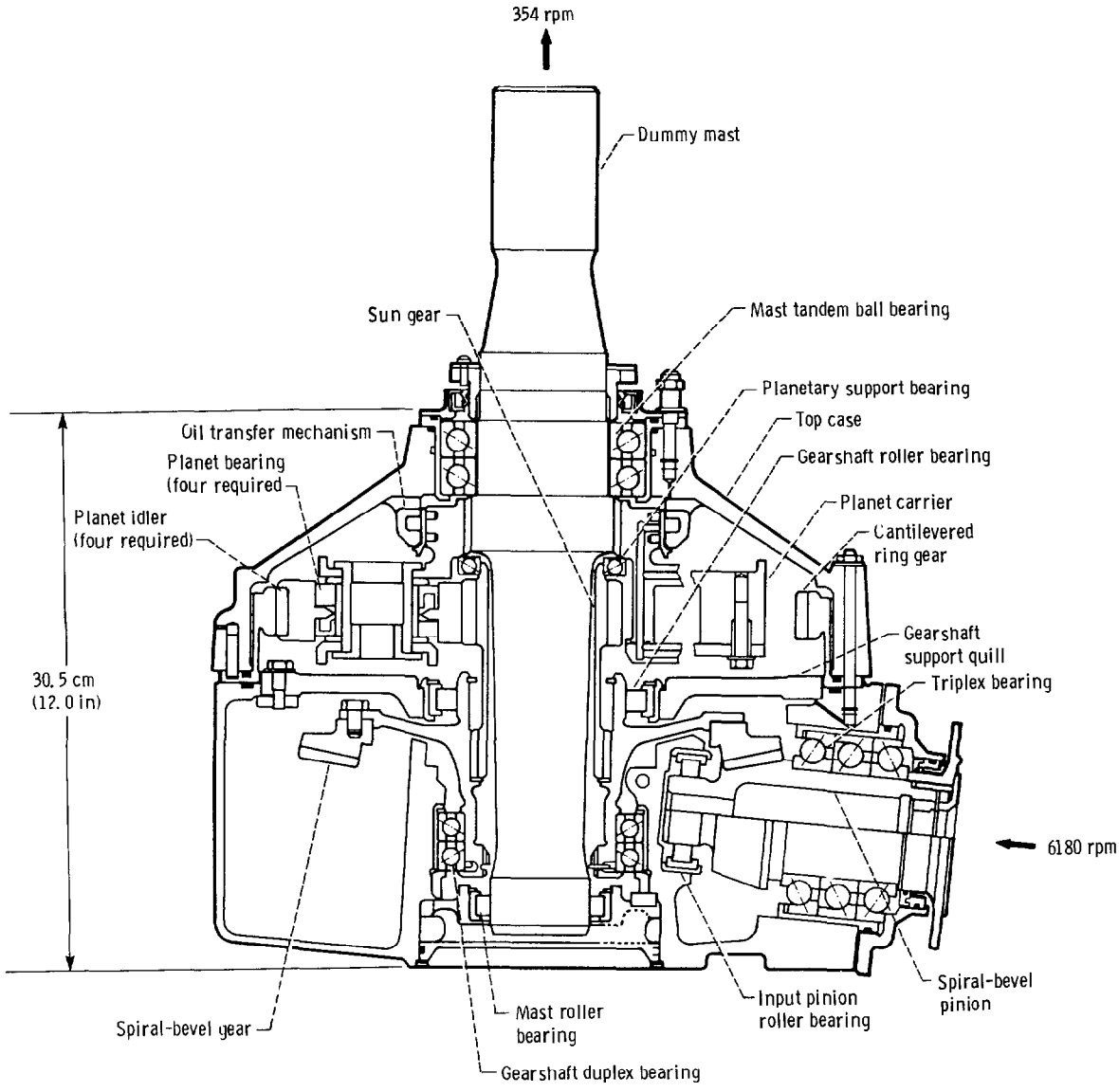

Figure 53.—373-kW (500-hp) helicopter transmission comprising a spiral-bevel gearset and four planet systems.

$N_{P,S}$ and $N_{P,R}$ are the numbers of teeth in the planet gears in contact with the sun and ring gears, respectively.

Coupled epicyclic trains.—Coupled epicyclic trains consist of two or more single epicyclic trains arranged so that two members in one train are common to the adjacent train (ref. 14).

Multispeed epicyclic trains.—Multispeed epicyclic trains are the most versatile and compact gear arrangement for a given ratio range and torque capacity. Tables 20 and 21 show the speed ratios possible with simple and compound epicyclic trains when one member is fixed and another is driving. With a suitable arrangement of clutches and brakes an epicyclic train can be the basis of a change-speed transmission. With the gears locked to each other an epicylic train has a speed ratio of 1 (ref. 14).

Most planetary gear transmissions are of the "automatic" type, in which speed changes are carried out automatically at a selected speed or torque level. Such transmissions are expensive transmissions because of the clutching and braking elements necessary to control operation of the unit. In addition, practical ratios available with planetary sets are limited (ref. 128).

TABLE 21.—SIMPLE EPICYCLIC TRAIN RATIOS[a]

[See fig. 54(a).]

Condition	Revolution of-		
	Sun	Arm	Ring
Sun fixed	0	1	$1+N_S/N_R$
Arm fixed	1	0	$-N_S/N_R$
Ring fixed	$1+N_R/N_S$	1	0

[a] N_S and N_R denote either pitch diameter or number of teeth in respective gears.

Bearingless planetary.—The self-aligning bearingless planetary transmission (fig. 55) covers a variety of planetary gear configurations that share the common characteristic that the planet carrier, or spider, is eliminated, as are conventional planet-mounted bearings. The bearings are eliminated by load balancing the gears, which are separated in the axial direction. All forces and reactions are transmitted through the gear meshes and contained by simple rolling rings. The concept was first demonstrated by Curtis Wright Corp. under sponsorship of the U.S. Army Aviation Research and Development Command (refs. 129 and 130).

Hybrid transmissions.—Geared planetary transmissions have a limitation on the speed ratio that can be obtained in a single stage without the planets interfering with each other. For example, a four-planet drive would have a maximum speed ratio of 6.8 before the planets interfered with each other. A five-planet drive would be limited to a ratio of 4.8, and so on.

A remedy to the speed ratio and planet number limitations of simple, single-row planetary systems was devised by A.L. Nasvytis (ref. 131). His drive system used the sun and ring roller of the simple planetary traction drive but replaced the single row of equal-diameter planet rollers with two or more rows of stepped, or dual-diameter, planets. With this new, multiroller arrangement practical speed ratios of 250 could be obtained in a single stage with three planet rows. Furthermore the number of planets carrying the load in parallel could be greatly increased for a given ratio. This

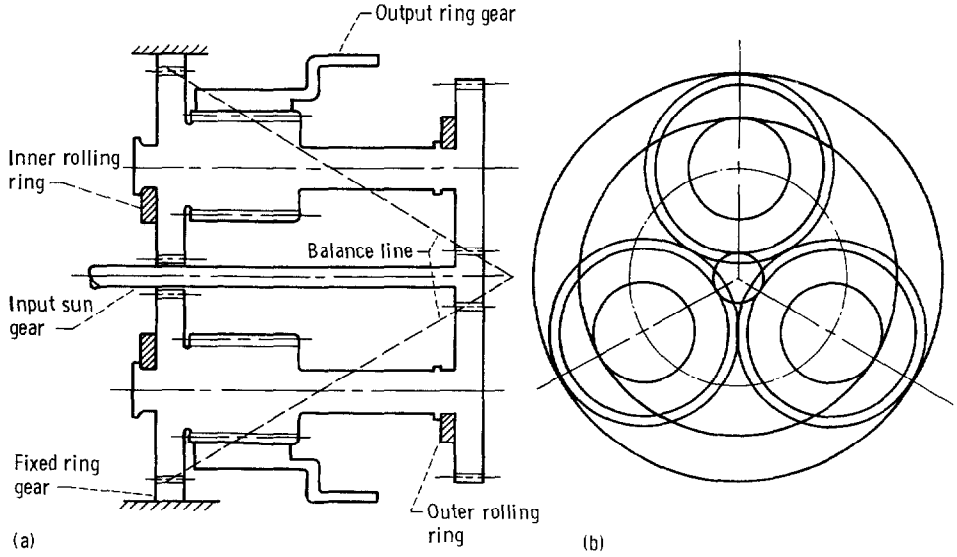

(a) Radial plane.
(b) Transverse plane.

Figure 55.—373-kW (500-hp) bearingless planetary transmission.

resulted in a significant reduction in individual roller contact loading with a corresponding improvement in torque capacity and fatigue life.

To further reduce the size and the weight of the drive for helicopter transmission applications, pinion gears in contact with a ring gear were incorporated with the second row of rollers (fig. 56). The ring gear was connected through a spider to the output rotor shaft. The number of planet roller rows and the relative diameter ratios at each contact are variables to be optimized according to the overall speed ratio and the uniformity of contact forces. The traction-gear combination is referred to as the "hybrid transmission." The potential advantages of the hybrid transmission over a conventional planetary transmission are higher speed ratios in a single stage, higher power-weight ratios, lower noise (by replacing gear contacts with traction rollers), and longer life because of load sharing by multiple power paths.

9.4 Split-Torque Transmissions

The power-weight ratio of a transmission and the unit stress of the gear teeth can be decreased by load sharing through multiple power paths. This concept, referred to as the "split-torque transmission" (refs. 132 to 134), is illustrated in figure 57 for single-input and double-input variants. Instead of a planetary gear arrangement the input power is split into two or more power paths and recombined in a bull gear to the output power (rotor) shaft. This concept appears to offer weight advantages over conventional planetary concepts without high-contact-ratio gearing. Incorporating high-contact-ratio gearing into the split-torque concept is expected to further reduce transmission weight.

9.5 Differential Gearing

Free differential gearing is an arrangement in which the normal ratio of the unit can be changed by driving into the unit with a second drive. This arrangement, or one having two outputs and one input, is used to vary the speed ratio. Simple differentials may use bevel gears (fig. 58(a)) or spur gears (fig. 58(b)). The bevel gear is used in automotive rear-end drives. The input-output speed relationship is

$$2\omega = \omega_1 - \omega_2 \tag{127}$$

where

ω speed of arm
ω_1, ω_2 shaft speeds

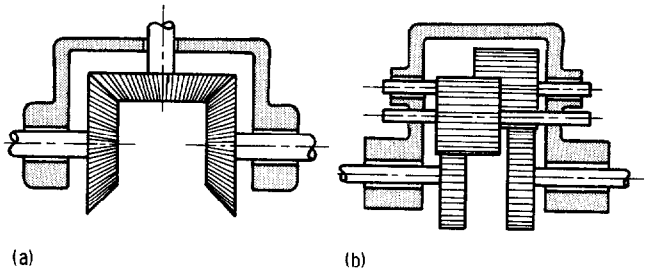

(a) Single input.
(b) Dual input.

Figure 57.—Conceptual sketch of split-torque transmission.

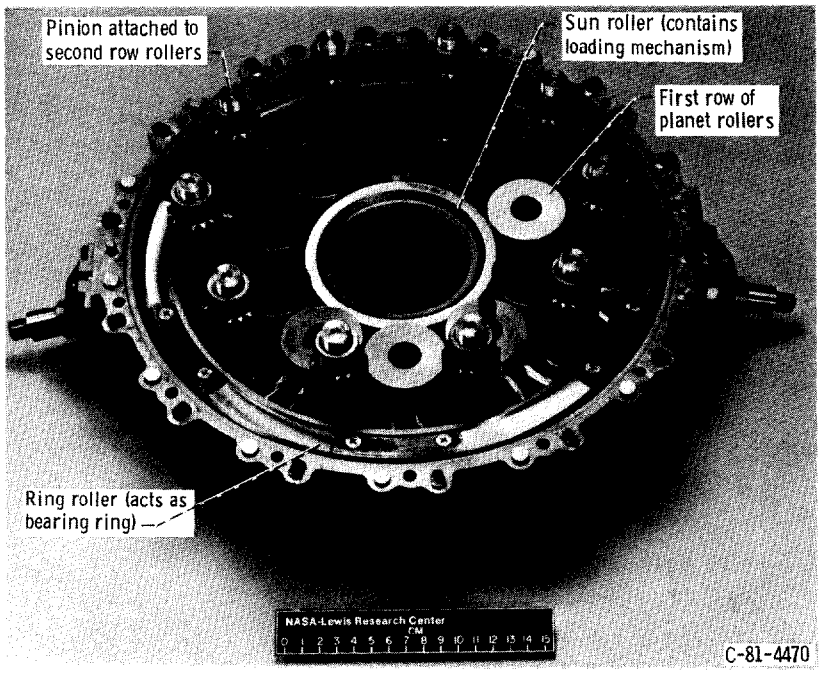

Figure 56.—373-kW (500-hp) hybrid transmission.

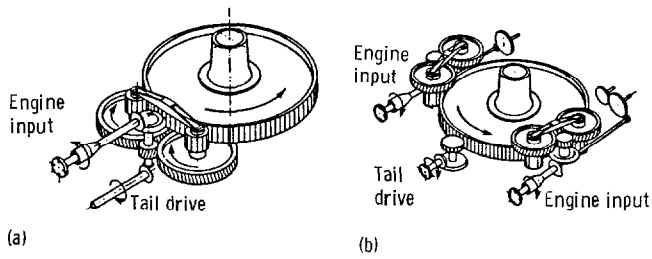

(a) Bevel gears.
(b) Spur gears.

Figure 58.—Simple differentials.

Another type of differential (called the fixed type) has a large, fixed ratio. Such a drive is an evolution of the compound epicyclic train (fig. 54(b)). If the ring gear is replaced with a sun gear which meshes with a planet gear $N_{P,R}$, the equations in table 22 apply except that the plus signs change to minus. If the sun and planet gears are made almost but not exactly equal, the output speed is the small difference between two terms that are almost equal. Such a drive is good for ratios from 10 to 3000.

Using two ring gears instead of a ring and a sun in figure 54(b) results in a fixed-differential drive suitable for ratios of 15 to 100. Any epicyclic geartrain can be designed for differential operation. For instance, instead of one of the elements, such as a sun or ring gear, being fixed, two of the elements may be driven independently. Output speed is then the net result of the two inputs.

Compound epicyclic trains can produce several input or output speeds by the addition of extra sun or ring gears meshing with the planet pinions. Thus the compound epicyclic train (fig. 54(b)) may have another sun gear

TABLE 22.—COMPOUND EPICYCLIC TRAIN RATIOS[a]

[See fig. 54(b).]

Condition	Revolution of–		
	Sun	Arm	Ring
Sun fixed	0	1	$1+N_R N_{P,R}/N_{P,S}N_R$
Arm fixed	1	0	$-N_S/N_{P,R}/N_{P,S}N_R$
Ring fixed	$1+N_{P,S}N_R/N_S N_{P,R}$	1	0

meshing with the ring gear $N_{P,R}$ and another ring gear meshing with the sun gear $N_{P,S}$. Any one of the four (two suns and two rings) could be fixed and the others available for input or output or free (ref. 14).

9.6 Closed-Loop Trains

Epicyclic geartrains with more than one planet pinion meshing with the same sun and ring gears have parallel paths through which power can flow. Other geartrains too sometimes use multiple-tooth contact to increase the capacity within a given space. Such gearing is sometimes called locked-train gearing.

Two considerations arise with multiple-tooth contact that are not present in open trains. One is the proper selection of tooth numbers and spacing to ensure assembly. The other is gear accuracy and adjustment to ensure equal distribution of the load to each mesh.

Multiple-mesh or locked-train gearing requires careful attention to tooth accuracy and support of the gears. Backlash and backlash tolerances should be as nearly equal as possible at each mesh to ensure equal load distribution (ref. 14).

Appendix—Symbols

A	cone distance, m (in)
a	semimajor axis of Hertzian contact ellipse, m (in)
ΔB	change in backlash, m (in)
B_{10}	bearing life at 90-percent reliability level
b	semiminor axis of Hertzian contact ellipse, m (in)
C	distance between centers, m (in)
ΔC	change in center distance, m (in)
C_1 to C_7	special constants (table 19)
C_{10}	special constant (eq. (68))
c	distance from neutral axis to outermost fiber of beam, m (in)
D	diameter of pitch circle, m (in)
D_{10}	special constant (eq. (79))
d	impingement depth, m (in)
E	Young's modulus of elasticity, Pa (psi)
E'	effective elastic modulus, Pa (psi)
e	Weibull slope, dimensionless
F	face width of tooth, m (in)
F_e	effective face width, m (in)
f	coefficient of friction
G	dimensionless materials parameter
G_{10}	life of gear at 90-percent reliability level, millions of revolutions or hr
H	dimensionless film thickness
H_B	Brinell hardness
ΔH	differential hardness
h	film thickness, m (in)
$\bar{h}$	central film thickness
I	area moment of inertia, m^4 (in^4)
J	geometry factor
K	load intensity factor, Pa (psi)
K_a	application factor
K_b	rim thickness factor
K_L	life factor
K_m	load distribution factor
K_R	reliability factor
K_S	size factor
K_T	temperature factor
K_V	dynamic load factor
K_X	cutter radius factor
k	ellipticity ratio, dimensionless
L	life, hr or millions of revolutions or stress cycles
L_W	lead of worm gear, m (in)
ℓ	length, m (in)
M	bending moment, N-m (lb-in)
m_c	contact ratio
m_G	gear ratio, N_2/N_1
N	number of teeth
N_e	equivalent number of teeth
n	angular speed, rpm
O	centerpoint location
P	diametral pitch, m^{-1} (in^{-1})
P_n	normal diametral pitch; m^{-1} (in^{-1})
P_t	transverse diametral pitch, m^{-1} (in^{-1})
p	circular pitch, m (in)
p_a	axial pitch, m (in)
p_b	base pitch, m (in)
p_n	normal circular pitch, m (in)
p_t	transverse circular pitch, m (in)
Δp	oil jet pressure, Pa (psig)
Q	power loss
q	number of planets
R_c	Rockwell C scale hardness
r	radius, m (in)
r_a	addendum circle radius, m (in)
r_{av}	mean pitch cone radius, m (in)
r_b	base circle radius, m (in)
r_c	cutter radius, m (in)
r_p	pitch circle radius, m (in)
S	stress, Pa (psi)
$S_{a,t}$	allowable tensile stress, Pa (psi)
$S_{a,y}$	allowable yield stress, Pa (psi)
S_b	bending stress, Pa (psi)
S_c	maximum Hertz compressive stress, Pa (psi)
S_r	residual shear stress, Pa (psi)
S_t	root fillet tensile stress, Pa (psi)
$\mathcal{S}$	probability of survival
$\mathcal{S}_T$	probability of survival of complete transmission including bearings and gears
s	distance measured from pitch point along line of action, m (in)
T	torque, N-m (lb-in)

T_{10}	tooth life at 90-percent reliability, millions of stress cycles or hr
t	tooth thickness, m (in)
U	dimensionless speed parameter
u	integer
V	stressed volume, m^3 (in^3)
v	pitch line velocity, m/s (ft/s)
v_j	oil jet velocity, m/s (ft/s)
v_r	total rolling velocity, m/s (ft/s)
$\bar{v}_r$	average total rolling velocity, m/s (ft/s)
v_s	sliding velocity, m/s (ft/s)
$\bar{v}_s$	average sliding velocity, m/s (ft/s)
W	dimensionless load parameter
W_N	load normal to surface, N (lb)
W_r	radial, or separating, component of load, N (lb)
W_t	transmitted or tangential, component of load, N (lb)
W_x	axial, or thrust, component of load, N (lb)
w	semiwidth of contact path, m (in)
X	distance from line of centers to impingement point, m (in)
Y	Lewis tooth form factor, dimensionless
Z	length of line of action, m (in)
z	depth to critical shear stress, m (in)
α	pressure-viscosity exponent, m^2/N (in^2/lb)
Γ	pitch angle, deg
γ	angle, deg
δ	tooth deflection, m (in)
ϵ	involute roll angle, deg (rad)
ϵ_c	pinion roll angle from base of involute to beginning of load (lowest point of double tooth-pair contact), deg (rad)
ϵ_H	increment of roll angle for which a single pair of teeth is in contact, deg (rad)
ϵ_L	increment of roll angle for which two pairs of teeth are in contact, deg (rad)
η	life, millions of stress cycles
θ	angle of rotation, rad
Λ	film thickness parameter, ratio of film thickness to rms surface roughness, dimensionless
λ_W	lead angle of worm gear, deg
μ	lubricant absolute viscosity, N s/m^2 (lb s/in^2)
μ_0	absolute viscosity at standard atmospheric pressure, N s/m^2 (lb s/in^2)
ν	Poisson's ratio, dimensionless
ξ	efficiency
ρ	radius of curvature, m (in)
$\Delta\rho$	curvature difference, dimensionless
Σ	shaft angle, deg
$\Sigma\rho$	curvature sum, m^{-1} (in^{-1})
σ	surface rms roughness, m (in)
τ	shear stress, Pa (psi)
τ_{max}	maximum shear stress, Pa (psi)
τ_o	maximum subsurface orthogonal reversing shear stress, Pa (psi)
Υ	parameter defined in table 15
φ	pressure angle, deg
φ_n	normal pressure angle, deg
φ_t	transverse pressure angle, deg
φ_x	axial pressure angle, deg
φ_w	angle between load vector and tooth centerline (fig. 34), deg
Ψ	helix angle, deg
ψ	spiral angle for spiral-bevel gear, deg
ω	angular velocity, rad/s

Subscripts:

a	at addendum, at addendum circle
av	average
B	bearing
b	binding
eq	equivalent
G	gear
in	input
j	jet
m	mesh
max	maximum
P	planet gear
p	pinion
R	ring gear
r	rolling
S	sun gear
s	sliding
T	total
t	transverse

W	worm gear
w	windage
x,y	mutually perpendicular planes in which maximum and minimum (principal) radii of surface curvature lie
1	pinion
2	gear

Superscripts:

c,h	exponents
α	pressure-viscosity exponent, m^2/N (in^2/lb)

References

1. Coy, John J.: Geared Powered Transmission Technology. Advanced Power Transmission Technology, George K. Fischer, ed., NASA CP-2210, 1983, pp. 49-77.
2. The New Encyclopedia Britannica, Fifteenth ed., Encyclopedia Britannica, Inc., 1974.
3. Price, Derek John deSolla: Gears from the Greeks. Science History Publications, 1975.
4. Drachmann, Aage Gerhardt: The Mechanical Technology of Greek and Roman Antiquity. Munksgaard (Copenhagen), 1963.
5. Dudley, Darle W.: The Evolution of the Gear Art. American Gear Manufacturers Association, 1969.
6. Reti, Ladislao: Leonardo on Bearings and Gears. Sci. Am., vol. 224, no. 2, Feb. 1971, pp. 100-110.
7. da Vinci, Leonardo (L. Reti, transl.): The Madrid Codices. McGraw-Hill Book Co., Inc., 1974.
8. Lewis, Wilfred: Investigations of the Strength of Gear Teeth. Proc. of Engineers Club of Philadelphia, 1893, pp. 16-23.
9. Grant, George B.: A Treatise on Gear Wheels. Twenty-first ed., Philadelphia Gear Works, Inc., 1980.
10. Buckingham, Earle: Dynamic Loads on Gear Teeth. American Society of Mechanical Engineers, 1931.
11. Tucker, A. I.: Bevel Gears at 203 Meters per Second (40,000 FPM). ASME Paper 77-DET-178, 1977.
12. Haas, L. L.: Latest Developments in the Manufacture of Large Spiral Bevel and Hypoid Gears. ASME Paper 80-C2/DET-119, 1980.
13. Drago, R. J.; and Brown, F. W.: The Analytical and Experimental Evaluation of Resonant Response in High-Speed, Light-Weight, Highly Loaded Gearing. J. Mech. Des., vol. 103, no. 2, Apr. 1981, pp. 346-356.
14. Crawshaw, S. L.; and Kron, H. O.: Mechanical Drives: Gears. Mach. Des., vol. 39, Sept. 21, 1967, pp. 18-23.
15. Gears and Gear Drives. Mach. Des., vol. 55, no. 15, June 30, 1983, pp. 16-32.
16. Kasuba, Romualdas: A Method for Static and Dynamic Load Analysis of Standard and Modified Spur Gears. Advanced Power Transmission Technology, George K. Fischer, ed., NASA CP-2210, 1983, pp. 403-419.
17. Wildhaber, E.: "Helical Gearing," U.S. Patent 1,601,750, 1926.
18. Wildhaber, E.: Method of Grinding Gears. U.S. Patent 1,858,568, May 1932.
19. Novikov, M.L.: U.S.S.R. Patent 109,750, 1956.
20. Shotter, B.A.: The Lynx Transmission and Conformal Gearing. SAE Paper 78-10141, Nov. 1978.
21. Shotter, B.A.: Experiences with Conformal/W-N Gearing. Machinery and Production Engineering, Oct. 5, 1977, pp. 322-326.
22. Costomiris, G.H.; Daley, D.P.; and Grube, W.: Heat Generated in High Power Reduction Gearing of Gas Turbine Rotors. PWA-3718. Pratt & Whitney Aircraft Division, 1969, p. 43. (AD-690923).
23. Fusaro, Robert L.: Effect of Atmosphere and Temperature on Wear, Friction and Transfer of Polyimide Films. ASLE Trans., vol. 21, no. 2, Apr. 1978, pp. 125-133.
24. Fusaro, Robert L.: Tribological Properties at 25 °C of Seven Polyimide Films Bonded to 440C High-Temperature Stainless Steel. NASA TP-1944, 1982.
25. Fusaro, R.L.: Polyimides: Tribological Properties and Their Use as Lubricants. NASA TM-82959, 1982.
26. Johansen, K.M.: Investigation of the Feasibility of Fabricating Bimetallic Coextruded Gears. AFAPL-TR-73-112, AiResearch Mfg. Co., 1973. (AD-776795.)
27. Hirsch, R.A.: Lightweight Gearbox Development for Propeller Gearbox System Applications—Potential Coatings for Titanium Alloy Gears. AFAPL-TR-72-90, General Motors Corp., 1972. (AD-753417.)
28. Delgrosso, E.J.; et al.: Lightweight Gearbox Development for Propeller Gearbox Systems Applications. AFAPL-TR-71-41-PH-1, Hamilton Standard, 1971. (AD-729839.)
29. Manty, B.A.; and Liss, H.R.: Wear Resistant Coatings for Titanium Alloys. FR-8400, Pratt & Whitney Aircraft, 1977. (AD-A042443.)
30. Dudley, Darle W.: Gear Handbook: The Design, Manufacture and Applications of Gears. McGraw-Hill, 1962.
31. Michalec, George W.: Precision Gearing Theory and Practice, John Wiley & Sons, Inc., 1966.
32. Rating the Strength of Spur Gear Teeth. AGMA 220.02, American Gear Manufacturers Association, Aug. 1966.
33. Surface Durability (Pitting) of Spur Gear Teeth. AGMA 210.02, American Gear Manufacturers Association, Jan. 1965.
34. Smith, W.E.: Ferrous-Based Powder Metallurgy Gears. Gear Manufacture and Performance, P. J. Guichelaar, B. S. Levy, and N. M. Parikh, eds., American Society for Metals, 1974, pp. 257-269.
35. Antes, H.W.: P/M Hot Formed Gears. Gear Manufacture and Performance, P. J. Guichelaar, Bernard S. Levy, and N. M. Parikh, eds., American Society for Metals, 1974, pp. 271-292.
36. Ferguson, B.L.; and Ostberg, D.T.: Forging of Powder Metallurgy Gears. TARADCOM-TR-12517, TRW-ER-8037-F, TRW, Inc., 1980. (AD-A095556.)
37. Townsend, Dennis P.; and Zaretsky, Erwin V.: Effect of Shot Peening on Surface Fatigue Life of Carburized and Hardened AISI 9310 Spur Gears. NASA TP-2047, 1982.
38. Straub, J.C.: Shot Peening in Gear Design. AGMA Paper 109.13, American Gear Manufacturers Association, 1964.
39. Anderson, Neil E.; and Zaretsky, Erwin V.: Short-Term, Hot-Hardness Characteristics of Five Case-Hardened Steels. NASA TN D-8031, 1975.
40. Hingley, C.G.; Southerling, H.E.; and Sibley, L.B.: Supersonic Transport Lubrication System Investigation. (AL65T038 SAR-1, SKF Industries, Inc.; NASA Contract NAS3-6267.) NASA CR-54311, 1965.
41. Bamberger, Eric N.; Zaretsky, Erwin V.; and Anderson, William J.: Fatigue Life of 120-mm Bore Ball Bearings at 600 °F with Fluorocarbon, Polyphenyl Ether, and Synthetic Paraffinic Base Lubricants. NASA TN D-4850, 1968.
42. Zaretsky, Erwin V.; Anderson, William J.; and Bamberger, Eric N.: Rolling-Element Bearing Life from 400° to 600 °F. NASA TN D-5002, 1969.
43. Bamberger, E.N.; Zaretsky, E.V.; and Anderson, W.J.: Effect of Three Advanced Lubricants on High-Temperature Bearing Life. J. Lubr. Technol., vol. 92, no. 1, Jan. 1970, pp. 23-33.
44. Bamberger, Eric N.; and Zaretsky, Erwin V.: Fatigue Lives at 600 °F of 120-Millimeter-Bore Ball Bearings of AISI M-50, AISI M-1, and WB-49 Steels. NASA TN D-6156, 1971.
45. Bamberger, E.N.: The Development and Production of Thermo-Mechanically Forged Tool Steel Spur Gears. (R73AEG284, General Electric Co.; NASA Contract NAS3-15338). NASA CR-121227, 1973.
46. Townsend, D.P.; Bamberger, E.N.; and Zaretsky, E.V.: A Life Study of Ausforged, Standard Forged, and Standard Machined AISI M-50 Spur Gears. J. Lubr. Technol., vol. 98, no. 3, July 1976, pp. 418-425.
47. Bamberger, E.N.: The Effect of Ausforming on the Rolling Contact Fatique Life of a Typical Bearing Steel. J. Lubr. Technol., vol. 89, no. 1, Jan. 1967, pp. 63-75.

48. Jatczak, C.F.: Specialty Carburizing Steels for Elevated Temperature Service. Met. Prog., vol. 113, no. 4, Apr. 1978, pp. 70–78.
49. Townsend, Dennis P.; Parker, Richard J.; and Zaretsky, Erwin V.: Evaluation of CBS 600 Carburized Steel as a Gear Material. NASA TP-1390, 1979.
50. Culler, R.A., et al.: Elevated Temperature Fracture Toughness and Fatigue Testing of Steels for Geothermal Applications. TERRATEK Report No. Tr 81-97, Terra Tek, Inc., Oct. 1981.
51. Roberts, G.A.; and Hamaker, J.C.: Strong, Low Carbon Hardenable Alloy Steels. U.S. Patent 3,036,912, May 1962.
52. Cunningham, R.J.; and Lieberman, W.N.J.: Process for Carburizing High Alloy Steels. U.S. Patent 3,885,995, May 1975.
53. Townsend, D.P.; and Zaretsky, E.V.: Endurance and Failure Characteristics of Modified Vasco X-2, CBS 600 and AISI 9310 Spur Gears. J. Mech. Des., vol. 103, no. 2, Apr. 1981, pp. 506–515.
54. Walp, H.O.; Remorenko, R.P.; and Porter, J.V.: Endurance Tests of Rolling-Contact Bearings of Conventional and High Temperature Steels under Conditions Simulating Aircraft Gas Turbine Applications. WADC-TR-58-392, Wright Air Development Center, 1959. (AD-212904.)
55. Baile, G.H., et al.: A Synopsis of Active SKF Research and Development Programs of Interest to the Aerospace Industry. AL-63M003, SKF Industries, Inc., 1963.
56. Scott, D.: Comparative Rolling Contact Fatigue Tests on En 31 Ball Bearing Steels of Recent Manufacture. NEL 69T96, National Engineering Laboratory, Glasgow, Scotland, 1969.
57. 1968 Aero Space Research Report. AL 68Q013, SKF Industries, Inc., 1968.
58. Scott, D.; and Blackwell, J.: Steel Refining as an Aid to Improved Rolling Bearing Life. NEL Report No. 354, National Engineering Laboratory, 1968.
59. Bamberger, E.N.; Zaretsky, E.V.; and Signer, H.: Endurance and Failure Characteristic of Main-Shaft Jet Engine Bearing at 3×10^6 DN. J. Lub. Technol., vol. 98, no. 4, Oct. 1976, pp. 580–585.
60. Carter, Thomas L.; Zaretsky, Erwin V.; and Anderson, William J.: Effect of Hardness and Other Mechanical Properties on Rolling-Contact Fatigue Life of Four High-Temperature Bearing Steels. NASA TN D-270, 1960.
61. Jackson, E.G.: Rolling Contact Fatigue Evaluations of Bearing Materials and Lubricants. ASLE Trans., vol. 2, no. 1, 1959, pp. 121–128.
62. Baughman, R.A.: Effect of Hardness, Surface Finish, and Grain Size on Rolling-Contact Fatique Life of M-50 Bearing Steel. J. Basic Eng., vol. 82, no. 2, June 1960, pp. 287–294.
63. Zaretsky, Erwin V., et al.: Bearing Life and Failure Distribution as Affected by Actual Component Differential Hardness. NASA TN D-3101, 1965.
64. Zaretsky, E.V.; Parker, R.J.; and Anderson, W.J.: Component Hardness Differences and Their Effect on Bearing Fatigue. J. Lubr. Technol., vol. 89, no. 1, Jan. 1967, pp. 47–62.
65. Anderson, W.J.; and Carter, T.L.: Effect of Fiber Orientation, Temperature and Dry Powder Lubricants on Rolling-Contact Fatigue. ASLE Trans., vol. 2, no. 1, 1959, pp. 108–120.
66. Carter, Thomas L.: A Study of Some Factors Affecting Rolling-Contact Fatigue Life. NASA TR R-60, 1960.
67. Bamberger, E.N.: The Effect of Ausforming on the Rolling Contact Fatigue Life of a Typical Bearing Steel. J. Lubr. Technol., vol. 89, no. 1, Jan. 1967, pp. 63–75.
68. Bamberger, E.N.: The Production, Testing, and Evaluation of Ausformed Ball Bearings. General Electric Co., 1966. (AD-637576.)
69. Parker, Richard J.; and Zaretsky, Erwin V.: Rolling-Element Fatigue Life of Ausformed M-50 Steel Balls. NASA TN D-4954, 1968.
70. AGMA Standard for Rating the Pitting Resistance and Bending Strength of Spur and Helical Involute Gear Teeth. AGMA 218.01, American Gear Manufacturers Association, Dec. 1982.
71. Cardou, A.; and Tordion, G.V.: Numerical Implementation of Complex Potentials for Gear Tooth Stress Analysis. J. Mech. Des., vol. 103, no. 2, Apr. 1981, pp. 460–465.
72. Rubenchik, V.: Boundary-Integral Equation Method Applied to Gear Strength Rating. Journal of Mechanisms, Transmissions, and Automation in Design, vol. 105, no. 1, Mar. 1983, pp. 129–131.
73. Alemanni, M.; Bertoglio, S.; and Strona, P.: B.E.M. in Gear Teeth Stress Analysis: Comparison with Classical Methods. Proceedings of the International Symposium on Gearing and Power Transmissions, Vol. II, Japan Society of Mechanical Engineers, Tokyo, 1981, pp. 177–182.
74. Wilcox, L.; and Coleman, W.: Application of Finite Elements to the Analysis of Gear Tooth Stresses. J. Eng. Ind., vol. 95, no. 4, Nov. 1973, pp. 1139–1148.
75. Wilcox, L.E.: An Exact Analytical Method for Calculating Stresses in Bevel and Hypoid Gear Teeth. Proceeding of the International Symposium on Gearing and Power Transmissions, Vol. II, Japan Society of Mechanical Engineers, Tokyo, 1981, pp. 115–121.
76. Frater, J.L.; and Kasuba, R.: Extended Load-Stress Analysis of Spur Gearing: Bending Strength Considerations. Proceedings of International Symposium on Gearing and Power Transmissions, Vol. II, Japan Society of Mechanical Engineers, Tokyo, 1981, pp. 147–152.
77. Coy, J.J.; and Chao, C. Hu-Chih: A Method of Selecting Grid Size to Account for Hertz Deformation in Finite Element Analysis of Spur Gears. J. Mech. Des., vol. 104, no. 4, Oct. 1982, pp. 759–766.
78. Drago, R.J.: Results of an Experimental Program Utilized to Verify a New Gear Tooth Strength Analysis. AGMA Technical Paper P229.27, American Gear Manufacturers Association, Oct. 1983.
79. Drago, R.J.; and Lutthans, R.V.: An Experimental Investigation of the Combined Effects of Rim Thickness and Pitch Diameter on Spur Gear Tooth Root and Fillet Stresses. AGMA Technical Paper P229.22, American Gear Manufacturers Association, Oct. 1981.
80. Chang, S.H.; Huston, R.L.; and Coy, J.J.: A Finite Element Stress Analysis of Spur Gears Including Fillet Radii and Rim Thickness Effects. Journal of Mechanisms, Transmissions, and Automation in Design, vol. 105, no. 3, Sept. 1983, pp. 327–330.
81. Drago, Raymond J.: An Improvement in the Conventional Analysis of Gear Tooth Bending Fatigue Strength. AGMA Technical Paper P229.24, American Gear Manufacturers Association, Oct. 1982.
82. Chong, Tae-Hyong, et al.: Bending Stresses of Internal Spur Gear. Bull. JSME, vol. 25, no. 202, Apr. 1982, pp. 679–686.
83. Wang, K.L.; and Cheng, H.S.: A Numerical Solution to the Dynamic Load, Film Thickness, and Surface Temperatures in Spur Gears, Part I-Analysis. J. Mech. Des., vol. 103, no. 1, Jan. 1981, pp. 177–187.
84. Wang, K.L.; and Cheng, H.S.: A Numerical Solution to the Dynamic Load, Film Thickness, and Surface Temperatures in Spur Gears, Part II-Results. J. Mech. Des., vol. 103, no. 1, Jan. 1981, pp. 188–194.
85. Dolan, T.J.; and Broghamer, E.L.: A Photoelastic Study of Stresses in Gear Tooth Fillets. University of Illinois, Engineering Experimental Station Bulletin 335, 1942.
86. Cornell, R.W.: Compliance and Stress Sensitivity of Spur Gear Teeth. J. Mech. Des., vol. 103, no. 2, Apr. 1981, pp. 447–459.
87. Coy, John J.; Townsend, Dennis P.; and Zaretsky, Erwin V.: Analysis of Dynamic Capacity of Low-Contact-Ratio Spur Gears Using Lundberg-Palmgren Theory. NASA TN D-8029, 1975.

88. Coy, John J.; and Zaretsky, Erwin V.: Life Analysis of Helical Gear Sets Using Lundberg-Palmgren Theory. NASA TN D-8045, 1975.
89. Coy, J.J.; Townsend, D.P.; and Zaretsky, E.V.: Dynamic Capacity and Surface Fatigue Life for Spur and Helical Gears. J. Lubr. Technol., vol. 98, no. 2, Apr. 1976, pp. 267–276.
90. Townsend, D.P.; Coy, J.J.; and Zaretsky, E.V.: Experimental and Analytical Load-Life Relation for AISI 9310 Steel Spur Gears. J. Mech. Des., vol. 100, no. 1, Jan. 1978, pp. 54–60.
91. Coy, John J.; Townsend, Dennis P.; and Zaretsky, Erwin V.: An Update on the Life Analysis of Spur Gears. Advanced Power Transmission Technology, George K. Fischer, ed., NASA CP-2210, 1983, pp. 421–433.
92. Lundberg, G.; and Palmgren, A.: Dynamic Capacity of Rolling Bearings. Acta Polytech., Mech. Eng. Ser., vol. 1, no. 3, 1947.
93. Bamberger, E.N., et al.: Life Adjustment Factors for Ball and Roller Bearings. American Society of Mechanical Engineers, 1971.
94. Savage, M.; Paridon, C.A.; and Coy, J.J.: Reliability Model for Planetary Gear Trains. Journal of Mechanisms, Transmissions, and Automation in Design, vol. 105, no. 3, Sept. 1983, pp. 291–297.
95. Krenzer, Theodore J.; and Knebel, Richard: Computer Aided Inspection of Bevel and Hypoid Gears, SAE Paper 831266, 1983.
96. Litvin, F.L.; and Gutman, Y.: Methods of Synthesis and Analysis for Hypoid Gear-Drives of 'Formate' and 'Helixform', Parts 1, 2 and 3. J. Mech. Des., vol. 103, no. 1, Jan. 81, pp. 83–113.
97. Litvin, F.L.; and Gutman, Y.: A Method of Local Synthesis of Gears Grounded on the Connections Between the Principal and Geodetic Curvatures of Surfaces. J. Mech. Des., vol. 103, no. 1, Jan. 1981, pp. 114–125.
98. Coy, J.J.; Rohn, D.A.; and Loewenthal, S.H.: Constrained Fatigue Life Optimization of a Nasvytis Multiroller Traction Drive. J. Mech. Des., vol. 103, no. 2, April 1981, pp. 423–429.
99. Coleman, W.: Bevel and Hypoid Gear Surface Durability: Pitting and Scuffing. Source Book on Gear Design, Technology and Performance, Maurice A.H. Howes, ed., American Society for Metals, 1980, pp. 243–258.
100. Anderson, W.J; and Zaretsky, E.V.: Rolling-Element Bearings. Mach. Des., vol. 42, no. 15, June 18, 1970, pp. 21–37.
101. Ertel, A.M.: Hydrodynamic Lubrication Based on New Principles. Prikl. Mat. Mek., vol. 3, no. 2, 1939 (in Russian).
102. Grubin, A.N.: Fundamentals of the Hydrodynamic Theory of Lubrication of Heavily Loaded Cylindrical Surfaces. Investigation of the Contact of Machine Components, Kh. F. Ketova, ed., Translation of Russian Book No. 30, Central Scientific Institute for Technology and Mechanical Engineering, Moscow, 1949. (Available from Dept. of Scientific and Industrial Research, Great Britain, Transl. CTS-235, and Special Libraries Assoc., Transl. R-3554.)
103. Hamrock, Bernard J.; and Dowson, Duncan: Minimum Film Thickness in Elliptical Contacts for Different Regimes of Fluid-Film Lubrication. NASA TP-1342, 1978.
104. Fein, R.S.: Chemistry in Concentrated-Conjunction Lubrication. Interdisciplinary Approach to the Lubricaton of Concentrated Contacts, NASA SP-237, 1970, pp. 489–527.
105. Godfrey, D.: Boundary Lubrication. Interdisciplinary Approach to Friction and Wear, NASA SP-181, 1968, pp. 335–384.
106. Bowden, Frank Philip; and Tabor, David: The Friction and Lubrication of Solids, Vol. 2. Clarendon Press, Oxford, 1964, p. 365.
107. Borsoff, V.A.: Fundamentals of Gear Lubrication. Annual Rep., Shell Development Co., June 1955. (Work under Contract NO.a(s) 53-356-c.)
108. Borsoff, V.A.; and Lulwack, R.: Fundamentals of Gear Lubrication. Final Rep., Shell Development Co., June 1957. (Work under Contract NO.a(s) 53-356-c).
109. Horlick, E.J.; and O'D. Thomas, D. E.: Recent Experiences in the Lubrication of Naval Gearing. Gear Lubrication Symposium, Institute of Petroleum, 1966.
110. Boner, Charles J.: Gear and Transmission Lubricant. Reinhold Pub. Co., 1964.
111. Townsend, D.P.; and Akin, L.S.: Study of Lubricant Jet Flow Phenomena in Spur Gears—Out of Mesh Condition. Advanced Power Transmission Technology, George K. Fischer, ed., NASA CP-2210, 1983, pp. 461–476.
112. Townsend, Dennis P.; and Akin, Lee S.: Gear Lubrication and Cooling Experiment and Analysis. Advanced Power Transmission Technology, George K. Fischer, ed., NASA CP-2210, 1983, pp. 477–490.
113. Akin, L.S.; Mross, J.J.; and Townsend, D.P.: Study of Lubricant Jet Flow Phenomena in Spur Gears. J. Lubr. Technol., vol. 97, no. 2, Apr. 1975, pp. 283–288, 295.
114. Townsend, D.P.; and Akin, L.S.: Study of Lubricant Jet Flow Phenomena in Spur Gears—Out of Mesh Condition. J. Mech. Des., vol. 100, no. 1, Jan. 1978, pp. 61–68.
115. Townsend, D.P.; and Akin, L.S.: "Analytical and Experimental Spur Gear Tooth Temperature as Affected by Operating Variables." J. Mech. Des., vol. 103, no. 1, Jan. 1981, pp. 219–226.
116. Akin, L.S.; and Townsend, D.P.: Into Mesh Lubrication of Spur Gears with Arbitrary Offset Oil Jet. Part 1: For Jet Velocity Less Than or Equal to Gear Velocity. Journal of Mechanismis Transmissions, and Automation in Design, vol. 105, no. 4, Dec. 1983, pp. 713–718.
117. Akin, L.S.; and Townsend, D.P.: Into Mesh Lubrication of Spur Gears with Arbitrary Offset Oil Jet. Part 2: For Jet Velocities Equal to or Greater Than Gear Velocity. Journal of Mechanisms, Transmissions, and Automation in Design, vol. 105, no. 4, Dec. 1983, pp. 719–724.
118. Patir, Nadir; and Cheng, H.S.: Prediction of the Bulk Temperature in Spur Gears Based on Finite Element Temperature Analysis. ASLE Trans., vol. 22, no. 1, Jan. 1979, pp. 25–36.
119. Anderson, Neil E.; and Loewenthal, S.H.: Spur-Gear-System Efficiency at Part and Full Load. NASA TP-1622, 1980.
120. Anderson, N.E.; and Loewenthal, S.H.: Effect of Geometry and Operating Conditions on Spur Gear System Power Loss. J. Mech. Des., vol. 103, no. 1, Jan. 1981, pp. 151–159.
121. Anderson, N.E.; and Loewenthal, S.H.: Design of Spur Gears for Improved Efficiency. J. Mech. Des., vol. 104, no. 3, Oct. 1982, pp. 767–774.
122. Anderson, N.E.; and Loewenthal, S.H.: Selecting Spur-Gear Geometry for Greater Efficiency. Mach. Des., vol. 55, no. 10, May 12, 1983, pp. 101–105.
123. Savage, M.; Coy, J.J.; and Townsend, D.P.: Optimal Tooth Numbers for Compact Standard Spur Gear Sets. J. Mech. Des., vol. 104, no. 4, Oct. 1982, pp. 749–758.
124. Savage, Michael; Coy, John J.; and Townsend, Dennis P.: The Optimal Design of Standard Gearsets. Advanced Power Transmission Technology, George K. Fischer, ed., NASA CP-2210, 1983, pp. 435–469.
125. Lynwander, P.: Gear Tooth Scoring Design Considerations. AGMA Paper P219.10, American Gear Manufacturers Association, Oct. 1981.
126. Savage, M.; Coy, J.J.; and Townsend, D.P.: The Optimal Design of Involute Gear Teeth with Unequal Addenda. AVRADCOM TR 82-C-7, NASA TM-82866, 1982.
127. Carroll, R.K.; and Johnson, G.E.: Optimal Design of Compact Spur Gear Sets. ASME Paper 83-DET-33, 1983.
128. Wadlington, R.P.: Gear Drives. Mach. Des., vol. 39, no. 22, Sept. 21, 1967, pp. 24–26.

129. DeBruyne, Neil A.: Design and Development Testing of Free Planet Transmission Concept. USAAMRDL-TR-74-27, Army Air Mobility Research and Development Laboratory, 1974. (AD-782857.)
130. Folenta, D.J.: Design Study of Self-Aligning Bearingless Planetary Gear (SABP). Advanced Power Transmission Technology, George K. Fischer, ed., NASA CP-2210, 1983, pp. 151-160.
131. Nasvytis, Algirdas L.: Multiroller Planetary Friction Drives. SAE Paper 660763, Oct. 1966.
132. White, G.: New Family of High-Ratio Reduction Gears with Multiple Drive Paths. Proc. Inst. Mech. Eng., vol. 188, no. 23, 1974, pp. 281-288.
133. Lastine, J.L.; and White, G.: Advanced Technology VTOL Drive Train Configuration Study. USAAVLABS-TR-69-69, Army Aviation Material Laboratories, 1970. (AD-867905.)
134. White, G.: Helicopter Transmission Arrangements with Split-Torque Gear Trans. Advanced Power Transmission Technology, George K. Fischer, ed., NASA CP-2210, 1983, pp. 141-150.

Bibliography

Buckingham, E.: Analytical Mechanics of Gears. Dover Publications, NY, 1963.

Boner, C. J.: Gear and Transmission Lubricants. Reinhold Publishing, NY, 1964.

Deutschman, A.; Michels, W. J.; and Wilson, C. E.: Machine Design, MacMillan, NY, 1975, pp. 519–659.

Dudley, D. W.: Practical Gear Design. McGraw-Hill, NY, 1954.

Dudley, D. W.: Gear Handbook. McGraw-Hill, NY, 1962.

Khiralla, T. W.: On the Geometry of External Involute Spur Gears. T. W. Khiralla, Studio City, Calif., 1976.

Michalec, G. W.: Precision Gearing: Theory and Practice. John Wiley & Sons, NY, 1966.

Mechanical Drives Reference Issue, Machine Design, 3rd ed., Vol. 39, No. 22, Sept. 21, 1967.

1. Report No.	2. Government Accession No.	3. Recipient's Catalog No.
NASA RP-1152 AVSCOM TR 84-C-15		

4. Title and Subtitle	5. Report Date
Gearing	December 1985
	6. Performing Organization Code

7. Author(s)	8. Performing Organization Report No.
John J. Coy, Dennis P. Townsend, and Erwin V. Zaretsky	E-2003
	10. Work Unit No.

9. Performing Organization Name and Address	11. Contract or Grant No.
Propulsion Directorate, USAARTA-AVSCOM and Lewis Research Center Cleveland, Ohio 44135	
	13. Type of Report and Period Covered
12. Sponsoring Agency Name and Address	Reference Publication
National Aeronautics and Space Administration Washington, DC 20546-0001 and U.S. Army Aviation Systems Command St. Louis, MO 63120-1798	14. Sponsoring Agency Code

15. Supplementary Notes

John J. Coy: Propulsion Directorate, U.S. Army Aviation Research and Technology Activity (USAARTA-AVSCOM), Lewis Research Center, Cleveland, Ohio.
Dennis P. Townsend and Erwin V. Zaretsky: Lewis Research Center, Cleveland, Ohio.

Ch. 38 in Mechanical Design and Systems Handbook, McGraw-Hill Book Company, 1985.

16. Abstract

Gearing technology in its modern form has a history of only 100 years. However, the earliest form of gearing can probably be traced back to fourth century B.C. Greece. This publication draws together current gear practice and integrates it with recent advances in the technology. The history of gearing is reviewed briefly in the Introduction. Subsequent sections describe types of gearing and their geometry, processing, and manufacture. Both conventional and more recent methods of determining gear stress and deflections are considered. The subjects of life prediction and lubrication are additions to the literature. New and more complete methods of power loss prediction as well as an optimum design of spur gear meshes are described. Conventional and new types of power transmission systems are presented.

17. Key Words (Suggested by Author(s))	18. Distribution Statement
Gearing; Gear geometry; Gear processing; Gear stress; Gear deflection	Unclassified - unlimited STAR Category 37

19. Security Classif. (of this report)	20. Security Classif. (of this page)	21. No. of pages	22. Price
Unclassified	Unclassified	72	A04

For sale by the National Technical Information Service, Springfield, Virginia 22161

NASA-Langley, 1985